STRUCTURAL, OPTICAL AND ELECTRICAL PROPERTIES OF COBALT DOPED ZINC OXIDE THIN FILMS PREPARED BY SPRAY PYROLYSIS

M. Phil. Thesis

(Physics)

By

Mahjabin Taskin

EXAMINATION ROLL NO. : 0409143013F

SESSION : April 2009

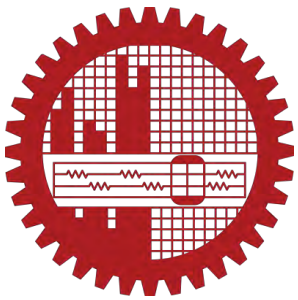

DEPARTMENT OF PHYSICS

BANGLADESH UNIVERSITY OF ENGINEERING & TECHNOLOGY

DHAKA 1000, BANGLADESH

October, 2011

STRUCTURAL, OPTICAL AND ELECTRICAL PROPERTIES OF COBALT DOPED ZINC OXIDE THIN FILMS PREPARED BY SPRAY PYROLYSIS

A Dissertation Submitted to the Department Of Physics, Bangladesh University of Engineering & Technology, Dhaka, in Partial Fulfillment of Requirement for the Degree of Master of Philosophy in Physics

By

Mahjabin Taskin

EXAMINATION ROLL NO. : 0409143013F

SESSION : April 2009

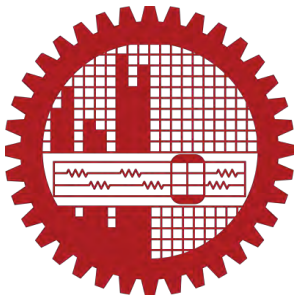

DEPARTMENT OF PHYSICS

BANGLADESH UNIVERSITY OF ENGINEERING & TECHNOLOGY

DHAKA 1000, BANGLADESH

October, 2011

CANDIDATE'S DECLARATION

It is hereby declared that this thesis or any part of it has not been submitted elsewhere for the award of any degree or diploma.

Mahjabin Taskin

DEDICATED TO
MY
BELOVED PARENTS

ACKNOWLEDGEMENTS

First of all I express all my admiration and devotion to the almighty Allah- Rabbul Alamin, the most beneficial who has enabled me to perform this research work and to submit this thesis.

I express my profound gratitude to my honorable supervisor Professor Dr. Jiban Podder, Department of Physics, BUET, for his constant direction, constructive criticism and inspiration in pursuing the whole investigation of the present research. Words are always insufficient to express his working capacities and unending enthusiasm for scientific rigorousness for innovative investigations. This always becomes the everlasting source of inspiration for his students.

I am thankful to Professor Dr. Md. Mostak Hossain, Head department of Physics, BUET for his best wishes and supports to carry out this work. He gives me a lot of instructive discussions and helpful suggestions.

I like to express my gratitude to, Professor Dr. Md. Abu Hashan Bhuiyan, Professor Dr. Md. Feroz Alam Khan, Professor Dr. A. K. M. Akther Hossain , Dr. Afia Begum, Dr. Md. Forhad Mina, Dr. Rafi Uddin, Dr. Nasreen Akter, and all other teachers of the Physics Department, for their cooperation.

I would like to give special thank to Dept. of Physics & Engineering Physics, University of Saskatchewan, Canada, for using their X-ray Diffractometer. The help provided by Dr. M. A. Gafur, Senior Engineer BCSIR, for UV-VIS measurements and Mr. Harinarayan Das, Scientific officer, AECD for EDX and SEM analysis is greatly appreciated

I am very much grateful to Professor Dr. M Khalilur Rahman Khan, Mr. Al Momin Md. Tanveer Karim and Mr. Md. Moniruzzaman, Department of Physics University of Rajshahi, Rajshahi for their kind help during the study of electrical property.

I am also thankful to Ms. Ferdousi Akhtar, Mr. Kamal Uddin Azad, Ms. Tamjida Rahman Luna, Mr. Amjad Hussain, Mr. Khorshed Alam, Mr. Sanjoy Das, Mr. Maruf Morshed, for their continuous cooperation and valuable suggestions during my research work in the solid state physics laboratory of the Department of Physics, BUET.

I am very grateful to Mr. Md. Idris Munsi, Mr. Md. Liakot Ali, Mr. Abu Thaher and all other official staff of this department for their sincere help.

Finally, I would like to express my deep gratitude to my parents and sisters for their multifaceted support through all these years. Last, but not least I am very grateful to my husband Kazi Sarwar Uddin for his constant support and encouragement during my research work. Thanks are also given to all of my friends who are always appreciating me to doing this work specially Sumaiya, Sharna, Rosy, Sifat and Bidhu. Thanks to Nijhu for helping me to prepare my presentation and poster. I am specially thankful to my friend Nayan who is very important to reach my goal.

The Author

Mahjabin Taskin

ABSTRACT

Diluted magnetic semiconductors (DMSs) have been extensively studied due to their great importance in spintronics devices. Among the family of DMSs, wide bandgap Zinc oxide (ZnO)-based DMS is rather significant as their potential in practical applications in opto-electronic device. Cobalt (Co) doped ZnO films were synthesized from the precursors $Zn(CH_3COO)_2.2H_2O$ and $Co(CH_3COO)_2.4H_2O$ by using a "Spray Pyrolysis Deposition" technique at 573 K substrate temperature containing 0.00, 0.05, 0.15, 0.25 and 0.35% Co concentrations. The surface morphological, structural, electrical and optical properties of the as-deposited ZnO films have been investigated as a function of Co-doping level. The thickness of the films was estimated by Fizeau fringes interference method which varied from 190 to 210 nm.

The scanning electron microscopy (SEM) micrographs of as-deposited films show uniform surface and deposition covers the substrate well. Nanofibers are observed around the nucleation centre of as-deposited thin films. Energy Dispersive Analysis of X-ray (EDAX) results clearly showed that the grains are typically comprised of both Zn and O for pure and Zn, O and Co for Co doped films. From EDAX (EDX) data it is found that atomic weight % of Co is increased with the increase of Co concentration in Co doped ZnO films.

X-ray diffraction studies showed the amorphous polycrystalline nature of the films with preferential orientation along the (100), (002), (101), (102), and (110) planes. Structure of the material has been identified as hexagonal wurtzite. The peaks are found to shift from their standard positions in the presence of the Co dopant. There is a deviation in the lattice parameters and it may be happened due to the positioning of dopant atoms into the interstitial lattice sites.

Various optical constants such as absorbance, transmittance, refractive index and dielectric constant of the films have been studied for the as-deposited films are recorded in the wavelength ranges from 300 to 1100 nm. For as-deposited $Zn_{1-x}Co_xO$ films, the band gap varies from 3.2 to 2.7 eV as Co increases. The optical transmittance of the films is found to decrease from 80 % to 70 % (at initial) with the addition of Co doping. Activation energy of $Zn_{1-x}Co_xO$ films is found to decreases with the incorporation of Co in the solution.

CONTENTS

CHAPTER 3

DEPOSITION TECHNIQUES 21-35

CHAPTER 4

EXPERIMENTAL DETAILS 36-60

CHAPTER 6

CONCLUSIONS AND SUGGESTIONS FOR FUTURE WORK

LIST OF FIGURES

LIST OF TABLES

CHAPTER 1
INTRODUCTION

1.1 Introduction

Modern day materials science depends largely on semiconductors which may be elemental systems such as silicon (Si) and germanium (Ge), or compound semiconductors such as gallium arsenide (GaAs), zinc oxide (ZnO) and indium phosphide (InP), or alloys such as silicon-germanium (Si-Ge) or aluminium gallium arsenide. This large family also consists of a smaller sub-set of wide band gap semiconductors (band gap ~ 2 to 3.5 eV) which have electronic band gaps larger than 1.7 eV. Wide band gap materials are often utilized in applications in which high-temperature operation is important. One of the most important II-VI wide band gap semiconductors, which is a hot topic of research in the 21st century is ZnO. ZnO is one of the most important materials that we come across in our day-to-day lives. ZnO transparent conducting oxide is one of the most promising material in many applications and commercial devices due to its unique properties, such as low resistivity and high transmittance in the visible solar region [1] , the material is composed of cheap and abundant elements, and is readily produced for large scale coatings, it can be used in photoconducting , piezoelectric and optical wave guide material[2], so ZnO is a good candidate for many device applications, such as transparent electrode, flat panel display, organic light emitting diode, solar cells, field emission device, sensors, ultrasonic oscillators, transducers, photoprotective coating, surface acoustic wave device and laser diodes [3-13].

Recently, theoretical works have predicted that ZnO based semiconductors can present ferromagnetic behavior at room temperature when doped with transition metals such as cobalt (Co) [14].This makes these systems very attractive for both fundamental and technological point of view.

Impurity doped ZnO thin films have been prepared by various techniques including, pulsed laser deposition, dc reactive magnetron sputtering, atomic layer deposition, sol–gel spin coating, radio frequency magnetron sputtering, metal orgainc chemical vapor deposition and chemical spray pyrolysis [15-21].

In this work we report on the growth of Co doped ZnO thin films on glass substrate by spray pyrolysis and the influence of Co doping percentages on the structural, optical and electrical properties of ZnO thin films.

1.2 Application of Thin Films

Thin films are deposited onto bulk materials (substrate) to achieve properties unattainable or not easily attainable in the substrates alone. Table 1.1 divides these properties into five basic categories and gives examples of typical applications within each category.

Table 1.1: Thin Film Applications

Thin-film Property category	**Typical applications**
Optical	Reflective/antireflective coatings, interference filters, decoration (color, luster), memory discs (CDs), waveguides and static-free coatings.
Electrical	Insulation, conduction, semiconductor devices, piezoelectric drivers, transparent electrodes in flat panel displays, electrochromic devices and transparent semiconducting device and photovoltaic cells etc.
Magnetic	Memory discs
Chemical	Barriers to diffusion or alloying, protection against oxidation or corrosion, gas/liquid sensors etc.
Mechanical	Tribological (wear-resistant) coatings, hardness, adhesion, micromechanics.
Thermal	Barrier layers, Heat sink

1.3 Diluted Magnetic Semiconductor

Diluted magnetic semiconductors (DMS) are semiconductors in which a fraction of the host cations can be substitutionally replaced by magnetic ions or appropriate rare earths, combining the two interesting properties: semiconducting and magnetic. Such a compound Fig 1.1 (b) is an alloy between a non-magnetic semiconductor Fig 1.1 (c) and

a magnetic element Fig 1.1 (a). Transition metals (TMs) that have partially filled d states (Sc, Ti, V, Cr, Mn, Fe, Co, Ni and Cu) and rare earth elements (e.g. Eu, Gd, Er), which have partially filled f states, have been as magnetic atoms in DMS. The partially filled d states or f states contain unpaired electrons, in terms of their spin, which are responsible for them to exhibit magnetic behavior.

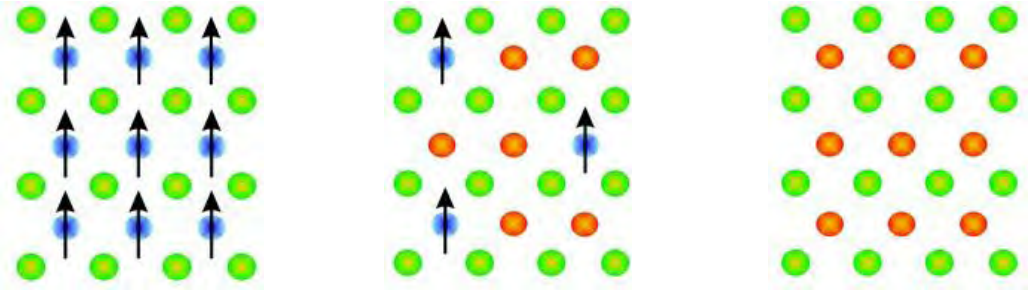

(a) **(b)** **(c)**

Figure 1.1: The different types of semiconductors: (a) a magnetic semiconductor, (b) a DMS and (c) a non-magnetic semiconductor

1.4 Importance of Diluted Magnetic Semiconductor:

Magnetic and semiconductor materials, respectively, have been extensively investigated and demonstrate significant results and applications in scientific and industrial categories in the past years. The spin property of electronics has been successfully utilized to achieve useful magnetic devices, such as magnetic sensors, Magnetoresistance (MR) read-heads and magnetic and magneto-optical recording elements. On the other hand, the semiconductor industry has used another property, charge, of electrons to fabricate a plenty of electronic devices, like integrated circuits (ICs), transistor, laser and light emitting diode (LED) devices, and has significantly promoted the development of computer and communication. With the development of semiconductor materials, advanced devices have the improving properties of high integrated density, high signal processing speed and good reliability. The operation principle of ICs is related to the control of carriers with the application of electric field, based on the charge property of carriers. In order to explore higher performance, the size of semiconductor devices has to be decreased to submicro-or nano-size. The effects of exchange interaction of carriers can become a more predominant factor influencing the properties of devices. Therefore, the use of both charge and spin properties may explore

advanced spin-dependent electronic (spintronics) devices [22]. In this, the spin of electrons that carries the information can be used as an added degree of freedom in novel electronic devices. Scientists have proposed the miniature of numarious spintronic devices, such as the magnetoresistive random access memory (MRAM), spin field effect transistor (Spin-FET), spin light emitting diode (Spin-LED), optical isolator and quantum computer. Therefore, the integration of magnetism and electronics to explore advanced spintronic devices is a very important research and application topic.

1.5 **Properties of ZnO**

The standard values relating to the physical properties of ZnO are mentioned below:

(i) Other Names: Zinc white, Calamine.

(ii) Molecular Formula: ZnO.

(iii) Inorganic Molar Mass: 81.408 g/mol.

(iv) Appearance: white powder.

(v) Density: 5.606 g/cm^3.

(vi) Melting point: 1975 °C.

(vii) Boiling point: 2360 °C.

(viii) Band gap energy: 3.3 eV (direct).

(ix) Exciton binding energy: 60 MeV.

(x) Crystal structure: Hexagonal wurtzite.

(xi) Lattice constant: a=3.249Å & c=5.206Å.

(xii) Semiconductor type: n-type.

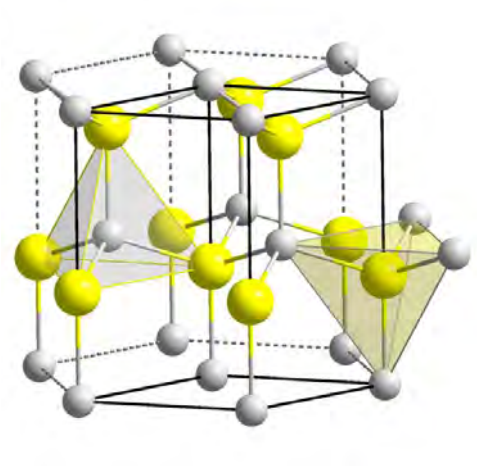

Figure 1.2: Crystal structure of ZnO

1.6 Information about Cobalt

The standard values relating to the physical properties of cobalt are mentioned below:

(i) Molecular Formula: Co.

(ii) Physical state: Solid.

(iii) Melting point: 1495 °C.

(iv) Boiling point: 2870 °C.

(v) Ionic radius: 0.58 Å.

(vi) Electron work function: 5 eV.

(vii) Electron configuration: $1s^2\ 2s^2\ 2p^6\ 3s^2\ 3p^6\ 3d^7$.

(viii) Crystal structure: Hexagonal.

(ix) Type of metal: Transition metal.

1.7 Brief Review of ZnO and $Zn_{1-x}Co_xO$ Thin Films

Studenikin et.al. [23] studied the optical and electrical properties of undoped ZnO films grown by spray pyrolysis of zinc nitrate solution. They deposited undoped ZnO films by spray pyrolysis using aqueous zinc nitrate solution at different substrate temperatures. The effect of the growth temperature on the structural, optical, electrical, and relaxation properties has been studied. It was found that there was a critical temperature T_c=180° C below which the thermal decomposition to ZnO did not occur or was incomplete. Films grown above T_c showed strong preferred orientation of polycrystals along the c-axis, while the films grown at T_c or below showed a powder-like, non-oriented polycrystalline structure when they were converted after wards to zinc oxide by annealing. A slight increase of the optical band gap was observed for as-prepared films as the substrate temperature was decreased near the critical temperature. After anneling they find the band gap as 3.30 eV. After illumination, the steady-state photoconductivity decayed very slowly with a time constant of about a week for as grown samples. The steady-state photoconductivity in the daylight was very close to saturation. Steady state photoconductivity in the daylight can be as much as four orders in magnitude larger than the dark value. Annealing in nitrogen at 400° c brought all samples to the same conductivity of 1023 Vcm^{-2} in daylight and 1024 Vcm^{-2} in the dark. The photoconductivity transients were complicated and changed from a power law to

multi exponential time dependence after annealing. The data are discussed on the basis of model in which hole traps located at the grain boundaries play the major role.

Islam et al [24] deposited good homogeneous and stoichiometric ZnO nanofiber thin films onto cleaned glass substrate by a simple spray pyrolysis technique under atmospheric pressure using zinc acetate precursor at temperature 200 °C. They obtained films of various thicknesses by varying the deposition time, while all other deposition parameters such as spray rate, carrier gas pressure and distance between spray nozzle to substrate were kept constant. They studied surface morphology and optical properties of the as deposited thin films by Scanning Electron Microscopy (SEM) attached with an EDX and UV visible spectroscopy. From EDX data, atomic weight % of Zinc and Oxygen were found to be 49.22 % and 49.62 % respectively. The SEM micrograph of the film showed uniform deposition and scattered nano fiber around the nucleation centers. The optical band gap of the ZnO thin films was found to be in the range 3.3 to 3.4 eV and the band gap decreased with thickness of the film. Optical constants such as refractive index, extinction coefficient, real and imaginary parts of dielelectric constants evaluated from reflectance and absorbance spectra.

Sahay et al [25] were prepared ZnO thin films by spray pyrolytic decomposition of zinc acetate onto a galss substrate. These films were analyzed for the optical and electrical properties. Optical studies show that in these films the electronic transition is of the direct transition type. The optical energy gap for the film of different thicknesses is estimated to be in the range 2.98-3.09 eV. Electrical studies indicate that the films exhibit thermally activated electronic conduction and the activation energies are found to be dependent on the film thickness. The complex impedance measurement was carried out over a wide range of frequencies at room temperature (300° C). All the impedance spectra contain only a single arc, but the arc has a non-zero intersection with the real axis in the high frequency region. Also, the arc has its centre lying below with the real axis which indicates the multirelaxation behavior of the films.

Ueda et al [26] formed 3d-transition-metal-doped ZnO films on sapphire substrates using a pulsed laser deposition technique, and there magnetic and electric

properties are examined. The Co doped ZnO films showed the maximum solubility limits. Some of the Co-doped ZnO films exhibit ferromagnetic behaviors with the Curie temperature higher than room temperature. The magnetic properties of Co-doped ZnO films depend on the concentration of Co ions and carriers.

Park et al [27] was investigated the origin of ferromagnetism in ZnO based systems using Co doped ZnO thin films as prototypical examples of II-VI based diluted magnetic semiconductors. In spite of the atomic scale dissolution of Co ions in wurtzite ZnO, both the magnetization-temperature curve and the magnetization-field curve demonstrated that $Zn_{1-x}Co_x$ thin films were paramagnetic for $x \leq 0.12$. On the other hand, $Zn_{1-x}Co_xO$ films with x greater than 0.12 were characterized by the Co-metal clustering and apparently showed room temperature ferromagnetism. The discrepancy between the zero-field cooling curves further indicates the Co-doped ZnO films (for $x \geq 0.12$) are superparamagnetic and the observed ferromagnetism originates from the nanometer-sized Co clusters.

Bhatti et al [28] deposited Cobalt doped zinc oxide thin films usuing spray prolysis method. They found single phasic films exhibited [100] preferential texture and small decrease in the lattice parameter on cobalt substitution. The films having different Co concentration have almost similar surface morphology and microstructure. These $Zn_{1-x}Co_xO$ ($x \leq 0.10$) thin films distinctly showed ferromagnetic character at room temperature. The optical transmission measured of these films clearly proved that in these films Co substitutes for Zn^{2+} and exists in +2state. Based on the optical structural and magnetic measurements, the possibility of occurrence of ferromagnetic ordering due to cobalt clustering is ruled out in these spray pyrolyzed films. A correlation of the observed ferromagnetic behavior in these $Zn_{1-x}Co_xO$ films with structural change resulting from the addition of Co is presented in this paper.

Subramanian et al [29] reported structural, optical and magnetization properties of cobalt-doped zinc oxide thin films prepared on Si substrates by spray pyrolysis technique. Grazing angle X-ray diffraction measurements confirms the wurtzite structure of $Zn_{1-x}Co_xO$ films. Optical reflectance measurements reveal that the optical

gap energy increases with increasing Co concentration indicating that Co^{2+} ions in the replaces Zn^{2+} ions in the ZnO lattice. Hysteresis measurements demonstrates that the Co doped ZnO films are magnetically anisotropic and they exhibit intrinsic ferromagnetic behaviour at room temperature. Higher magnetization in 3kOe values are observed for a field applied perpendicular to the sample surface compared to in plane direction.

1.8 Objectives with specific aims

The spray pyrolysis method for the deposition of thin solid films is a good method for the preparation of thin films suitable for scientific studies and for many applications in technology and industry. This method was used for the preparation of thin films of the important semiconductors II-VI.

In recent years the II-VI compound semiconductors thin films have varieties of applications as electroluminescent, photoluminescent and photoconductor devices and especially in photovoltaic cells.

The knowledge of optical constants of materials is frequently of great interest in the design and analysis of materials to be used in optoelectronics. Moreover, optical measurements are extensively used for characterization of composition and quality of the materials. So, it is essential to have an insight into the optical properties, which include the optical band gap, reflectivity, absorption coefficient, the dielectric constant and the refractive index as a prerequisite in using the suitable material for device applications.

Although much work has been done on the electronic and optical properties of ZnO thin films but scarce information is available on the ternary $Zn_{1-x}Co_xO$ system. The reason is the possibility of tailoring its semiconductor properties between the values corresponding to the pure binaries. This fact allows us to adapt the material properties to the device requirements.

The focus of this work is to prepare $Zn_{1-x}Co_xO$ thin film on glass substrate by spray pyrolysis deposition and investigation of various properties such as morphological, structural, optical and electrical properties of the films. From technological point of interest, ternary alloys from II-IV compound semiconductor $Zn_{1-x}Co_xO$ is deposited onto

the glass substrate and its structural, optical and electrical properties is studied in details. Based on these research challenges, the objectives of this work are as follows:

(a) Surface morphology of the deposited films is studied by optical microscope.

(b) The elemental compositions are estimated by Energy Dispersive Analysis of X-ray (EDX).

(c) The crystal structure of the deposited films are analyzed by XRD.

(d) The optical constants e. g. absorbance, transmittance, optical band gap, extinction coefficient, refractive index, dielectric constants, dielectric loss, optical conductivity etc. are determined by UV visible spectroscopy in the wavelength range 300 nm ~ 1100 nm.

(e) Electrical conductivity measurement is carried out by van-der Pauw four probe method.

(f) Activation energy of $Zn_{1-x}Co_xO$ films are determined.

References:

[1] Minami, T., "New n-Type Transparent Conducting Oxides", Mater. Res. Soc., Vol-25, No.08, pp. 38-44, 2000.

[2] Moustaghfir, A., Tomasella, E., Ben, A. S., Jacquet, M., Cellier J., and Sauvage, T., "Structural and Optical Studies of ZnO Thin Films Deposited by r.f. Magnetron Sputtering: Influence of Annealing", Surf. and Coat. Technol., Vol-174-175, pp 193-196, 2003.

[3] Owen, J., Son, M. S., Yoo, K. H., Ahn, B. D. and Lee, S.Y., "Organic Photovoltaic Devices with Ga-doped ZnO Electrode" Appl. Phys. Lett., Vol-90, No. 3, pp 033512-033515, 2007.

[4] Oh, B. Y., Teong, M. C., Moon, T. H., Lee, W., Myoung, J. M., .Hwang, J. Y and Seo, D. S., "Transparent Conductive Al-doped ZnO Films for Liquid Crystal Displays", Appl. Phys., Vol-99, No. 124505, pp 2206417-2206420, 2006.

[5] Fay, S., Kroll, V., Bucher, C., Valets – Sauvian, E. and Shah, A., "Low Pressure Chemical Vapour Deposition of ZnO Layers for Thin Film Solar Cells: Temperature-Induced Morphological Changes", Sol. Energy Mater., Vol-86, No. 3, pp 385-397, 2005.

[6] Nomura, K., Ohta, H., Ueda, K., Kamiya, T., Hirano, M. and Hosono, H., "Thin Film Transistor Fabricated in Single-Crystalline Transparent Oxide Semiconductor", Sci, Vol-300, No. 5623, pp 1269-1272, 2003.

[7] Wang, W., Zhang, G., Yu, L., Bai, X., Zhang, Z. and Zhao, X., "Field Emission Properties of Zinc Oxide Nanowires Fabricated by Thermal Evaporation", Physica E, Vol-36, No. 1, pp 86-91, 2007.

[8] Breivik, T. H., Diplas, S., Ulyashin, A. G., Gunnaes, A. E., Olaisen, B. R., Wright, D. N., Hott, A., and Olsen, A., "Nano-Structural Properties of ZnO Films for Si Based Heterojunction Solar Cells", Thin Solid Films, Vol-515, No. 24, pp 8479-8483, 2007.

[9] Park Y. R., Nam E. and Kim Y. S., "Electrical Properties of Sputtered ZnO Films with Nitrogen and Phosphorous Co-doping", Appl. Phys., Vol-14, No. 4, pp 471-475, 2008.

[10] Xu, D., Deng, Z., Xu, Y., Xiao, J., Liang, C., Pci, Z., and San, C., "An Anode with Aluminum Doped on Zinc Oxide Thin Films for Organic Light Emitting Devices", Phys. Lett., Vol-346, No. 1-3, pp 148-152, 2005.

[11] Ruske, F., Jacobs, C., Sittinger, V., Szyszka, B. and Werner, W., "Large Area ZnO:Al Films with Tailored Light Scattering Properties for Photovoltaic Applications" Thin Solid Films, Vol-515, No.24, pp 8695-8698, 2007.

[12] Tanaka, H., Shimakawa, T., Miyata, T., Sato, H. and Minami, T., "Effect of AZO Film Deposition Conditions on the Photovoltaic Properties of AZO–Cu_2O Heterojunctions", Appl. Surf. Sci., Vol-244, No. 1-4, pp 568-572, 2005.

[13] Fadi, A. A. E., Maghraby, E. M. E., and Mohamed, G. A., "Influence of Gamma Radiation on the Absorption Spectra and Optical Energy Gap of Li- doped ZnO Thin Films", Cryst. Res. Technol., Vol-39, No. 2 pp 143-150, 2004.

[14] Ueda K., Tabata H. and Kawai T., "Magnetic and Electric Properties of Transition-Metal-doped ZnO Films", Appl. Phys. Lett., Vol-79, No. 988, pp 1384478-1384481, 2001.

[15] Lin J. M., Zhang Y. Z., Ye Z. Z., Gu X. Q., Pan X. H., Yang Y. F., Lu J. G., He H. P. and Zhao B. H., "Nb-doped ZnO Transparent Conducting Films Fabricated by Pulsed Laser Deposition", Appl. Surf. Sci., Vol-255, No. 13-14, pp 6460-6463, 2009.

[16] Hong, R., Huang, J., He, H., Fan, Z. and Shao, J., "Influence of Different Post-Treatments on the Structure and Optical Properties of Zinc Oxide Thin Films", Appl. Surf. Sci., Vol-242, No. 3-4, pp 346-352, 2005.

[17] Lim, J., and Lee, C., "Dependence of the Structural and Optical Properties of ZnO Thin Films on the Substrate Temperature in Atomic Layer Deposition and Post-Annealing", Allo and Compoun, Vol-449, No. 1-2, pp 371-374, 2008.

[18] Srinivasan, G., Kumar, R. R. T., and Kumar, J., "Influence of Al dopant on Microstructure and Optical Properties of ZnO Thin Films Prepared by Sol–gel Spin Coating Method" Opti Mater, Vol-30, No. 2, pp 314-317, 2007.

[19] Huang, B., Li, J., Wu, Y., Guo, D. and Wu, S., "Optical Constants of Transparent ZnO Films by RF Magnetron Sputtering", Mater Lett, Vol-62, No. 8-9, pp 1316-1318, 2008.

[20] Kong, B. H., Mohanta, S. K., Kim, D. C., and Cho, H. K., "Optical and Structural Properties of ZnO Thin Films Grown on Various Substrates by Metalorganic Chemical Vapor Deposition", Condens Matt, Vol-401-402, No. 15, pp 399-403, 2007.

[21] Caglar, Y., Ilican, S., Caglar, M., and Yakaphanoglu, F., "Effects of In, Al and Sn Dopants on The Structural and Optical Properties of ZnO Thin Films", Molecul and Biomolecul Spectro, Vol-67, pp 1113-1119, 2007.

[22] Wolf, S. A., Awschalom, D. D. , Buhrman, R. A., Dauhhton, J. M., von Molnar, S., Roukes, M. L., Chtchelkanova, A. Y., Treger, D. M., "Spintronics: A Spin-Based Electronics Vision for the Future", Sci., Vol-294, No. 5546, pp 1488-1495, 2001.

[23] Studenikin, S. A., Golego, N., and Cocivera, M., "Optical and Electrical Properties of Undoped ZnO Films Grown by Spray Pyrolysis of Zinc Nitrate Solution", App. Phys., Vol-83, No. 4, pp 2104-2111, 1998.

[24] Islam, M. R., and Podder, J. "Optical Properties of ZnO Nano Fiber Thin Films Grown by Spray Pyrolysis of Zinc Acetate Precursor", Cryst. Res. Technol., Vol-44, No. 3, pp 286-292, 2009.

[25] Sahay, P. P., Tewari, S., and Nath, R. K., "Optical and Electrical Studies on Spray Deposited ZnO Thin Films", Cryst. Res. Technol., Vol-42, No. 7, pp 723-729, 2007.

[26] Ueda, K., Tabata, H, and Kawai, T., "Magnetic and Electric Properties of Transition-Metal-doped ZnO films", Appl. Phys. Lett., Vol-79, No. 7, pp 988-990, 2001.

[27] Park, J. H., Kim, M. G., Jang, H. M., and Ryu, S., "Co-Metal Clustering as the Origin of Ferromagnetism in Co-doped ZnO Thin Films", App. Phys. Lett., Vol-84, No. 8, pp 1338-1340, 2004.

[28] Bhatti, K. P., Malik, V. K., and Chaudhary, S., "Cobalt Substituted ZnO Thin Films: a Potential Candidate for Spintronics', Mater. Sci. Elec. Vol-10, No. 19, pp 849-854, 2007.

[29] Subramanian, M. Tanemura, M., Hihara, T., Ganesan, V., Soga, T., and Jimbo, T., "Magnetic Anisotropy in Nanocrystalline Co-doped ZnO", Che. Phys. Lett., No. 487, pp 97-100, 2010.

Chapter 2

Theoretical Background

2.1 Introduction

Spray pyrolysis technique involves spraying of an ionic solution, usually aqueous, containing soluble salts of the constituent cluster of atoms of the desired compound onto heated substrates. Hydrolysis and pyrolysis are the main chemical reactions involved in the process. In this technique, the chemicals vaporized and react on the substrate surface after reaching on it. In principle spray pyrolysis technique is very simple and is suitable for industrial applications. The apparatus needed to carry out the chemical spray process consists of a optimizer the spray solution and a substrate heater.

2.2 Formation Stages of Thin Films

There are three mechanisms of thin film condensation can be distinguished, depending on the strength of interaction between the atoms of the growing film and between the atoms of the film and substrate: These are

(a) Layer-by-layer growth (Frank - van der Merwe mechanism) –for the chemical entities more strongly bound to the substrate than to each other. During the process, the small stable nuclei extend, growing in two dimensions, forming planar sheets. A first monolayer forms, and further layers cover, but the bonds between atoms are less strong.

(b) Island growth (Volmer – Weber mechanism) – specific for the chemical entities which are bound to each other more strongly than to the substrate. During the growth small stable clusters nucleate on the surface and then grow in the three dimension, forming islands.

(c) Layer-plus-island growth (Stranski – Krastanow mechanism) – involves an intermediate combination of the previous two models. During the thin film growth, after monolayer(s) formation on the substrate, islands formation occurs, probably as result of the decreased bonding energy of the chemical species to the existing layers.

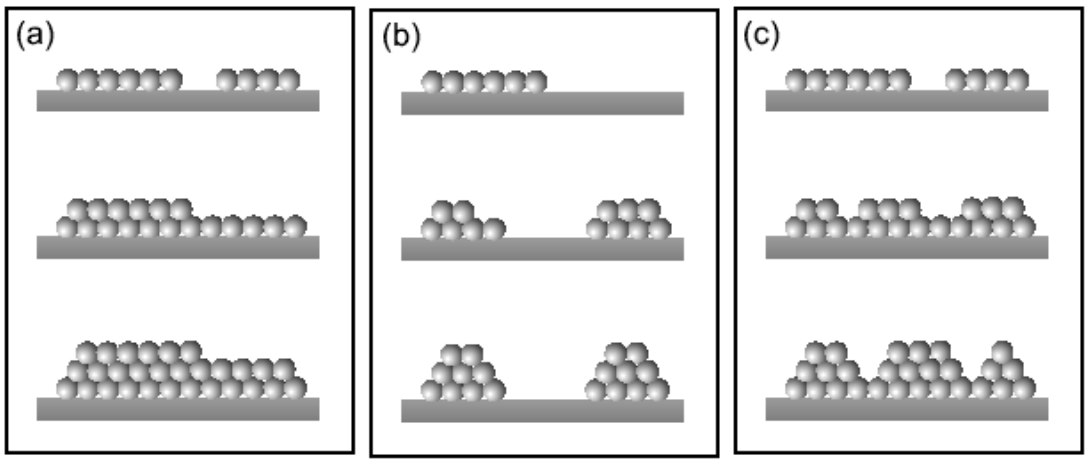

Figure 2.1: (a) Layer-by-layer or **Frank-van der Merwe** mode → 2D islands

(b) Island or **Vollmer-Weber** mode → 3D islands

(c) Layer plus island or **Stranski-Krastanov** mode → 2D layer + 3D islands

In most cases mechanism (b) takes place and a brief description of it is given below. The important processes involved in the formation of thin film are condensation, nucleation and growth on the substrate. Transformation of a substance from its vapour phase to the liquid or solid phase is called condensation, which in this case is initiated by the formation of small clusters or nuclei through combination of several incident atoms adsorbed on the substrate to form finally a coherent film is termed as growth.

2.2.1 Condensation

Thermodynamically, for condensation to occur on a substrate, the partial vapour pressure in the gaseous phase should be equal to or greater than its vapour pressure in the condensed phase at the same temperature. The substrate material is different from the vapour material, so impinging vapour atoms are first adsorbed on the surface of the substrate and condensation is initiated by the formation of small clusters of the adsorbed atoms. These small clusters then act as the initial centers of condensation. The process can be visualized as follows:

The impinging vapour atoms on approaching the substrate surface within a few atomic diameters come under the influence of the field of force of the surface atoms of the

substrate and then several interactions may follow. They are: (1) an impinging atom may be reflected almost instantly retaining most of its kinetic energy, (2) there may be physical adsorption of vapour atoms under influence of Van der Waals force of the substrate atoms, (3) there may be chemical adsorption due to force of the type forming chemical bond between a vapour atom and a substrate atom, (4) impinging atom may form immediate association with other atom or atoms already adsorbed after finite stay time, or it may strike to the surface of the substrate and then migrate literally to join a cluster of adsorbed atoms. Adsorption of incident vapour atom is possible only when there is thermal accommodation with the substrate atoms. If the kinetic energy of an incident atom is less than the energy of desorption, the thermal accommodation takes place by giving up its excess kinetic energy through lattice vibration of the substrate and the atom is adsorbed. Under appropriate conditions, when the rate of adsorption becomes greater than the rate of desorption, the small clusters (consisting of monomers) begin to enlarge, leading to stable nucleation and growth. Several workers [1-2] have studied condensation phenomena experimentally.

2.2.2 Nucleation

Nucleation is the onset of a first-order phase transition by which a metastable phase transforms into a more stable one. Such a phase transition occurs when an initial system initially in equilibrium is destabilized by the change of an external parameter like the temperature or the pressure In the process of depositing thin film on a substrate the first stage is the formation of adsorbed monomers of one or more atoms which in the second phase, under the action force similar to surface tension, or capillarity combine to form small clusters. These clusters like the monomers are not stable and likely to be desorbed unless they attain a certain critical size corresponding to a particular temperature of the substrate. On reaching a critical size, they continue to grow forming stable condensates. Several theories are proposed to explain the formation of critical clusters leading to the growth of stable condensates. Out of all these, the two principal theories are the capillarity model and the atomistic model [3]. Capillarity model predicts that the free energy of a cluster passes through a maximum as it increases in size, and this maximum of free energy corresponds to the critical size of the cluster, which becomes stable above this critical size, but may re-evaporate below this critical size. This is similar to the process of formation of liquid droplets from vapours as explained

by classical capillarity theory. Thus in order to condense a permanent deposit, aggregates of critical size or larger have to be created first. Critical nuclei can grow to super critical size either by direct incorporation of impinging atoms from the gaseous phase or by incorporation of the adsorbed monomers diffusing over the surface of the substrate. In the latter process, the rate at which the critical nuclei grow is given by the initial number of nuclei per unit area of the substrate and the rate at which the adsorbed monomers diffuse to join them. In this case emphasis is given not on the free energy but on the dissociation energy of a critical cluster under specific condition of super saturation, and then the rate of nucleation corresponding to such a critical cluster is computed, leading to an expression involving parameters like number of monomers in the critical cluster, activation energy for desorption, activation energy for diffusion, substrate temperature, etc. The prediction of the nucleation theories, in general have been found to be true even through relatively crude experimentations. However, the observations have revealed distinct stages of film growth leading to a continuous film. There are two types of nucleation occur during the formation of a film;

i) Homogeneous nucleation: The total free energy is used in the formation of a cluster of adatoms.

ii) Heterogeneous nucleation: Particular shapes of clusters are formed by collisions of atoms on the substrate surface, and in the vapor phase its super saturation is sufficiently high. [4].They initially developed within increase in free energy until a critical size is reached above which growth continues with a decrease in free energy. In atomistic theory, in low substrate temperature or very high super saturations, the critical nucleus may be a single atom which will form a pair with another atom by random occurrence to become a stable cluster and grow spontaneously.

2.2.3 Growth

Growth is the final and completion stage of thin film formation. The process of enlargement of the nuclei to finally form a coherent is termed as growth. The growth sequence of a film was originally deduced by Andrade from the observed optical transmission behavior of Ag films. This deduction is in remarkable agreement with the electron-microscopic observations first made by Uyeda and later in detailed by Levinstein. The clusters become larger and ultimately continuous film is produced.

Pashley et al. distinguished four stages of the growth process based on the electron microscopic observations.These stages are:

(i) Nucleation and island formation:

The existence of nuclear barriers as predicted by nucleation theories favours the formation of islands in the initial stage of film growth. When the nucleation barrier is large, a few large islands are formed initially, which persist up to relatively high average film thickness, resulting in the formation of a coarse grained film. Under the small nucleation barrier, large number of islands is formed, which becomes continuous at relatively low average film thickness and finer grained film is obtained. The tendency to form an island structure is increased by (1) at high substrate temperature, (2) at low boiling point film material, (3) at low deposition rate, (4) weak binding energy between film material and substrate, (5) a high surface energy of the film material and (6) a low surface energy of the substrate.

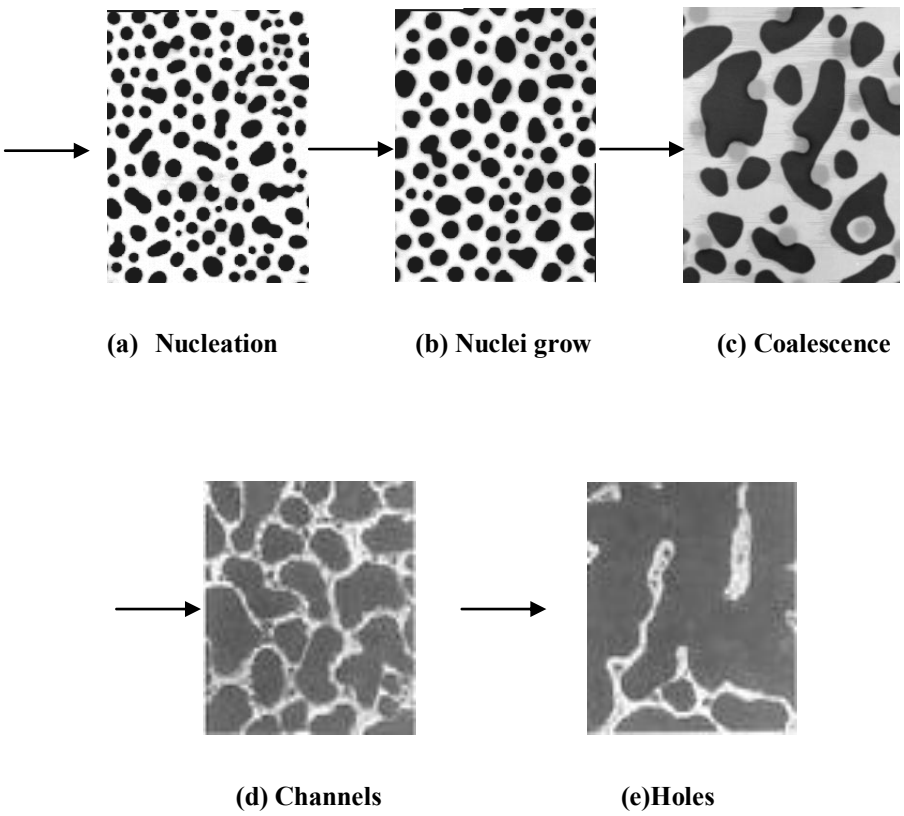

Figure 2.2: Different stages of film growth

(ii) Coalescence of islands:

As the deposition is continued, the islands grow in their sizes and come to each other. The large islands appear to grow by coalescence of smaller islands and the island density decreases monotonically. Surface diffusion is predominant for mass transfer between the islands during coalescence. Shape and area of an island, which has just been formed by coalescence, change during and after coalescence. According to Pashley et al. [5] the driving force for the coalescence process is provided by the change in the surface energy. Fig. 2.3 illustrates the manner of coalescence of two rounded nuclei. The coalescence occurs in less than 0.1s for the small nuclei and is characterized by a decrease in total projected area of the nuclei on the substrate (an increase in their height). In addition, nuclei having well-defined crystallographic shapes before coalescence become rounded during the event [6]. The composite island takes on a crystallographic shape again if left for a sufficiently long time before interacting with its neighbors. The triangular profile of the crystallites is characteristic of the nucleation stage. After coalescence has taken place, the islands assume a more hexagonal profile and are often faulted. A sequence of micrographs illustrating the effects is shown in Fig. 3.7, where islands A and B have formed a compound island which eventually becomes crystallographically shaped.

Figure 2.3: Schematic of shape changes during coalescence

The liquid like character of the coalescence leads to enlargements of the uncovered areas of the substrate, with the result that secondary nuclei form between the islands. This effect becomes noticeable when the primary islands have grown to about 1000 Å and continues until the final hole-free film is formed. The small nuclei surrounding island B are examples of those secondary nuclei. A secondary nucleus grows until it touches a neighbor and if this happens to be a much larger island, the secondary nucleus coalesces very rapidly and becomes completely incorporated in the large island.

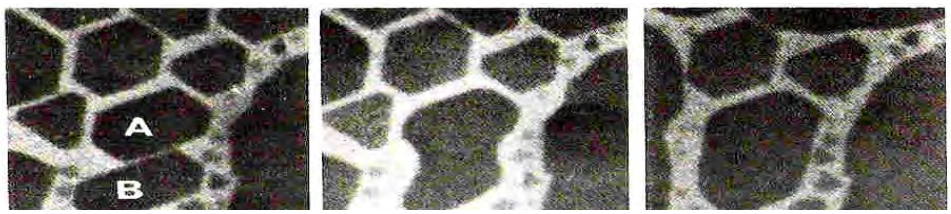

(a) (b) (c)

Figure 2.4: Electron micrograph shows the change in shape of islands during and after coalescence (a) at zero (b) after 1 to 2 sec. (c) after 60 sec.

(iii) Channel formation:

As the islands grow, there is a decreasing tendency for them to become completely rounded after coalescence. Large shape changes still occur, but these confined mainly to the regions in the immediate vicinity of the junction of the islands. Consequently, the islands become elongated and join to form a continuous network structure in which the deposit material is separated by long, irregular, and narrow channels of width 50 to 200 Å. As deposition continues, secondary nucleation occurs in these channels, and the nuclei are incorporated into the bulk of the film as they grow and touch the sides of the channel. At the same time, channels are bridged at some points and fill in rapidly in a liquid like manner.

Eventually, most of the channels are eliminated and the film is continuous but contains many small irregular holes. Secondary nucleation takes place on the substrate within these holes and the growing nuclei are incorporated (in a liquid like manner) into the continuous regions of the deposit. The hole contains many secondary nuclei which coalescence with each other to form secondary islands, which then touch the edge of the hole and coalesce with the main film to leave a clean hole. Further, secondary nuclei then form and the process are repeated until the hole finally fills in.

(iv) Formation of continuous film:

The final stage of film growth is a slow process of filling the empty channels, which requires a considerable amount of deposits. In channel stage large areas are vacated by coalescence. These empty channels are filled by secondary nucleation, growth and coalescence and in this way a continuous film is formed.

References

[1] Palatnik, L. S., and Komnik, Y. F., "The Kinetics of Condensation of Metals in Vacuo", Sov. Phys. Doklady, Vol-4, No. 196, pp 663, 1959.

[2] Lewis, B., and Champbell, D. S., "Nucleation and Initial-Growth Behavior of Thin-Film Deposits", Vac Sci. Technol., Vol-4, No. 5, pp 209, 1967

[3] Neugebaner, C. A., "Hand Book of Thin Film and Technology", Maissel, L. I. and Gang, R., (eds); Mc Graw Hill Com., New York, 1970.

[4] Altiokka, B., Aksay, S., "Optical Properties of $CuInS_2$ Films Produced by Spray Pyrolysis Method", Arts and Sci, Vol-31, pp 27-34, 2005.

[5] Pashley, D. W., Stowell, M. J., Jacobs, M. H., and Law, T. J., Phil. Mag., Vol-10, pp 127, 1964.

[6] Pashley, D. W., and Stowell M. J., in S.S. Breese (Ed.), Proc.5^{th} Intern. Cogner. Electron microscope, P.GGI. Academic Press Inc; New York, 1962.

CHAPTER 3
DEPOSITION TECHNIQUES

3.1 Classification of Deposition Technologies

There are many dozens of deposition technologies for material formation [1]-[4]. Since the concern here is with thin-film deposition methods for forming layers in the thickness range of a few nanometers to about ten micrometers, the task of classifying the technologies are made simpler by limiting the number of technologies to be considered. Basically, thin-film deposition technologies are either purely physical, such as evaporative methods, or purely chemical, such as gas and liquid-phase chemical processes. A considerable number of processes that are based on glow discharges and reactive sputtering combine both physical and chemical reactions; these overlapping processes can be categorized as physical-chemical methods. A classification scheme is presented in Table 1, where there is a group of thin-film deposition technologies according to evaporative glow discharge, gas-phase chemical, and liquid-phase chemical processes.

Table 3.1: Classification of Thin-Film Deposition Technologies

EVAPORATIVE METHODS

• ***Vacuum Evaporation***

Conventional vacuum evaporation
Electron-beam evaporation
Molecular-beam epitaxy (MBE)
Reactive evaporation

GLOW-DISCHARGE PROCESSES

• ***Sputtering***

Diode sputtering
Reactive sputtering
Bias sputtering (ion plating)
Magnetron sputtering
Ion beam deposition
Ion beam sputter deposition
Reactive ion plating
Cluster beam deposition (CBD)

• ***Plasma Processes***

Plasma-enhanced CVD
Plasma oxidation
Plasma anodization
Plasma polymerization
Plasma nitridation
Plasma reduction
Microwave ECR plasma CVD
Cathodic arc deposition

GAS-PHASE CHEMICAL PROCESSES

• ***Chemical Vapor Deposition (CVD)***	• ***Thermal Forming Processes***
CVD epitaxy	Thermal oxidation
Atmospheric-pressure CVD (APCVD)	Thermal nitridation
Low-pressure CVD (LPCVD)	Thermal polymerization
Metalorgainc CVD (MOCVD)	
Photo-enhanced CVD (PECVD)	
Laser-induced CVD (PCVD)	
Electron-enhanced CVD	Ion implantation

LIQUID-PHASE CHEMICAL TECHNIQUES

• ***Electro Processes***	• ***Mechanical Techniques***
Electroplating	Spary pyrolysis
Electroless plating	Spray-on techniques
Electrolytic anodization	Spin-on techniques
Chemical reduction plating	
Chemical displacement plating	
Electrophoretic deposition	Liquid phase epitaxy

3.2 Overview of various thin-film deposition technologies

The following is a brief description of the principles, salient features, and applications of the more important technologies for thin-film deposition and formation categorized in Table 1.

3.2.1 Evaporative Technology

Although one of the oldest techniques used for depositing thin films, thermal evaporation or vacuum evaporation, is still widely used in the laboratory and in industry for depositing metal and metal alloys [1, 3]. The following sequential basic steps take place: (*i*) a vapor is generated by boiling or subliming a source material, (*ii*) the vapor is transported from the source to the substrate, and (*iii*) the vapor is condensed to a solid film on the substrate surface. Although deceptively simple in principle, the skilled practitioner must be well versed in vacuum physics, material science, mechanical and electrical engineering, as well as in elements of thermodynamics, kinetic theory of gases, surface mobility, and

condensation phenomena. Evaporants cover an extraordinary range of varying chemical reactivity and vapor pressures. This variety leads to a large diversity of source components including resistance-heated filaments, electron beams; crucibles heated by conduction, radiation, or rf-induction; arcs, exploding wires, and lasers. Additional complications include source-container interactions, requirements for high vacuum, precise substrate motion (to ensure uniformity) and the need for process monitoring and control.

3.2.1.1 Molecular Beam Epitaxy (MBE)

Molecular beam epitaxy is a technique for epitaxial growth via the interaction of one or several molecular or atomic beams that occurs on a surface of a heated crystalline substrate. In Figure 8 scheme of a typical MBE system is shown. The substrate, on which the heterostructure to be grown, is placed on a sample holder which is heated to the necessary temperature and, when needed, continuously rotated to improve the growth homogeneity [5]. The growth in the MBE requires ultra high-vacuum (UHV), typically 10^{-6}–10^{-4} mbar during growth. After outgasing under such a high vacuum, O_2, CO_2, H_2O, and N_2 contamination on the growing surface can be neglected. The typical growth conditions make possible to reduce the rate down to nm/sec, so that precise control of the growth thickness is possible – this is a great advantage [6]. Although simple in principle MBE is not simple in practice. The substrates are carefully prepared and cleaned with extreme purity if their properties are not to be spoil by contamination. This in turn requires pure starting materials, only ultra pure sources are used. The background pressure in the evaporator must be kept low to reduce contamination. The flux of effusion cell must be uniform across the substrate. The reaction chamber is evacuated to $<10^{-8}$ mbar and the walls of the chamber cooled with liquid nitrogen. Even so the highest mobility layers are only grown after an extended run when the machinary has completely cleaned it. An important feature of MBE is that it takes place in UHV, which means that some diagnostic techniques can be used to monitor the growth. The most common is reflected high-energy electron diffraction (RHEED). The surface changes in a periodic way as each monolayer is grown and this can be seen in the intensity and pattern of the RHEED signal. Thus growth can be controlled precisely at the monolayer level. During the MBE process, growth can be monitored in situ by a number of methods: RHEED, low energy electron diffraction (LEED); Auger electron spectroscopy (AES), modulated beam mass spectrometry (MBMS).

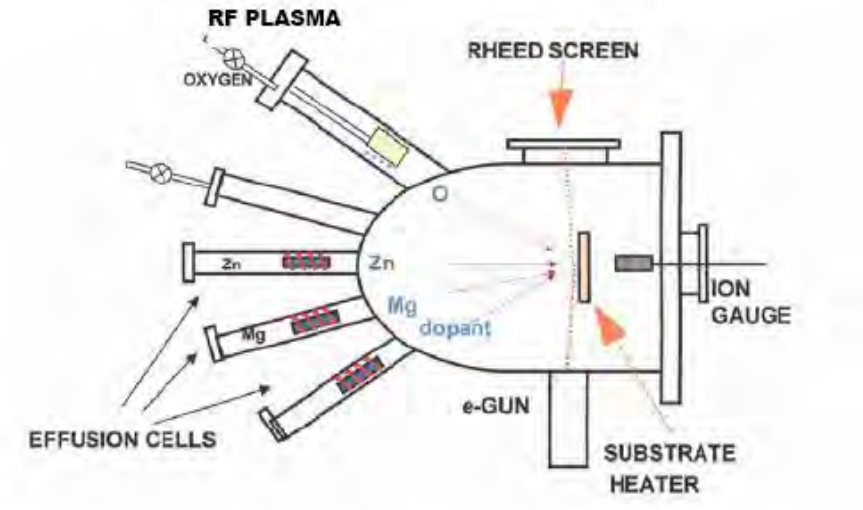

Figure 3.1: Schematic of MBE system

Advantages of MBE: (1) excellent interface and surface morphology, (2) abrupt hetero-junctions, (3) growth of complex heterostructures with many different layers, (4) in-situ characterization techniques (RHEED), (5) high purity starting materials, easy chemistry, (6) safer for some material growth than CVD (As and Se exceptions) (7) low growth temperature.

Disadvantages of MBE: (1) graded interfaces, (2) structures with many different compositions (only 4 metal sources in most machines), (3) run-to-run reproducibility, (4) low growth rates, (5) high temperatures are hardly reached, (6) very difficult and costly to implement and maintain.

3.2.2 Glow-Discharge Technology

The electrode and gas-phase phenomena in various kinds of glow discharges (especially rf discharges) represent a rich source of processes used to deposit and etch thin films. Creative exploitation of these phenomena has resulted in the development of many useful processes for film deposition (as well as etching), as listed in Table 1.

3.2.2.1 Sputtering

The most basic and well-known of these processes is sputtering, the ejection of surface atoms from an electrode surface by momentum transfer from bombarding ions to

surface atoms. From this definition, sputtering is clearly an etching process, and is, in fact, used as such for surface cleaning and for pattern delineation. Since sputtering produces a vapor of electrode material, it is also (and more frequently) used as a method of film deposition similar to evaporative deposition. Sputter deposition has become a generic name for a variety of processes.

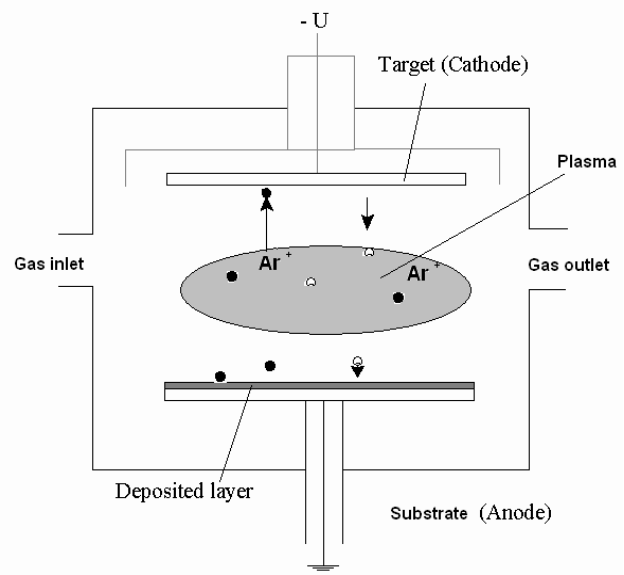

Figure 3.2: Schematic representation of sputter deposition system

Magnetron Sputtering

The planar magnetron sputtering source was invented at the beginning of the seventies [7]. This technique is now one of the most versatile used for the deposition of transparent conducting oxides (TCO). The basic feature of a magnetron discharge is the confinement of the plasma in front of the target (cathode). This is achieved by the combination of electric and magnetic fields [8]. The magnetic field strength is adjusted in such a way (about 50 to 200 mT) that the electrons are significantly influenced by the magnetic field while the ions are not. The electrons perform cycloidal orbits in the crossed electric and magnetic fields, leading to very high ionization efficiency. Therefore, magnetron discharges can be sustained at much lower pressures ($<10^{-4}$ Torr) and/or higher current densities than the glow discharges without magnetic assistance.

In standard sputtering processes there are usually two modes of powering the magnetron sputtering system. These two modes are direct current (DC) magnetron sputtering or by radio frequency (RF) magnetron sputtering. In DC magnetron sputtering, a direct voltage is applied between the cathode and anode. This method works well with conductive targets (zinc,

molybdenum, silver, aluminum, etc). The second method involves the use of a radio frequency source with atypical frequency of 13.56 MHz. This method is preferred for both conductive as well as non-conductive targets (ceramic targets). This mode was mainly employed in the present study. A schematic diagram of both magnetron sputtering discharge configurations is shown in the Figure 3.3. The external discharge parameters such as working pressure, discharge power, design of the magnetic field (i.e. balanced or unbalanced magnetrons) and the excitation mode (dc or rf) influence the potential distribution and hence the particle energies.

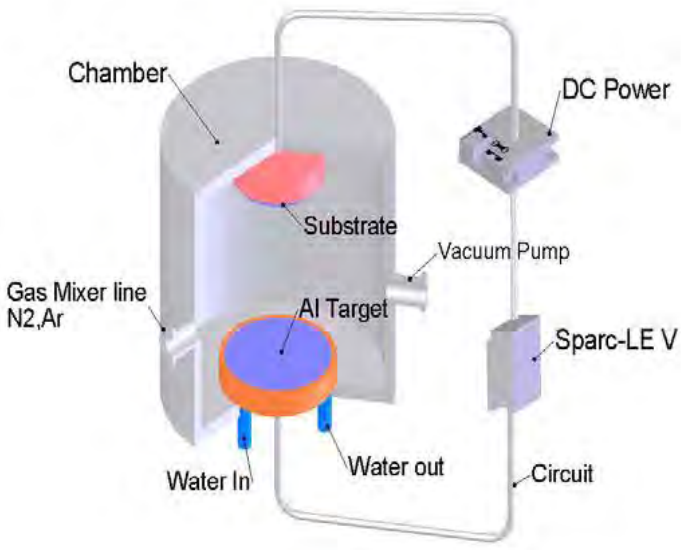

Figure 3.3: Schematic diagram of a magnetron sputtering configuration for simultaneous rf and dc excitation

3.2.2.2 Plasma Processes.

The fact that some chemical reactions are accelerated at a given temperature in the presence of energetic reactive-ion bombardment is the basis of processes for surface treatments such as plasma oxidation, plasma nitriding, and plasma carburizing. A metal to be oxidized, nitrided or carburized is made the cathode of a glow discharge and is simultaneously heated by radiant or rf induction means. The discharge gas is either O_2, N_2 plus H_2, or CH_4. Very thick (0.1–2 mm) protective coatings on a variety of metals can be produced in this way to render surfaces hard and/or corrosion resistant.

Plasma-Enhanced Chemical Vapor Deposition (PECVD):

Plasma-enhanced chemical vapor deposition (PECVD) is one of the most attractive ones for high perfection films at low and moderate temperatures. It is a method of depositing

thin films from source gases or vapors that can be either fed into or generated within the reactor. Coupling of a radio frequency (RF) electric field (typically 13.56 MHz) into the plasma reactor results in dissociation of the source precursor molecules. Free electrons present in the chamber are accelerated by the applied RF electric field and collide with precursor molecules. Impact ionization by these free electrons yield avalanches that continue until steady-state plasma is established. In this way, the precursor molecules are excited to higher energy states, primarily by inelastic collisions with the energetic electrons, and dissociate into a variety of radicals, ions, atoms, and more electrons [9]. Radicals and atoms, generated in the plasma, travel to the surface of the growing film. On arrival, they are adsorbed onto the surface where some then diffuse on the growing film surface and make chemical bonds at favorable sites to form an amorphous film. Others are desorbed depending on their respective sticking coefficients. Figure 3.4 shows a schematic of the plasma reactor for this technique.

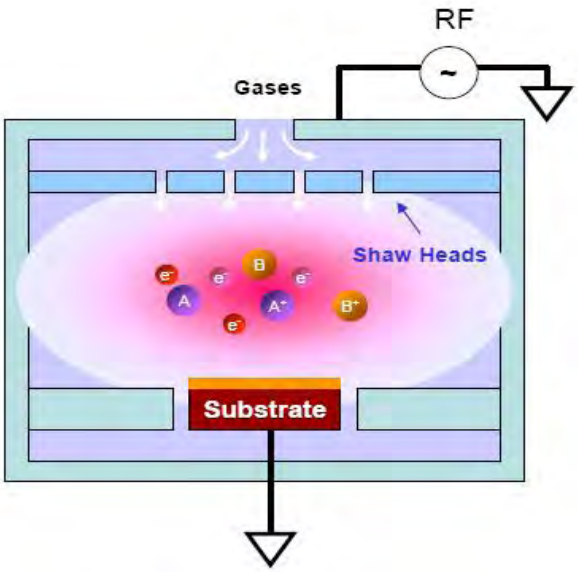

Figure 3.4: Plasma-Enhanced Chemical Vapor Deposition system.

3.2.3 Gas-Phase Chemical Processes

Methods of film formation by purely chemical processes in the gas or vapor phases include chemical vapor deposition and thermal oxidation. Chemical vapor deposition (CVD) is a materials synthesis process whereby constituents of the vapor phase react chemically near or on a substrate surface to form a solid product. The deposition technology has become one of the most important means for creating thin films and coatings of a very large variety of materials essential to advanced technology, particularly solid-state electronics where some of

the most sophisticated purity and composition requirements must be met. The main feature of CVD is its versatility for synthesizing both simple and complex compounds with relative ease at generally low temperatures. Both chemical composition and physical structure can be tailored by control of the reaction chemistry and deposition conditions. Fundamental principles of CVD encompass an interdisciplinary range of gas-phase reaction chemistry, thermodynamics, kinetics, transport mechanisms, film growth phenomena, and reactor engineering.

Chemical reaction types basic to CVD include pyrolysis (thermal decomposition), oxidation, reduction, hydrolysis, nitride and carbide formation, synthesis reactions, disproportionation, and chemical transport. A sequence of several reaction types may be involved in more complex situations to create a particular end product. Deposition variables such as temperature, pressure, input concentrations, gas flow rates and reactor geometry and operating principle determine the deposition rate and the properties of the film deposit. Most CVD processes are chosen to be heterogeneous reactions. That is, they take place at the substrate surface rather than in the gas phase. Undesirable homogeneous reactions in the gas phase nucleate particles that may form powdery deposits and lead to particle contamination instead of clean and uniform coatings. The reaction feasibility (other than reaction rate) of a CVD process under specified conditions can be predicted by thermodynamic calculations, provided reliable thermodynamic data (especially the free energy of formation) are available. Kinetics control the rate of reactions and depend on temperature and factors such as substrate orientation. Considerations relating to heat, mass, and momentum transport phenomena are especially important in designing CVD reactors of maximum efficiency. Since important physical properties of a given film material are critically influenced by the structure (such as crystallinity), control of the factors governing the nucleation and structure of a growing film is necessary. Thin-film materials that can be prepared by CVD cover a tremendous range of elements and compounds. Inorganic, organometallic, and organic reactants are used as starting materials. Gases are preferred because they can be readily metered and distributed to the reactor. Liquid and solid reactants must be vaporized without decomposition at suitable temperatures and transported with a carrier gas through heated tubes to the reaction chamber, which complicates processing, especially in the case of reduced-pressure systems. Materials deposited at low temperatures (e.g., below 600°C for silicon) are generally amorphous. Higher temperatures tend to lead to polycrystalline phases. Very high temperatures (typically 900°C to 1100°C in the case of silicon) are necessary for growing singlecrystal films. These

films are oriented according to the structure of the substrate crystal; this phenomenon, known as *epitaxy*, is of crucial practical importance in solid-state device technology. CVD has become an important process technology in several industrial fields. As noted, applications in solid-state microelectronics are of prime importance. Thin CVD films of insulators, dielectrics (oxides, silicates, nitrides), elemental and compound semiconductors (silicon, gallium arsenide, etc.), and conductors (tungsten, molybdenum, aluminum, refractory metal silicides) are extensively utilized in the fabrication of solid-state devices. Hard and wear-resistant coatings of materials such as boron, diamond-like carbon, borides, carbides and nitrides have found important applications in tool technology. Corrosion resistant coatings, especially oxides and nitrides, are used for metal protection in metallurgical applications. Numerous other types of materials, including vitreous graphite and refractory metals, have been deposited mainly in bulk form or as thick coatings. Many of these CVD reactions have long been used for coating of substrates at reduced pressure, often at high temperatures.

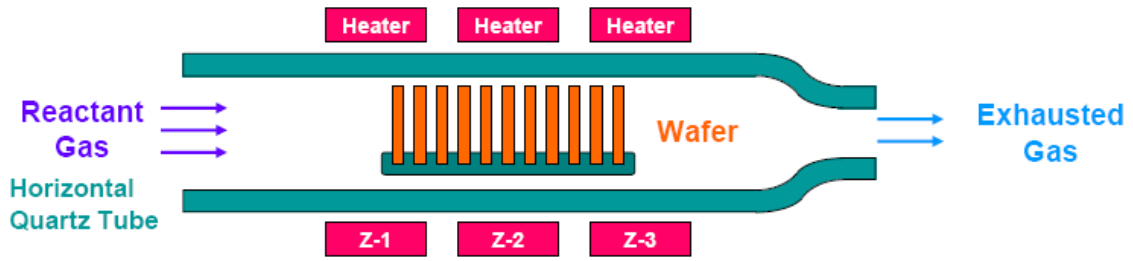

Figure 3.5: Chemical vapor deposition

3.2.3.1 Laser-Induced Chemical Vapor Deposition (LCVD).

LCVD utilizes a laser beam for highly localized heating of the substrate that then induces film deposition by CVD surface reactions [10]. Another mode of utilizing laser (or electron radiation) is to activate gaseous reactant atoms or molecules by their absorption of the specific wavelength of the photonic energy supplied. The resulting chemical gas phase reactions are very specific, leading to highly pure film deposits. On the other hand, the activation matching of the spectral properties with the reactant species limits the choice of reactions and hence the film deposits that can be obtained. LCVD is still in its early development stages but promises many interesting and useful applications in the future.

3.2.3.2 Ion Implantation

Recently, ion implantation has been used to form silicon-on-insulator structures by implanting large doses of atomic or molecular oxygen ions in single-crystal silicon substrates to produce a buried oxide layer with sharp interfaces after annealing. Simultaneous high-dose implantation of low energy oxygen and nitrogen ions into silicon yields very thin films of silicon oxynitride, whereas low-energy implantation of nitrogen or ammonia into silicon yields a low-density silicon nitride layer [11].

3.2.4 Liquid-Phase Chemical Formation

The growth of inorganic thin films from liquid phases by chemical reactions is accomplished primarily by electrochemical processes (which include anodization and electroplating), and by chemical deposition processes (which include reduction plating, electroless plating, conversion coating, and displacement deposition). A number of extensive reviews of these film formation processes discuss theory and practice. Another class of film forming methods from the liquid phase is based on chemically reacting films that have been deposited by mechanical techniques. Finally, liquid phase epitaxy is still being used for growing a number of single-crystal semiconductors.

3.2.4.1 Electroplating

In electroplating a metallic coating is electrodeposited on the cathode of an electrolytic cell consisting of a positive electrode (anode), a negative electrode (cathode), and an electrolyte solution (containing the metal ions) through which electric current flows. The quantitative aspects of the process are governed by Faraday's laws. Important electroplating variables include current efficiency, current density, current distribution, pH, temperature, agitation, and solution composition. Numerous metals and metal alloys have been successfully electroplated from aqueous solutions. However, the technically most useful electroplated metals are chromium, copper, nickel, silver, gold, rhodium, zinc, and a series of binary alloys including chromium/nickel composites. Electroplating is widely used in industry and can produce deposits that range from very thin films to very thick coatings (electroforming).

3.2.4.2 Mechanical Methods

Mechanical techniques for depositing coatings from liquid media that are subsequently reacted chemically to form the inorganic thin film product are spraying; spinning, dipping and draining, flow coating, roller coating, pressure-curtain coating, brushing, and offset printing of reagent solutions. Chemical reaction of the coating residue, often by thermal oxidation, hydrolysis, or pyrolysis (in the case of metalorganics) produces the desired solid film. Spin-on deposition of film forming solutions is widely used in solid-state technology. Liquid spray coating is probably the most versatile mechanical coating technique of the deposition techniques noted, and it is particularly well suited for high-speed automated mass production. Deposition of very thin films is possible by judicious selection and optimization of spray machine parameters for forming "atomized" droplets and the reagent and solvent systems used to formulate the spray liquid. An example of the capability of this refined method is the mass production spray-on deposition of organometallic alkoxy compounds, such as titanium-(IV)-isopropoxide, in an optimally formulated spray solution. Controlled pyrolysis of the deposit can form TiO2 films of 70 nm thickness which serves as a highly effective and low-cost antireflection coating for silicon solar cells [12]. It should be noted that spray deposition encompasses several other types of spraying processes that are based on either liquid sources, such as harmonic electrical spraying, or on dry source reactants that include flame spraying, arc plasma spraying, electric arc spraying, and detonation coating.

3.2.4.2.1 Spray Pyrolysis

The spray pyrolysis technique is a method that has been widely used for more than two decades, due to its simple, inexpensive technique and possibility to produce large area films [13]-[15]. Because the film formation is carried out in air by a simple apparatus in SPD, the technique is one of the most attractive film preparation methods. This technique dissolves elements of the compound material in solution and solution fed into the spray nozzle at a predetermined pressure and flow rates. The substrate temperature is controlled by a heater power supply with a feedback circuit. The solution is sprayed onto a heated substrate in the form of small droplets generated by an ultrasonic spray generator or aerosol generator. The spray nozzle can be driven by gravity or forced by gas pressure. Gas pressure can be controlled by the flow and used as part of the compounds, such as oxygen or dry air, to deposit oxides and nitrogen or inert gas to avoid chemical reactions between the compound

materials. The film formation depends on the the reactant/solvent evaporation and on the process of droplet landing. The ideal deposition condition is considered when the solvent is completely removed at the moment the droplet approaches the substrate where the chemical reaction occurs [16]. The reactant molecules undergo processes of absorption, surface diffusion and chemical reaction, leading to nucleation and layer growth, while volatile by-products evaporate and diffuse away from the surface [17]. On the other hand, it is also important to heat the substrate enough to make sure that the compound solvents are completely evaporated. The film's thickness depends on the concentration of the solution and deposition time.

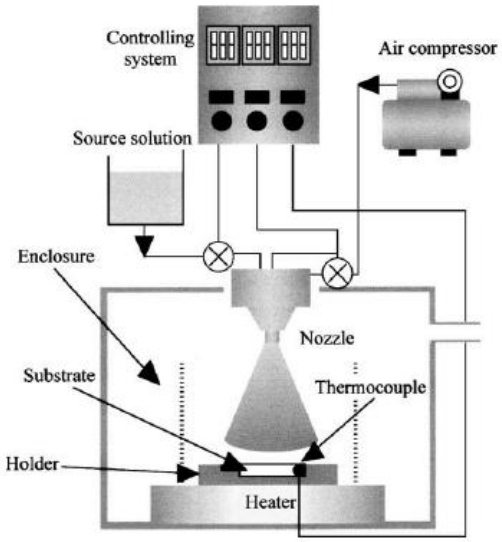

Figure 3.6: Schematic representation of a spray pyrolysis deposition (SPD)

Advantages of Spray Pyrolysis Deposition:

1. Inexpensive technique.
2. Possibility to produce large area film.
3. ability to form crystalline or amorphous deposition.
4. ability to control deposition parameters such as deposition temperature, deposition rate, thickness etc.
5. Particles are more uniform in size.
6. Simple & continuous operation.
7. Easy fabrication.
8. Easy to control.
9. Vacuum less

3.3 Current & Future Developments

Thin film technologies and their applications are constantly evolving. In fact, with the growing need for component and assembly miniaturization, well established thick film processes are rapidly approaching their technological limits. As a result, more and more manufacturers of electronic, mechanical, chemical, optical and energy supply devices are replacing the conventional thick film processes with thin film technologies in order to manufacture smaller components and parts.

In recent years several deposition devices have been developed in order to fabricate complex multilayer and structures and to optimize the thin film deposition conditions and the quality and homogeneity of the obtained thin films. These devices utilize either physical vapour deposition techniques or chemical vapour deposition techniques and a few of the recent patents in thin film deposition have been revised in this paper.

Applications of thin film technology include very large scale integrated circuits (VLSI), electronic packaging, magneto-optical recording media, sensor technology etc. One of the most promising applications concerns photovoltaic systems in order to reduce their cost. Thin-film modules are expected to be cheaper to manufacture due to their reduced material costs, energy costs, handling costs and capital costs. According to by 2015 thin film photovoltaic (TFPV) systems will be generating 26GW of power worldwide and represent a market worth $20bn. The prediction about TFPV is based on the rapid growth of all types of photovoltaics but also on the low cost of manufacturing and flexibility of deployment associated with TFPV - especially in residential applications – compared with currently dominant crystalline silicon photovoltaic technologies. “NanoMarkets” expects TFPV to account for more than half the world's production of photovoltaic systems by 2015. In the automotive industry surface and thin film techniques are also extensively used mainly in sensors, optics, electronics and surface modification assuring the production of safer and more comfortable automobiles. additionally, the 2007 German Future Prize winning thin film technology of Dr. Klaus Streubel, Dr. Stefan Illek (both of OSRAM) and Dr. Andreas Bräuer (of the Fraunhofer-Institute for Applied Optics and Precision Engineering) is the key to producing LED chips of extremely high brightness and also enables them to be packed tightly together to create a large illuminating surface. High-efficiency light emitting diodes from OSRAM that are based on this innovative technology will open up new applications ranging from mini projectors and rear projection televisions to night vision systems in vehicles and general room lighting.

All the deposition methods have their inherent advantages and limitations. Hence the choice of certain deposition technique for some application is to be made very carefully. Among these techniques, the spray pyrolysis is well studied for the preparation of pure and cobalt doped zinc oxide thin films. This technique has the advantage of simple and inexpensive experimental arrangement. In this case though, intrinsic advantages of **SPRAY PYROLYSIS TECHNIQUE** have been used to deposit ZnO thin films.

References:

[1] Maissel, L. I., and Glang, R., (eds.), "Handbook of Thin Film Technology", McGraw Hill, New York, pp 10-12, 1970.

[2] Vossen, J. L., and Kern, W., (eds.), "Thin Film Processes", Academic Press, New York, 1978.

[3] Bunshah, R. F., (ed), "Deposition Technologies for Films and Coatings: Developments and Applications", Noyes Publications, Park Ridge, New Jersey, pp 27-54, 1982.

[4] Ghandhi, S. K., "VLSI Fabrication Principles: Silicon and Gallium Arsenide" John Wiley and Sons, New York, pp 288-290, 1983.

[5] Davies, H. J., "The Physics of Low-Dimensional semiconductors: an introduction". Cambridge University Press, 1997.

[6] Rinaldi, F., "Basics of Molecular Beam Epitaxy (MBE) - Annual Report. – 2002, Optoelectronics Department, University of Ulm.

[7] Ellmer, K., "Magnetron sputtering of transparent conductive zinc oxide: relation between the sputtering parameters and the electronic properties" Appl. Phys, Vol-33 No. 4, 2000.

[8] Heller, R. B., McGannon, J., and Weber, A.H., "Precision Determination of the Lattice Constants of Zinc Oxide", Appl. Phys., Vol-21, No. 12, pp 1283-1284, 1950.

[9] Lieberman, M. A., and Lichtenberg, A. J., "Principles of Plasma Discharges and Materials Processing", John Wiley and Sons, New York, 1994.

[10] Solanski, R., Moore, C. A., and Collins, G. J., "Laser-Induced CVD", Solid State Technol., Vol-28, No. 6, pp 220–227, 1985.

[11] Chiu, T. Y., Hovland. C., and Oldham, W. G., Solar Energy; Semiconductor Materials; Electron Transfer; Seebeck Effect; Alloys; Doped Materials; Electric Conductivity; Electron Mobility; Thermoelectricity; Electrical Properties; Electricity; Materials; Mobility; Particle Mobility; Physical Properties", Electrochem. Soc., Vol-131, No. 9, pp 2110–2115, 1984.

[12] Kern, W., and Tracy, E., "Titanium dioxide antireflection coating for silicon solar cells by spray deposition", RCA Review, Vol-41, No. 2, pp 133–180, 1980.

[13] Isac, L.; Duta, A., Kriza, A., "Copper sulfides obtained by spray pyrolysis - Possible absorbers in solidstate solar cells". Thin Solid Films, Vol-15, pp 5755-5758, 2007.

[14] Ienei, E.; Isac, L., Duta, A., "Synthesis of alumina thin films by spray pyrolysis. Revue Roumaine de Chimie, , Vol-3, pp 161-165, 2010.

[15] Krunks, M., Bijakina, O., Mikli, V., Rebane, H., Varema, T., Altosaar, M., and Mellikov, E., "Sprayed $CuInS_2$ thin films for solar cells: The effect of solution composition and post-deposition treatments". Solar Energy Materials and Solar Cells, Vol-69, No. 1, pp 93-98, 2001.

[16] Patil, P.S., "Versatility of chemical spray pyrolysis technique". Mater Chem and Phys, Vol-59, No. 3, pp 185-198, 1999.

[17] Oktik, S., Russell, G. J., and Brinkman, A. W., "Properties of ZnO layers deposited by "photo-assisted" spray pyrolysis", Crystal Growth, Vol-159, No. 1-4, pp 195-199, 1996.

CHAPTER 4

EXPERIMENTAL DETAILS

Thin films can be prepared from a variety of materials such as metals, semiconductors, insulators or dielectrics etc., and for this purpose various preparation techniques has also been developed. Spray pyrolysis is the most commonly used technique adopted for the deposition of metals, alloys and many compounds.

This chapter deals mainly with the description of the apparatus and the preparation of the sample. In this chapter the preparation of $Zn_{1-x}Co_xO$ thin films on glass substrate by spray pyrolysis process is discussed. Various steps of the film deposition procedure of the spray pyrolysis method have been discussed below.

4.1 Experimental Equipments

4.1.1.1 Masks for generation of pattern in the deposited films

The desired shapes or patterns of films are generally obtained by masking substrates during deposition so that only desired areas receive the vapour atoms. A mask should be stable over the temperature range encountered during deposition and chemically inactive with the vapour atoms. Mask was made from stainless steel plate with the desired pattern cut into it. The aperture was made in a bath machine. In the present case, freshly cleaved good quality mica sheets were also used under the metal mask for making different masks according to requirement. They were cut into metal mask shapes by shaving blades and micro punch.

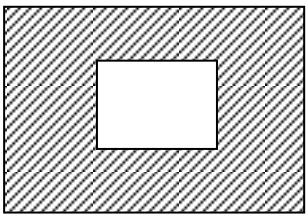

Figure 4.1: Mask for the sample

The masks were thoroughly cleaned by detergent and finally washed in acetone. They were dried properly by hot air blower. The mask was prepared in such a way that the

edge of the mask is smooth so that it is helpful for determining the film thickness accurately.

4.1.1.2 Heater

The heater „H" is an ordinary hot plate 2k-watt nichrome wire heater. The top of the plate is covered with a piece of asbestos sheet having a small open area at the center where a mica sheet is attached. A thick stainless steel plate is placed on this mica sheet. Substrate is placed on this susceptor plate to have a uniform temperature throughout the substrate surface. An electrical voltage variac controls the heater power.

4.1.1.3 The Design of the Reactor

The design of the reactor is shown in Fig. 4.2. It is a vertical batch type reactor composed of a galvanized iron enclosure „E", heater „H" and heat susceptor „G". For the rapid expulsion of the by-product gases there are opening at the side and at the top of the reactor. It helps focusing the incoming sprayed solution towards the substrate and also provides a chimney action to the exhaust gas upwards.

Figure 4.2: Design of a reactor

4.1.1.4 The Fume Chamber

It is a large type chamber with a slanting top and is provided with a chimney. There is an exhaust fan fitted at the mouth of the chimney to remove the unused gases from the chamber. The slanting top and the sidewalls are made of glass and wood. There

are airtight doors in the front side. The chamber has purging facilities. The whole spray system and the reactor are kept inside this fume chamber at the time of film deposition because of the safety grounds and to check air current disturbances at the deposition site. These two points just stated are very important for the spray process when deposition is carried out in open- air atmosphere.

4.1.1.5 Air Compressor

It is reservoir type electrical air compressor. A rotary pump in this section mode draws atmospheric air and keeps it reserved in a large capacity air tank. At the outlet of the tank a pressure gauge is attached which records the pressure of the air at the time of supplying it from the tank. There is a bypass control valve which can keep the output pressure constant.

4.1.1.6 Spray Head/Nozzle

The single spray nozzle consists of capillary tubes (stainless steels) fitted perpendicular to the other tube as shown in Fig. 4.3. When compressed air is passed rapidly through the upper tube „P" in direction tangential to the mouth of the lower tube „A", a partial vacuum is created at the front part of the tube „A" whose other end is kept immersed in the spray liquid. Due to this partial vacuum the liquid rises up through the tube „A" and the compressed air drives it away in the form of fine spray particles. The thinner spray nozzle would give the finer spray particles. A very fine needle shaped capillary tube was used for the spray nozzle and it may vary from nozzle to nozzle. It was ensured that solutions do not come into contact with any metal parts except the spray needle.

4.1.2.1 Selection of substrate

For deposition of thin films of a material suitable supporting material known as substrate is required. The surface of the substrate plays a major role in the nucleation and growth process of the film and thereby influences the thin film properties considerably. An ideal substrate should have the following requirements [1, 2].

(a) The surface should be flat and smooth.

(b) High mechanical strength to enable the substrate to withstand strain during processing and monitoring

(c) High resistivity

(d) High thermal conductivity.

(e) Nearly same coefficient of thermal expansion with that of the film to minimize thermal stress.

(f) Zero porosity to minimize out gassing and to ensure film uniformity, and

(g) Low cost.

For thin film deposition, several types of substrates are used. Generally, glass, quartz, plastic and ceramic substrates are used for polycrystalline films. It has been observed that there is no material that would satisfy all these requirements. Glass is most widely used as substrate material for deposition of polycrystalline films. However, in the present work, thin films were deposited on glass substrates. The most commonly microscope glass slides having 5 cm long, 2 cm wide and 0.1 cm thickness were used. These were fine smooth high quality microscope glass slides.

4.1.2.2 Cleaning of substrate

The substrates should be highly cleaned and uncontaminated for proper adhesion of the films and for producing reproducible film properties. Usually the fine dust particles due to packaging, fingerprints and sticking of different impurity atoms are the common contaminants. The removal of these contaminants by different cleaning techniques depends upon the nature of the substrate and the type of contaminants. The chemical reagents, such as acids, alcohol or alkalis with proper concentrations remove the contaminants by breaking the bonds between the contaminants molecules as well as between the contaminants and substrate. Acid converts oxide layer if any and greases into water-soluble compounds. The ultrasonic cleaning is another recommended process for removing gross contaminants such as greasy particles and fingerprints. This procedure enhances the dissolution of residues sticking on the substrate by the intense local stirring action by the shock waves created in the solvent.

The substrates of appropriate sizes cut from the glass slides were first washed with ordinary detergent solution and then these were treated in a mixture of nitric acid. Taking out from this solution the substrates were washed by freshly prepared distilled water and then immersed in chromic acid and after wards these are again rinsed with de-ionised water. The drying of cleaned wet substrates is also critical because of probable recontamination due to adsorption of gaseous particles and dust. So, necessary precautions were taken in drying the substrate in an atmosphere free from any air borne contaminants. Taking out the substrates from the deionised water, the substrates were put vertically in a clean pettry dish so that there is no water stick mark on the substrate. Finally, these were dried in hot air and preserved for use. During the whole process the substrates were always held by slide holding forceps.

4.1.3 Working Solution

The working solution was prepared by taking zinc acetate [$Zn(CH_3COO)_2.2H_2O$] as a source material. The most commonly used solvents are water and ethanol. As [$Zn\ (CH_3COO)_2.2H_2O$] dissolves in water at room temperature, water was taken as solvent. Since the spray system used in the present experiment operates via a partial vacuum path as the mouth of the spray nozzle, the concentration of the solution prepared by the solvent was made in such a way that it could be at least be drawn by the nozzle. The higher the solution concentration the lower the spray rate. A typical value of solution concentration 0.1 M was used in this work. Also, in order to prepare the

$Zn_{1-x}Co_xO$ thin film the aqueous solution of zinc acetate [$Zn(CH_3COO)_2.2H_2O$], cadmium acetate [$Co(CH_3COO)_2.4H_2O$] as the precursor solution were taken. In the work the concentration of the solution was kept at 0.1 M.

4.1.4 Film Deposition Parameters

In the chemical spray deposition technique the structure, composition and other characteristics of the deposited films depend on a number of process variables [deposition parameters]. The variable quantities such the substrate temperature, solution and gas flow rate, deposition time, quality of the substrate material, size of atomized particles, solution concentration, and substrate to spray outlet distance, etc. are affected

on the film properties. It is obvious that the substrate temperature is the most important deposition parameter and it is controlled with great care.

For the deposition of $Zn_{1-x}Co_xO$ thin film, all the above mentioned parameters except

(i) Substrate temperature (T_s)
(ii) Deposition time (t_d)
(iii) Solution concentration (C)
(iv) Spray rate (S_r)
(v) Spray outlet to substrate distance (d_s) and
(vi) Carrier air pressure (P_a),

were kept at their optimum values. To study the effect of any one of these six parameters on the film properties the remaining other were kept constant. Air current disturbances become another parameter, which creates problem to get uniformity of thickness and homogeneity of the film.

4.1.5 Sample Preparation

It has been stated earlier that spray pyrolysis method for preparing ZnO thin film is an economically attractive method, which consist basically of spraying solution on a heated glass substrate. The apparatus needed to carry out the chemical spray process consists of a device to atomize the spray solution and a substrate heater. Fig. 4.3 shows a typical experimental setup of spray pyrolysis technique.

A considerable amount of (100 mL) solution taken in the container „F" fitted with the spray nozzle „A". The clean substrate with a suitable mask was put on the susceptor of the heater „H". The distance between the tip of the nozzle and the surface of the glass substrate was kept 25 cm. Before supplying the compressed air the substrate temperature „T_s" was to be kept at a level slightly higher than the required substrate temperature because at the onset of spraying a slight fall of temperature is likely. The temperature of a substrate was controlled by controlling the heater power using a variac. The substrate temperature was measured by placing a copper constantan thermocouple on the substrate.

When compressed air is passed through „P" at constant pressure (0.5 bar), a fine $Zn_{1-x}Co_xO$ was produced and was automatically carried to the reactor zone where film was deposited on the heated substrate. A situation have been adjusted such that 5 minutes of spray produces $Zn_{1-x}Co_xO$ thin film, thickness of the range 200 nm keeping substrate temperatures at 573 K. The possible chemical reaction that takes place on the heated substrate to produce $Zn_{1-x}Co_xO$ may be as follows:

$$\left.\begin{array}{l} Zn(CH_3COO)_2.2H_2O \\ \quad + \\ Co(CH_3COO)_2.4H_2O \end{array}\right\} \xrightarrow[\text{Decomposes}]{573\ K} ZnCoO\ /\ Zn_{1-x}Co_xO\downarrow + CO_2\uparrow + CH_4\uparrow + \text{Steam}$$

4.1.5.1 Rate of Deposition

Spray rate is a parameter influencing the properties of films formed. It has been reported that properties like crystallinity, surface morphology, resistivity and even thickness are affected by changes in spray rate [3]. It is generally observed that smaller spray rate favours formation of better crystalline films. Smaller spray rate requires higher deposition time for obtaining films of the same thickness prepared at higher spray rate. The rate of flow of the working solution can be controlled by a suitable nozzle „A" and adjusting the airflow rate.

4.1.5.2 Thickness Control

In the present spray deposition process, the deposition time is the main factor for the thickness control, provided the other parameters, remain constant. Since the deposition is carried out in normal atmosphere a direct and insitu control of thickness is not so easy. To control the film thickness therefore calibration chart may be used. These charts are generally plots of deposition time vs. thickness, and can be prepared at different constant substrate temperatures prior to the preparation of particular experimental samples using the same solution and deposition variables.

4.1.6 Optimization of the Deposition Process

To obtain the optimum condition of the film deposition process, it is essential to select at first the requirements with respect to which the process should be optimized. The optimization process is very lengthy because there are a number of process variables. The basic requirement was to get a film of high transparency as well as high electrical conductivity.

For the process of optimization following set of films have been deposited:

(i)The first set of films was deposited at various substrate temperatures, keeping all other deposition parameters constant at an arbitrary level. From the set of films the optimum substrate temperature T_s was selected with respect to the best conducting and transparent films.

(ii) After obtaining the optimum value of T_s, second set of films were deposited by varying the substrate to spray outlet distance, d_s using the optimized T_s and other parameters were kept constant to the arbitrary level as they were in the first set. From this second set of films the optimum distance d_s was selected corresponding to the best film.

(iii) Fixing the distance d_s and substrate temperature T_s, a third set of films were deposited by varying the pressure of the carrier gas P_a. From this set, optimum carrier air pressure P_a was selected. Keeping T_s, d_s and P_a as fixed fourth set of films were deposited by taking spray rate S_r as variable parameters. From this set, optimum spray rate S_r was selected. The fifth set of films were deposited keeping T_s, d_s, P_a and S_r at their optimum values. In this case, the solution concentration C was varied for selecting the optimum concentration of the working solution.

Thus in all cases the optimum values of the parameters were selected for deposition of films that exhibit good conductivity and high transparency. The resulting optimization is undoubtedly a tentative one because the process variables are in some degree mutually interdependent.

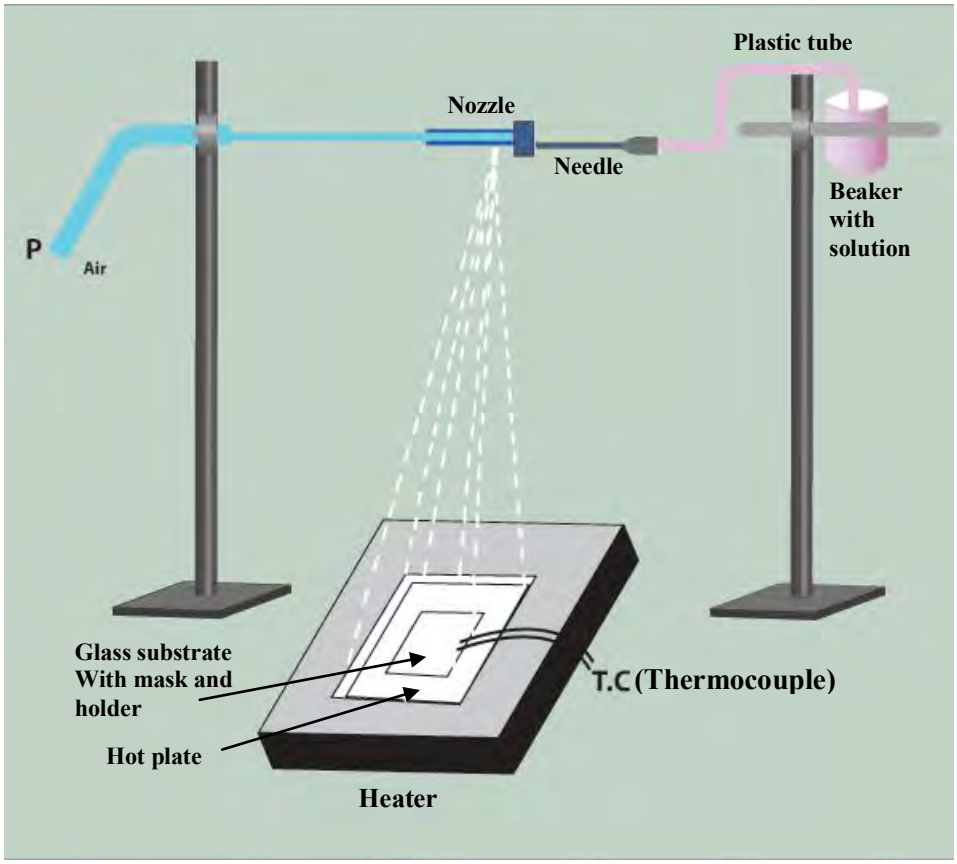

Figure 4.3. Experimental setup of spray pyrolysis technique.

Thin films are usually characterized by their structural, stochiometric, optical, electrical and mechanical properties. In this section, the characterization methods used in this work are reviewed briefly. These techniques include optical microscope, scanning electron Microscope (SEM) for surface morphology, Energy Dispersive X-ray (EDX) for compositional study, x-ray diffraction (XRD) for structural characterization, absorption spectra, for the optical characterization.

4.2 Measurement Details

4.2.1.1 Scanning Electron Microscopy (SEM)

SEM is a type of electron microscope that creates various images (surface morphology) by focusing a high energy beam of electrons onto the surface of a sample and detecting signals from the interaction of the incident electron with the sample's surface. The type of signals gathered in a SEM varies and can include secondary electrons, characteristic x-rays, and back scattered electrons. In a SEM, these signals

come not only from the primary beam impinging upon the sample, but from other interactions within the sample near the surface. The SEM is capable of producing high resolution images of a sample surface in its primary use mode, secondary electron imaging. Due to the manner in which this image is created, SEM images have great depth of field yielding a characteristic three-dimensional appearance useful for understanding the surface structure of a sample. This great depth of field and the wide range of magnifications are the most familiar imaging mode for specimens in the SEM. Characteristic x-rays are emitted when the primary beam causes the ejection of inner

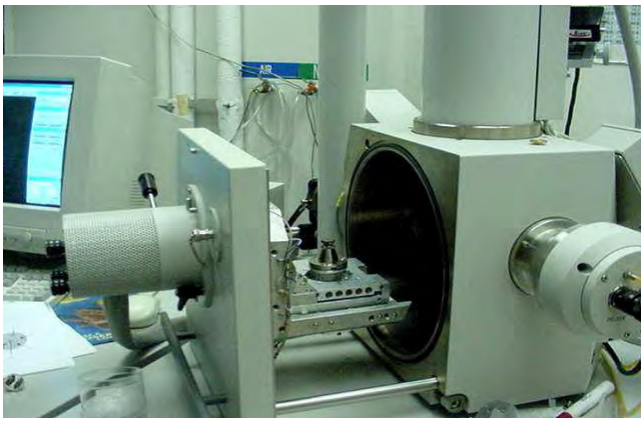

Figure 4.4: Photograph of Scanning Electron Microscope (SEM).

shell electrons from the sample and are used to tell the elemental composition of the sample. The back-scattered electrons emitted from the sample may be used alone to form an image or in conjunction with the characteristic x-rays as atomic number contrast clues to the elemental composition of the sample.

4.2.1.2 Scanning process and image formation

In a typical SEM, an electron beam is thermionically emitted from an electron gun fitted with a tungsten filament cathode. Tungsten is normally used in thermo ionic electron guns because it has the highest melting point and lowest vapour pressure of all metals, thereby allowing it to be heated for electron emission, and because of its low cost. The electron beam, which typically has an energy ranging from a few hundred eV to 40 keV, is focused by one or two condenser lenses to a spot about 0.4 nm to 5 nm in diameter. The beam passes through pairs of scanning coils or pairs of

deflector plates in the electron column, typically in the final lens, which deflect the beam in the x and y axes so that it scans in a raster fashion over a rectangular area of the sample surface.

When the primary electron beam interacts with the sample, the electrons lose energy by repeated random scattering and absorption within a teardrop-shaped volume of the specimen known as the interaction volume, which extends from less than 100 nm to around 5 μm into the surface. The size of the interaction volume depends on the electron's landing energy, the atomic number of the specimen and the specimen's density. The energy exchange between the electron beam and the sample results in the reflection of high-energy electrons by elastic scattering, emission of secondary electrons by inelastic scattering and the emission of electromagnetic radiation, each of which can be detected by specialized detectors. The beam current absorbed by the specimen can also be detected and used to create images of the distribution of specimen current. Electronic amplifiers of various types are used to amplify the signals which are displayed as variations in brightness on a cathode ray tube. The raster scanning of the CRT display is synchronized with that of the beam on the specimen in the microscope, and the resulting image is therefore a distribution map of the intensity of the signal being emitted from the scanned area of the specimen. The image may be captured by photography from a high resolution cathode ray tube, but in modern machines is digitally captured and displayed on a computer monitor.

4.2.2 Energy dispersive X-ray spectroscopy

The EDX analysis system works as an integrated feature of a scanning SEM and cannot operate on its own without the latter. During EDX analysis, the specimen is bombarded with an electron beam inside the scanning electron microscope. The bombarding electrons collide with the specimen atoms' own electrons, knocking some of them off in the process. A position vacated by an ejected inner shell electron is eventually occupied by a higher-energy electron from an outer shell. To be able to do so, however, the transferring outer electron must give up some of its energy by emitting an X-ray. The amount of energy released by the transferring electron depends on which shell it is transferring from, as well as which shell it is transferring to. Furthermore, the atom of every element releases X-rays with unique amounts of energy during the

transferring process. Thus, by measuring the amounts of energy present in the X-rays being released by a specimen during electron beam bombardment, the identity of the atom from which the X-ray was emitted can be established.

The output of an EDX analysis is an EDX spectrum. The EDX spectrum is just a plot of how frequently an X-ray is received for each energy level. An EDX spectrum normally displays peaks corresponding to the energy levels for which the most X-rays had been received. Each of these peaks is unique to an atom, and therefore corresponds to a single element. The higher a peak in a spectrum, the more concentrated the element is in the specimen.

An EDX spectrum plot not only identifies the element corresponding to each of its peaks, but the type of X-ray to which it corresponds as well. For example, a peak corresponding to the amount of energy possessed by X-rays emitted by an electron in the L-shell going down to the K-shell is identified as a K-Alpha peak. The peak corresponding to X-rays emitted by M-shell electrons going to the K-shell is identified as a K-Beta peak.

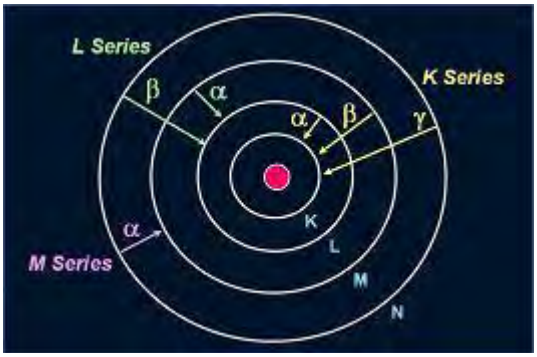

Figure 4.5: Elements in an EDX spectrum are identified based on the energy content of the X-rays emitted by their electrons as these electrons transfer from a higher-energy shell to a lower-energy one

4.2.3 X-ray Diffraction

Bragg reflection is a coherent elastic scattering in which the energy of the x-ray is not changed on reflection. If a beam of monochromatic radiation of wavelength λ is incident on a periodic crystal plane at an angle θ and is diffracted at the same angle as shown in Fig. 4.6, the Bragg diffraction condition for x-rays is given by

$$2d\,Sin\theta = n\lambda \qquad (4.1)$$

where *d* is the distance between crystal planes and *n* is the positive integer which represents the order of reflection. Equation (4.1) is known as Bragg law. This Bragg law suggests that the diffraction is only possible when $\lambda \leq 2d$ [4]. For this reason we cannot use the visible light to determine the crystal structure of a material. The X-ray diffraction (XRD) provides substantial information on the crystal structure.

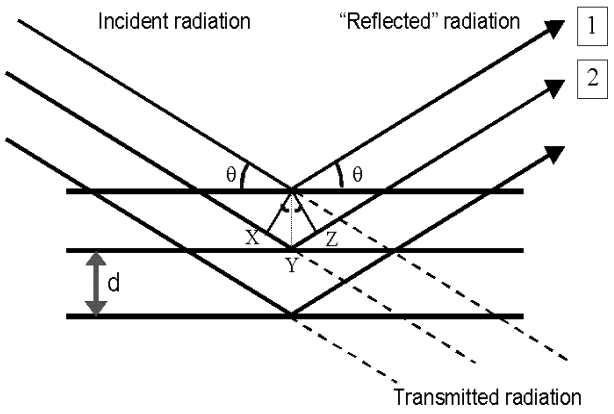

Figure 4.6. Bragg law of diffraction.

X-ray diffraction is the most precise technique for studying the crystal structure of solids, generally requiring no elaborate sample preparation and is essentially nondestructive [5,6]. Thin surface films, up to about 1000Aº thick, can be investigated using X-ray diffraction [7, 8]. Thicker films can be characterized by RHEED. Analysis of the diffraction patterns obtained by these techniques and comparison with standard ASTM data can reveal the existence of different crystallographic phases in the film, their relative abundance, the lattice parameters, and any preferred orientations. From the width of the diffraction line, it is possible to estimate the average grain size in the film [9].

4.2.4 Methods for the Film Thickness Measurement

Film thickness plays an important role on the properties of thin film and those it is one of the most significant film parameter and thickness measurement is a most essential job. Therefore, the thickness should be measured with great care as far as possible to have an accurate value. The thickness may be measured either by monitoring the rate of deposition or after the film is taken out of the deposition chamber. The latter type is appropriate for the spray deposition for the spray deposition technique because it is operated in open atmosphere. In the present work, the film thickness is measured after

taking out the film from the chamber. There are many techniques for measuring film thickness, such as Gravimetric Method, Microbalance Technique, Stylus Method, Photometric, Crystal Oscillatory, Color Comparison and Optical Interference etc. Thickness may be directly known by in-site monitoring the rate of deposition or it may be measured after the film is taken out of the deposition chamber. In the present work the later method was used. There are several methods for the measurement of film thickness and in the present work optical interference fringe method was used.

4.2.4.1 Optical Interference Method

The thickness of the film can be measurement accurately by optical interference method and it is one of the best method comparative others process. In this method two reflecting surfaces are brought into close proximity to produce interference fringes. Weiner was the first to use interference fringes for the measurement of film thickness. Latter on using Fizeau fringes, Tolansky developed this method to a remarkable degree and is now accepted as a standard method [10].When two reflecting surfaces are brought into close proximity, interference fringes are produced, the measurement of which makes possible a direct determination of film thickness and surface topography with high accuracy. In this method, two types of fringes are utilized for thickness measurement. The first produces Fizeu fringes of equal thickness, using a monochromatic light source. The second uses a white light source and produces fringes of equal chromatic order. The second method is prepared for thinner films.

The Fizeu fringes method was used in the present work for the measurement of film thickness. For the experimental set up a low power microscope, a monochromatic source of light, a glass plate and an interferometer are required. To make the Fizeau fringes of equal thickness visible in a multiple beam interferometer formed by a thin absorbing film on a glass substrate, generally and auxiliary reflecting coating on the film surface is required. But if the experimental sample is transparent with a very smooth surface no such auxiliary coating is necessary [11].

The film whose thickness is to be measured is required to form a step on a glass substrate and over it another plane glass plate (Fizeau plate) is placed. This illuminated with a parallel monochromatic beam of light a fringe system as shown in figure (4.4) is produced and is viewed with low power microscope. In this method, thickness from 3

nm to 2000 nm can be measured with an accuracy of ± 5nm. The fringe spacing and fringe displacement across the step are measured and used to calculate the film thickness. The displacement „h" of the fringe system across the film substrate step is then measured to calculate the film thickness „t" using the relation

$$t = \frac{h}{fringes - spacing} \times \frac{\lambda}{2} \qquad (4.2)$$

Where λ is the wavelength of the monochromatic light (sodium light) employed.

If d is the fringe spacing then the film thickness t is given by,

$$t = \frac{h}{d} \times \frac{\lambda}{2} (nm) \qquad (4.3)$$

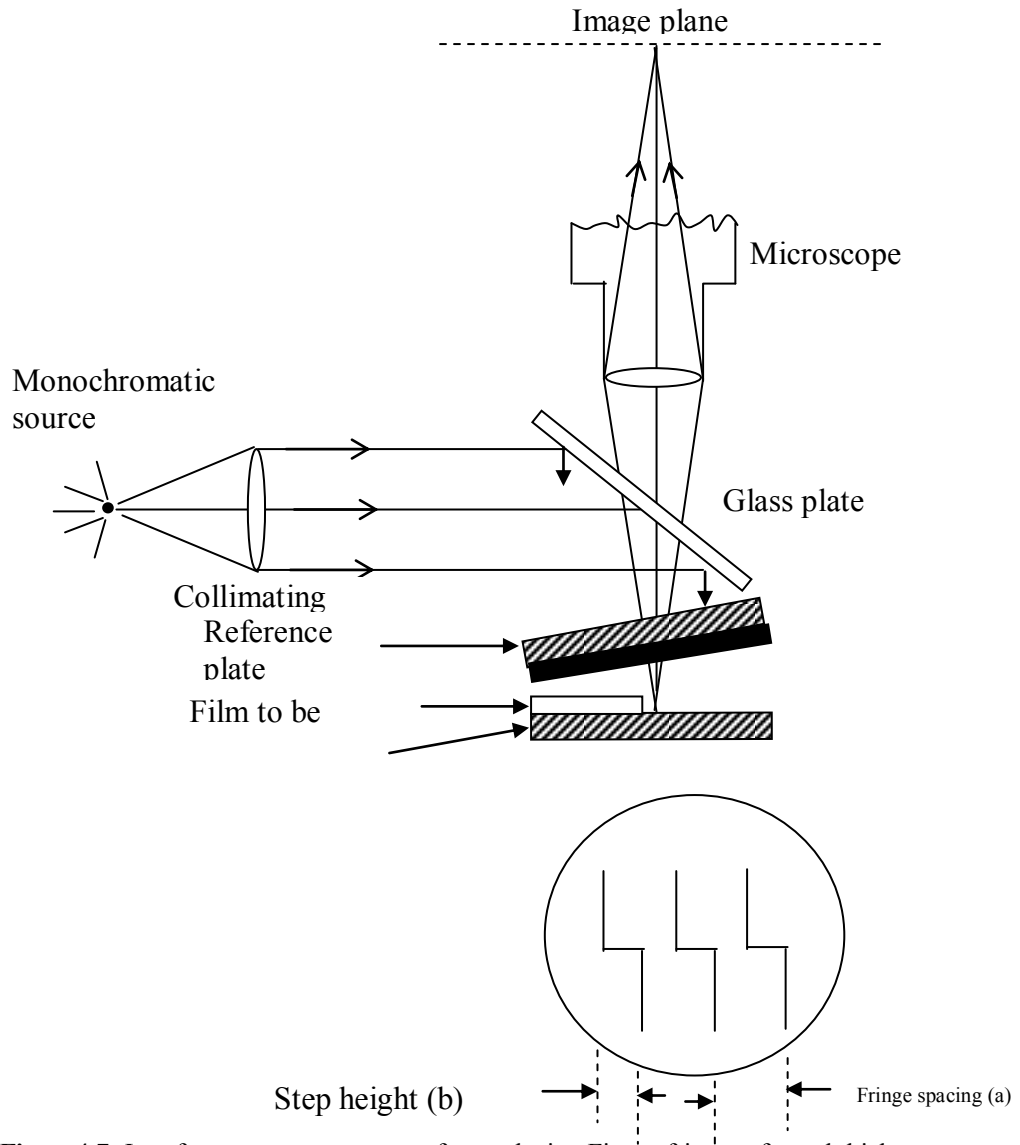

Figure4.7: Interferometer arrangements for producing Fizeau fringes of equal thickness

4.2.5 Optical Properties of Thin Film

4.2.5.1 Absorption coefficient

When a semiconductor is illuminated by light, photon strikes the surface, a fraction of photons are reflected, some of these are absorbed within the semiconductor and the remainder transmitted into the semiconductor. The absorption of radiation by any medium occurs through the excitation of electrons and photons. For semiconductor, it is convenient to consider several types of absorption arising from

i) Electronic transitions between different energy bands.

ii) Electronic transitions within energy band.

iii) Electronic transitions to localized states of impurity atoms.

iv) Lattice vibrations.

v) Vibrations of impurity atoms.

In the fundamental absorption region the transmission T is given by

$$T = A \exp\left(-\frac{4\pi kt}{\lambda}\right) \qquad (4.4)$$

Where A is a constant, k is the extinction co-efficient and t is the thickness. For $K^2 << n^2$, the principle variation of T occurs in the exponential term and pre-exponential term A. Therefore,

$$T = \exp(-\alpha t) \qquad (4.5)$$

Figure 4.8: Photograph of a Spectrophotometer

Where $\alpha = \frac{4\pi k}{\lambda}$ is the absorption co-efficient of the film. Thus the value of absorption co-efficient may be calculated from the relation

$$\alpha = -\frac{\ln T}{t} \qquad (4.6)$$

Otherwise from equation (4.4) Plotting Eqn. 4.2 as ln ($\frac{1}{T}$) Vs t curve at a fixed wavelength, a straight line will be obtained. The slope of the straight line will give α and intercept will give A.

According to Bardeen [12], the relationships that exist for possible transition across the energy gap of a semiconductor show that the absorption co-efficient α may be written as

$$\alpha = \frac{A(h\nu - E_g)^n}{t} \qquad (4.7)$$

Where A is a constant, hν is the photon energy, n is a index related to the density of state (n= ½ for direct transition and n=2 for indirect transition) and E_g is the optical band gap of the semiconductor. By plotting $(\alpha h\upsilon)^n$ against hν for the several values of n it is possible to determine which of these conditions dominate and hence determine the appropriate energy gap of the sample.

4.4.5.2 Determination of Optical Band Gap

The energy difference between the valence band and conduction band on energy level diagram is known as band gap. Large energy band indicates that valance electrons are lightly bound with the nucleus. For conduction of electrons, required energy must be equal to or greater than the forbidden energy gap or band gap E_g.

Mainly there are two types of band gap found in crystal are

(a) Direct band gap

(b) Indirect band gap

(a) Direct band gap:

If the lowest point of the conduction band occurs at the same value of wave vector space k as the highest point of the valence band Fig.4.9 [4] is called direct band

gap. A direct optical transition is drawn vertically with no significant change of k, because the absorbed photon has a very small value of wave vector k. The threshold frequency ω_g for absorption by direct transition determines the band gap $E_g = h\omega_g/2\pi$. A simple theoretical treatment gives the result

Where A is a constant having the numerical value of 2×10^{14} when k is expressed in cm^{-1} and hυ and E_g are in eV.

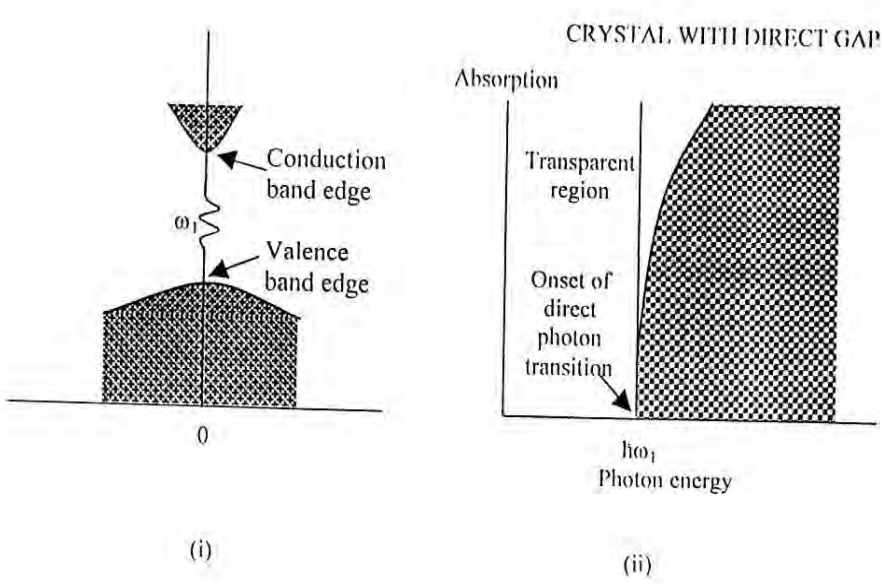

Figure 4.9: (i) Crystal diagram of direct band gap, **(ii)** Absorption process.

(b) Indirect band gap

In indirect semiconductor crystal, the lowest point of conduction band and highest point of valence band occurs at different values of the crystal momentum i.e. different values of wave vector k. In the indirect absorption process a photon is absorbed by the crystal with the creation of electron-hole pair and in this process a photon is produced having an energy $h\Omega/2\pi$. Indirect band gap and absorption are shown in Fig 4.9 [4].

So that the minimum photon energy required exciting an electron from the valence band to the conduction band is given by

$$h\upsilon = E_g \pm E_p \qquad (4.8)$$

Where E_p is the for photon energy either absorbed (+) or released (-) in this process.

Since the indirect band gap absorption process required an extra "particle" be involved, the probability of light being absorbed by this process is much less than in the direct band gap case. Hence the absorption coefficient is low and light can pass a reasonable

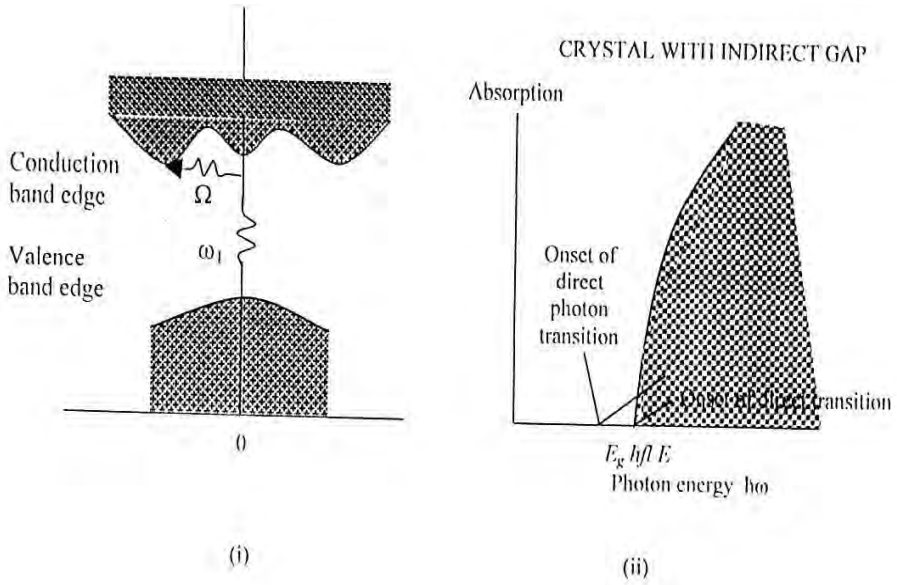

Figure.4.9: (i) Crystal diagram of indirect band gap, **(ii)** Absorption process.

distance into the semiconductor prior to absorption. Since, both photon emission and absorption are possible for hυ > ($E_g \pm E_p$), the absorption coefficient is then

$$K(h\upsilon) = k_i(h\upsilon) + k_d(h\upsilon) \qquad (4.9)$$

According to Bardeen et al [12] the relationships that exist for possible transition across the energy gap of the semiconductor show that the absorption coefficient k is given by the following conditions.

Direct transitions: For direct transition, absorption coefficient is given by the equation

$$k(h\nu) = A\,(h\nu - E_g)^n \qquad (4.10)$$

where n=1/2 for allowed transitions and n=3/2 for forbidden transitions and A is a constant.

Indirect transitions: In this condition, the absorption coefficient k is given by

$$k(h\nu) = B\,(h\nu - E_g \pm E_p)^n \qquad (4.11)$$

where n=2 for allowed transitions and n=3 for forbidden transitions and B is another constant.

E_g is the energy for direct transition, $_g$ is the energy for indirect transition and E_p is the phonon energy either absorbed (+) or emitted (-).

From all the above expressions, it is clear that a plot of $(kh\nu)^{1/n}$ and $(kh\nu)^n$ Vs $E_p(h\nu)$ curves would give the value of optical band gap E_g when carefully drawn for a particular transition process.

4.2.5.3 Refractive index and extinction coefficient

One of the most important optical constants of a material is its refractive index, which in general depends on the wavelength of the electromagnetic wave, through a relationship called dispersion. In materials where an electromagnetic wave can lose its energy during its propagation, the refractive index becomes complex. The real part is usually the refractive index, *n*, and the imaginary part is called the extinction coefficient, *K*. In this section, the refractive index and extinction coefficient will be presented in detail along with some common dispersion relations.

The refractive index of an optical or dielectric medium, is the ratio of the velocity c in vacuum to its velocity V in the medium; **n**=c/v. Using this and Maxwell"s equations, one obtains the well known Maxwell"s formula for the refractive index of substance as $n = \sqrt{\varepsilon_r \mu_r}$ where ε_r is the static dielectric constant or relative permittivity and μ_r the relative permeability. As μ_r = 1 for nonmagnetic substances, one gets, $n = \sqrt{\varepsilon_r}$, which is very useful in relating the dielectric properties to optical properties of materials at any particular frequency of interest. As ε_r depends on the wavelength of light, the refractive index also depends on the wavelength of light, and this dependence is called dispersion. In addition to dispersion, an electromagnetic wave propagating through a lossy medium experiences attenuation, which means it loses its energy, due to various loss mechanisms such as the generation of phonons (lattice waves), photogeneration, free carrier absorption, scattering, etc. In such materials, the refractive index becomes a complex function of the frequency of the light wave. The complex refractive index, denoted by *n**, with real part *n*, and imaginary part *K*, called the extinction coefficient, is related to the complex relative permittivity, $\varepsilon_r = \varepsilon_r' - j\varepsilon_r''$ by:

$$n^* = n - jk = \sqrt{\varepsilon_r} = \sqrt{\varepsilon_r' - j\varepsilon_r''} \quad (4.12)$$

where ε_r' and ε_r'' are, respectively, the real and imaginary parts of ε_r. Equation (4.13) gives:

$$n^2 - k^2 = \varepsilon_r'' \text{ and } 2nk = \varepsilon_r'' \quad (4.13)$$

In explicit terms, *n* and *K* can be obtained as:

$$n = (1/2^{1/2})[(\varepsilon_r'^2 + \varepsilon_r''^2)^{1/2} + \varepsilon_r']^{1/2} \quad (4.14)$$

$$k = (1/2^{1/2})[(\varepsilon_r'^2 + \varepsilon_r''^2)^{1/2} - \varepsilon_r']^{1/2} \quad (4.15)$$

The optical constants *n* and *K* can be determined by measuring the reflectance from the surface of a material as a function of polarization and the angle of incidence. For normal incidence, the reflection coefficient, *r*, is obtained as

$$r = \frac{1-n^*}{1+n^*} = \frac{1-n+jk}{1+n-jk} \quad (4.16)$$

The reflectance *R* is then defined by:

$$R = |r|^2 = \left|\frac{1-n+jk}{1+n-jk}\right|^2 = \frac{(1-n)^2+k^2}{(1+n)^2+k^2} \quad (4.17)$$

And we have calculated refractive index by using following equation

$$n = \left(\frac{1+\sqrt{R}}{1-\sqrt{R}}\right) + \sqrt{\frac{4R}{(1-R)^2} - K^2} \quad (4.18)$$

Notice that whenever *K* is large, for example over a range of wavelengths, the absorption is strong, and the reflectance is almost unity. The light is then reflected, and any light in the medium is highly attenuated.

4.2.6 Electrical Property Analysis of Thin Films

4.2.6.1 Measurements of the Resistivity and Electrical Conductivity

Resistivity and electrical conductivity of SnO2 thin film was measured by van-der Pauw"s method. van-der Pauw Method [13] is one of the standard and widely used techniques for the measurement of resistivity of thin film. The van-der Pauw method is a

technique for doing 4-probe resistivity and Hall effect measurements. The advantages of this method include low cost and simplicity. The van-der Pauw technique can be used on any thin sample of material and the four contacts can be placed anywhere on the perimeter/boundary, provided certain conditions are met:

- The contacts are on the boundary of the sample (or as close to the boundary as possible)
- The contacts are infinitely small (or as close as possible)
- The sample is thin relative to the other dimensions

A brief account of this method is given bellow because in our measurement we have used van-der Pauw Method.

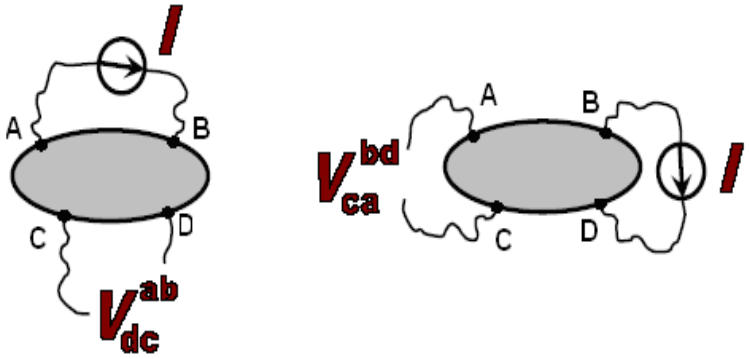

Figure 4.10: van-der Pauw method for resistivity measurements of a thin film of arbitrary shape

At first we select a region on the sample where four electrical contacts were made at four corners, say A, B, C, and D as shown in Fig 4.10. Silver past was used to the contact. The sample should not need to be of the shape as shown in figure. This method is applicable for any arbitrary shape of uniform sheet of material with four contacts applied to the periphery. Through commutative switches the connections are made between the film and the meter terminals.

If a dc current I_{AB} entering the specimen through the contact A and leaving through the contact, B produces a potential difference V_D-V_C between C and D then the resistance $R_{AB,CD}$ can be expressed as

$$R_{AB,CD} = \frac{V_D - V_C}{I_{AB}} = \frac{V_{CD}}{I_{AB}} \qquad (4.19)$$

Similarly,

$$R_{BC,DA} = \frac{V_A - V_D}{I_{BC}} = \frac{V_{DA}}{I_{BC}} \tag{4.20}$$

$$R_{CD,AB} = \frac{V_B - V_A}{I_{CD}} = \frac{V_{AB}}{I_{CD}} \tag{4.21}$$

And

$$R_{DA,BC} = \frac{V_C - V_B}{I_{DA}} = \frac{V_{BC}}{I_{DA}} \tag{4.22}$$

The resistivity of a thin film can be expressed as by the equation

$$\rho = \frac{\pi t}{\ln 2}\left[\frac{R_{AB,CD} + R_{BC,AD}}{2}\right] \times f\left[\frac{R_{AB,CD}}{R_{BC,DA}}\right] \tag{4.23}$$

or,

$$\rho = 4.53t \times \left[\frac{R_{AB,CD} + R_{BC,AD}}{2}\right] \times f\left[\frac{R_{AB,CD}}{R_{BC,DA}}\right] \tag{4.24}$$

Where t is the thickness of the film and the function f can be evaluated from the equation

$$\left[\frac{R_{AB,CD} - R_{BC,DA}}{R_{AB,CD} + R_{BC,DA}}\right] = \frac{f}{\ln 2} \arccos h \frac{\exp(\ln 2 / f)}{2} \tag{4.25}$$

If, $R_{AB,CD}$ and $R_{BC,DA}$ is almost equal, f may approximately equal to unity and then the equation (4.25) takes the form,

$$\rho = 2.265t\left(R_{AB,CD} + R_{BC,DA}\right) ohm - cm \tag{4.26}$$

4.2.6.2 Activation energy

The energy requisite to transfer charge from one neutral island to another is known as activation energy and it is denoted by ΔE. This is equivalent to the electrostatic binding energy of the charge to the island. The activation energy, which is related to the electron transport process in the material, can be expressed by a conventional type relation

$$\sigma = \sigma_0 \exp\left(\frac{-\Delta E}{2kT}\right) \tag{4.27}$$

Where k is the Boltzmann constant and T is the absolute temperature.

Equation (4.27) can be written as,

$$\ln \sigma = \ln \sigma_0 + \left(\frac{-\Delta E}{2kT} \right) \qquad (4.28)$$

The activation energy ΔE is calculated from the slop of a curve lnσ vs. (1/T). So the activation energy is given by

$$\Delta E = -\frac{\ln \sigma}{1/T} 2k \qquad (4.29)$$

The circuit arrangements used for the resistivity and conductivity measurement are shown in Fig.4.10

References:

[1] Brown, R., Maissel, L. I., and Glang, R. (eds) Hand Book of Thin Film Technology, Mc Graw Hill, New. York, 1970.

[2] Tareev, B., "Physics of Dielectric Materials", Mir publisher, Moscow, pp 46, 1975.

[3] Sebastian, T., Jayakrishnan, R., Kartha, C. S., Vijayakumar, K. P., "Characterization of Spray Pyrolysed $CuInS_2$ Thin Films", The Open Surf Sci, Vol 1, No. 1, pp 1-6, 2009.

[4] Kittel, C., "Introduction to Solid State Physics", 7th edition, Jhon Wiley and Sons, Inc., New York, 1996.

[5] Howland, R., and Benatar, L., "A Practical Guide to Scanning Probe Microscopy", Park Scientific Instruments, Sunnyvale, 1997.

[6] Cullity, B. D., "Elements of X-ray Diffraction", Addison-Wesley Publishing Company. Inc. USA, 1959.

[8] Vankar, V. D., Das, S. R., Nath, P.and Chopra, K. L., "Structure of vacuum, evaporated $Cd_xZn_{1-x}S$ thin films" Phys. Stat. Sol., Vol-45, PP 665-669, 1978.

[9] Nahrwold, R., Ann Physik, Vol-31, pp 467, 1887.

[10] Tolansky, S., "Multiple Beam Interferometry of Surface and Films", Oxford University Press, London, 1948.

[11] Gottling, J. G., and Nikol, W. S., "Double-Layer Interference in Air-CdS Films", Opt. Soc. Am., Vol-56, No. 9, pp1227-1230, 1966.

[12] Barden, J., Blatt, F. J., and Hall, L. H., Proc of Atlantic City Photoconductivity Conference, 1954.

[13] van-der Pauw, L. J., Philips Res. Rept., Vol-13, pp-1, 1958.

CHAPTER 5
RESULTS AND DISCUSSION

5.1 Introduction

The objectives of this study are to synthesis and characterize $Zn_{1-x}Co_xO$ (x=0.00, 0.05, 0.15, 0.25, 0.35) thin films by spray pyrolysis method. In this chapter the results and discussion of the various experimental studies namely surface morphology, structural, optical and electrical properties of $Zn_{1-x}Co_xO$ thin films have been presented and discussed step by step.

5.2 Surface Morphology and Structural Investigation

5.2.1 SEM study

Surface morphology of $Zn_{1-x}Co_xO$ thin films was observed using SEM under 10000 magnification. Fig. 5.1 (a-d) is shown that all the films are found well covered on the glass substrate. SEM reveals that sprayed particles (cluster of atoms) are adsorbed onto the glass substrate. Nanofibers are observed in pure ZnO thin film. The average diameter of the fibers is around 600 nm fig 5.1 (a). Similar feature was also reported by other researchers [1, 2]. Due to interstitial holes of ZnO are filled with cobalt, nanofibers are observed more clearly and the average diameter of the fiber increases around 750 nm in 5% doping concentration fig 5.1 (b). But after 5% doping due to Zn are substituted by cobalt nanofibers are observed but the diameter of the fiber decreases around 620 nm in 15% doping fig 5.1 (c). Finally for 25% doping fibers become narrower around 300 nm. SEM photograph reveals that sprayed particles (cluster of atoms) are adsorbed onto the glass substrate.

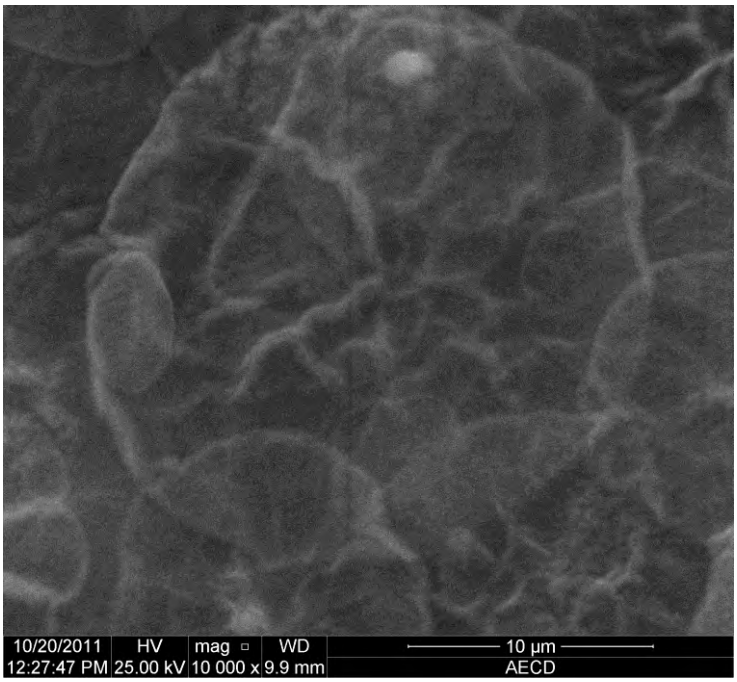

Figure 5.1 (a): SEM image of pure ZnO thin film

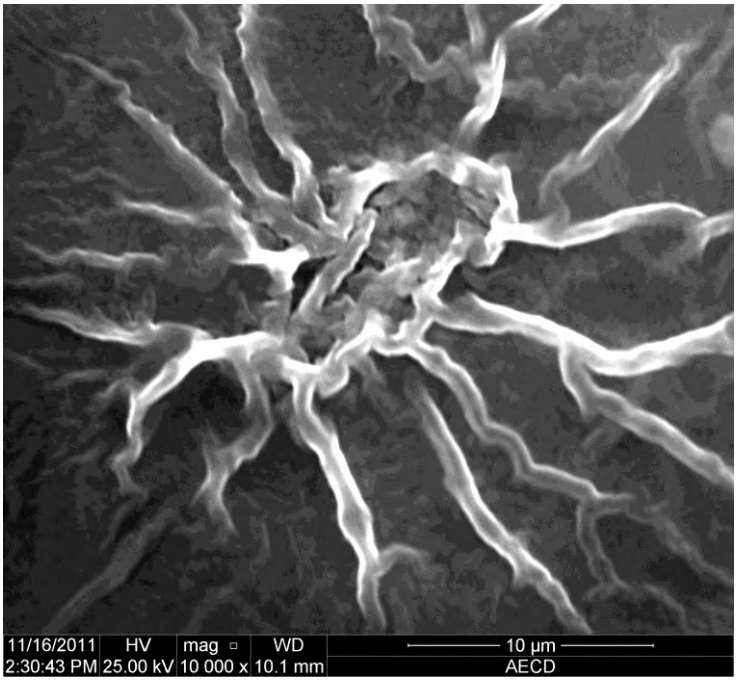

Figure 5.1 (b): SEM image of 5% Co doped ZnO thin film

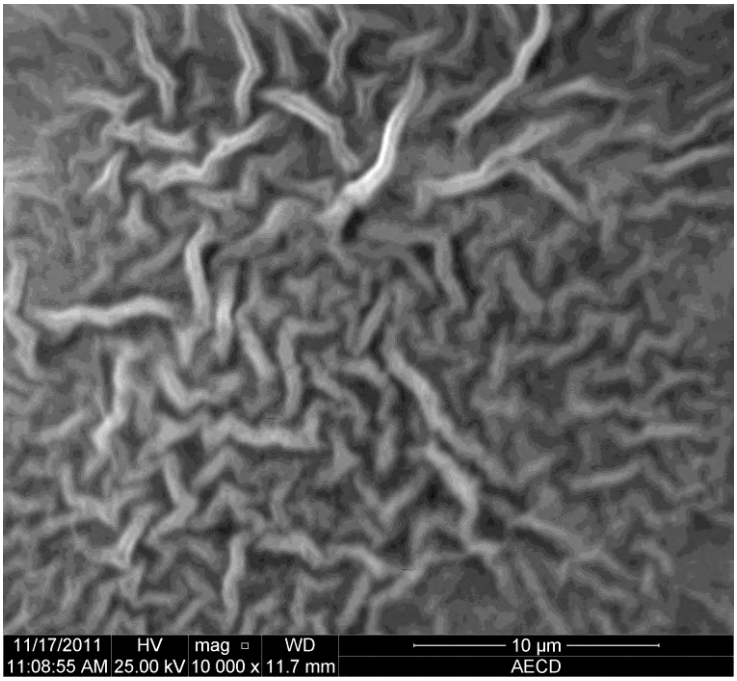

Figure 5.1 (c): SEM image of 15% Co doped ZnO thin film

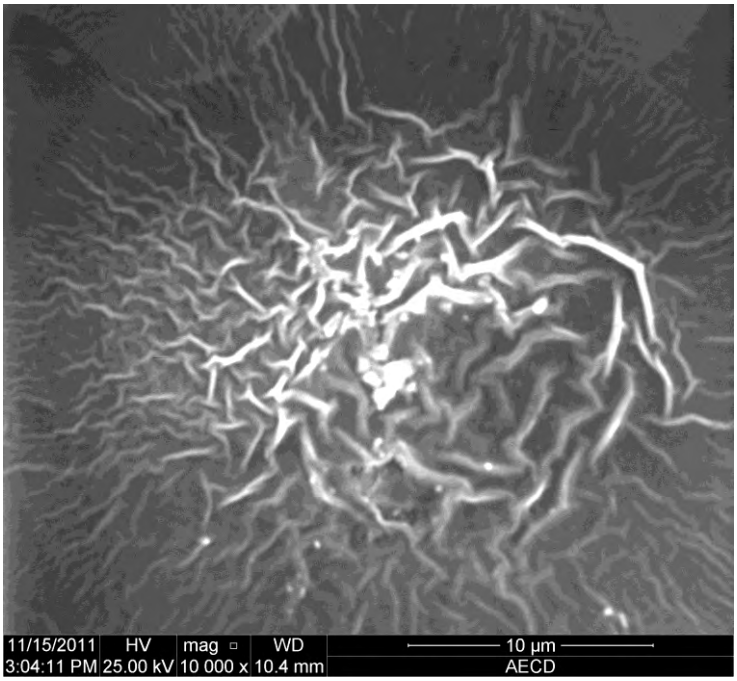

Figure 5.1 (d): SEM image of 25% Co doped ZnO thin film

5.2.2 EDX studies

The quantitative analysis of the as-deposited ZnO films carried out by EDX is shown in Figure 5.2 (a). Two strong peaks corresponding to Zn and O were found in the

spectrum, which confirms the high purity of the ZnO thin film. At high operating voltage the electron beam penetrates the film and reaches the glass surface, which results the Si peak. And all peaks for Zn, Co and O are obtained for 15% doping concentration. From the EDX pattern it is observed that the height of the peak for Zn decreases and Co increases with the increase of doping concentration. The percent of Zn, Co and O present in different values of Co are shown in the table 5.1.

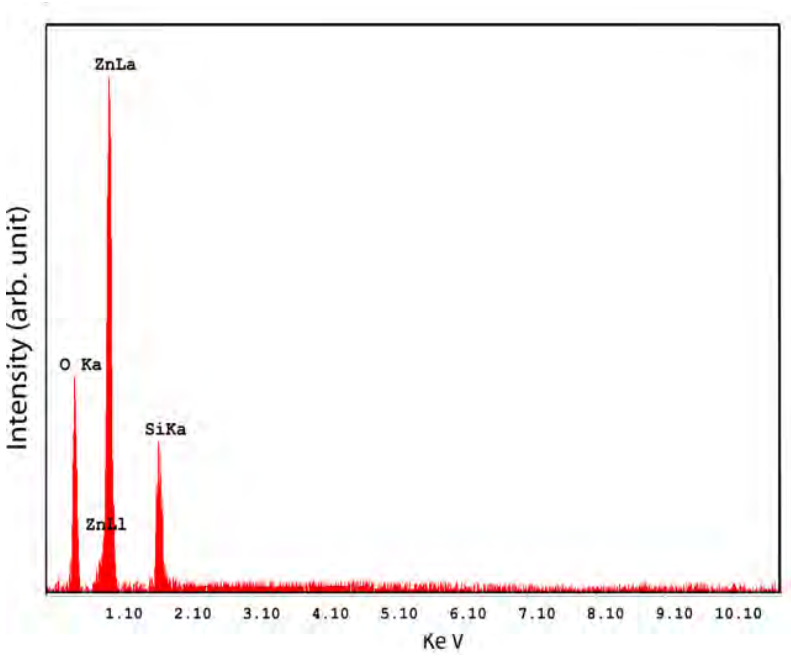

Figure 5.2 (a): EDX spectrum of pure ZnO thin films

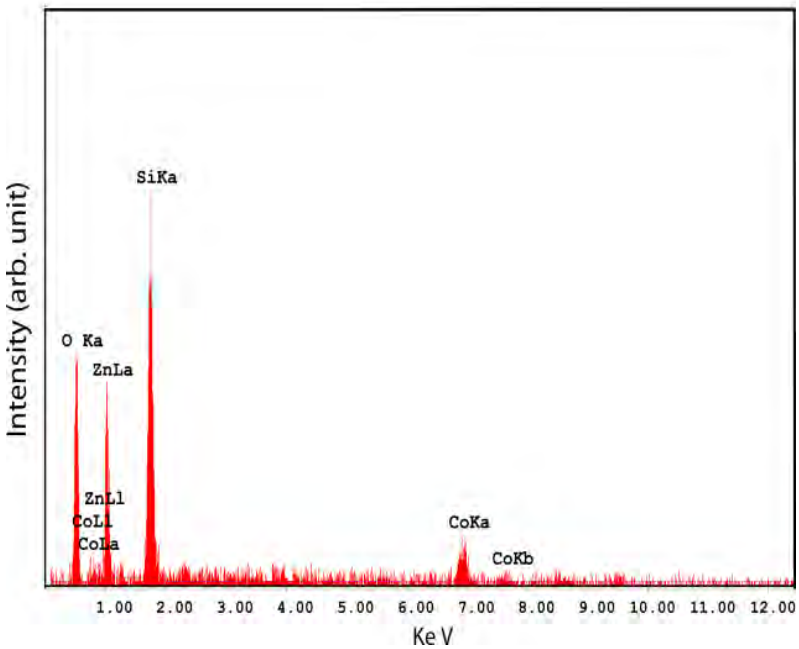

Figure 5.2 (b): EDX spectrum of 15% Co doped ZnO thin films

Table: 5.1 Atomic% of different Co compositions of $Zn_{1-x}Co_xO$ thin films.

Sample	Element, Atomic %			
	Zn	**O**	**Si**	**Co**
Pure ZnO	76.32	17.08	6.48	0.00
15% Co ZnO	38.19	42.50	7.45	10.26

From the above data it is evident that for all the films the amount of Zn, Co and O are present at stoichiometric ratio.

5.2.3 XRD Study

The XRD has been taken on as-deposited pure and Co doped ZnO thin film. X-ray diffractograms of all the samples have been recorded using monochromatic CoK_α radiation (λ = 1.7902 Å), scanning speed 2 degree/min**,** starting from 10º and ending at 70º to ensure the information of the single phase nature of the sintered product. Peak intensities are recorded corresponding to their 2θ values.

Using the data of diffractogram, the d_{hkl} (inter-planar distance) values and their corresponding <hkl> values have been calculated. The d_{hkl} values of pure and Co doped films and their corresponding <hkl> values from the standard JCPDS Card and the calculated lattice parameter (a, c) values, deviation of 2θ and grain size of these samples are tabulated in table 5.2. The X-ray diffractogram of ZnO samples with different concentration of Co are shown in Fig 5.3. It is seen from these diffractograms that the pure and Co doped ZnO films respectively, have different peak at d_{hkl} values with its corresponding crystal planes in JCPDS card. Different fundamental peaks were identified as (100), (002), (101), (102) and (110), for pure ZnO films which indicate the hexagonal wurtzite structure of ZnO. Grain size of the prepared ZnO thin film was determined from the stronger peaks of (002) from each XRD patterns using Scherrer formula,

$$D_g = \frac{0.94\lambda}{\Delta \cos\theta}$$

Where D_g is the average grain size, λ is the wavelength of the radiation used as the primary beam of CoK_α (λ= 1.7902 Å), θ is the angle of incidence in degree (Bragg angle) and Δ is the full width at half maximum (FWHM) of the peak in radian, which was determined experimentally after correction of instrumental broadening (in the present case it is 0.05°). Thin films, where two strong peaks (100) and (002) are shown in expanded form to understand the variation of FWHM and peak shift of Bragg peaks with temperature. Lattice parameters a and c were determined from the 2θ value. It is seen that the value of lattice parameter a was observed 3.232 Å for pure ZnO and it shifted to 3.215 Å after 5% Co doping. Similarly the value of a was observed changed due to different percentage of Co dopping is given in table 5.3. Similarly the value of the parameter c was 5.172 Å for pure ZnO films and it shifted to 5.142 Å for 5% Co doping. Both the values of a and c change with increasing of Co doping. It was observed that $\Delta 2\theta^o$ value is different for Co doped ZnO films than pure ZnO thin films. It is observed that the peaks in the doped films shift from their standard positions in the presence of the dopant. The shift in the lattice parameter is mainly due to the dopant occupying interstitial positions in the lattice. No peaks corresponding to either Co metal or any of its oxides are observed in any of the diffractograms, which indicates that there is no additional phase present in $Zn_{1-x}Co_xO$ films, at least within the limit of (35%). When the Co concentration increases the intensity of the (002) peak decreases with increase in FWHM. This is due to the lattice disorder and strain induced by Co^{2+} substitution in the host lattice [3].

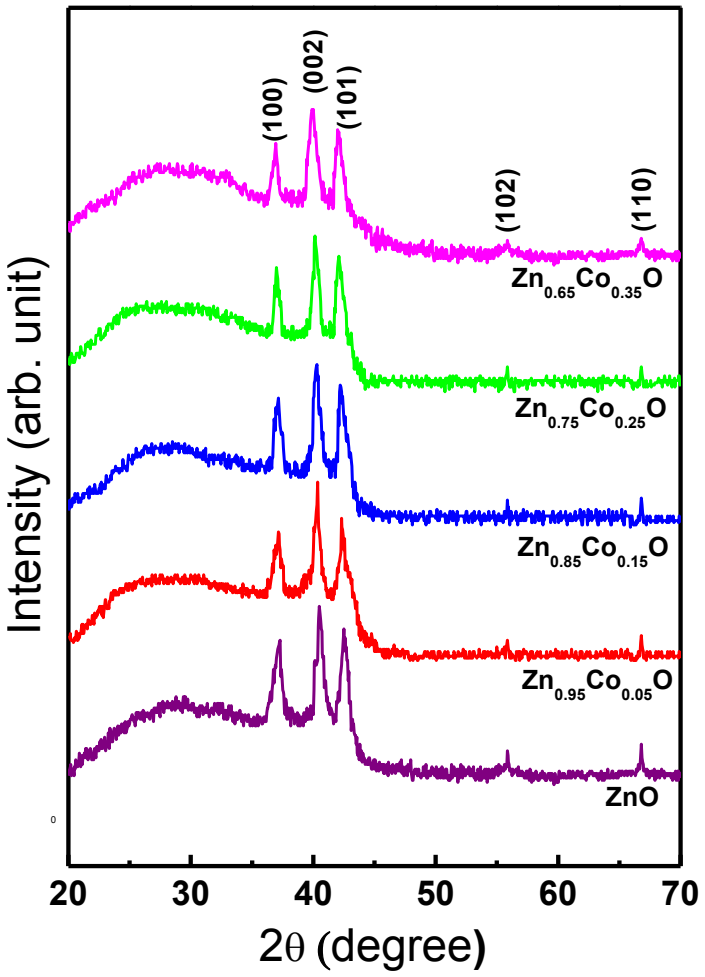

Figure 5.3: X-ray diffraction patterns of $Zn_{1-x}Co_xO$ thin films

Table 5.2: X-ray diffraction data, lattice parameters, grain size for pure and Co doped ZnO thin films.

Composition	For (100) reflection			For (002) reflection			Grain size from (002) reflection	c/a Ratio
	2θ°	d_{hkl}(Å)	a (Å)	2θ°	d_{hkl}(Å)	c(Å)	nm	
ZnO	37.30	2.799	3.232	40.50	2.586	5.172	57	1.602
$Zn_{0.95}Co_{0.05}O$	37.50	2.784	3.215	40.75	2.571	5.142	41	1.599
$Zn_{0.85}Co_{0.15}O$	37.40	2.791	3.223	40.60	2.580	5.160	42	1.601
$Zn_{0.75}Co_{0.25}O$	37.65	2.773	3.203	40.80	2.568	5.136	43	1.602
$Zn_{0.65}Co_{0.35}O$	37.60	2.777	3.207	40.70	2.574	5.148	46	1.605

5.3 Optical Properties

5.3.1 Optical Absorbance

Optical properties of pure and Co doped ZnO as deposited thin films such as transmittance, absorbance, direct band gap, refractive index, etc were calculated. Absorbance spectra were taken within range of 300 to 1100 nm for films. Fig 5.4 shows the variation of absorbance with wavelength of pure and Co doped ZnO thin films. It is found that the absorbance is decreased with higher wavelength slowly. It is also observed that absorption is rapid increase at lower wavelength. Absorbance spectra shows low absorbance in the entire wavelength region but it high at wavelength < 350 nm. This increase of absorbance in Co doped samples can be explained as due to sp-d exchange interections between the band electrons and the localized d electrons of Co^{2+} ions.

The important optical characteristic of ZnO film is that they are transparent in the wavelength ranging from 400 to 1100 nm. At wavelengths shorter than 400 nm, absorption occurs due to the fundamental band gap, and thus light cannot be transmitted due to quantum phenomenon. At longer wavelengths, reflection occurs because of the plasma edge, and light cannot be transmitted due to a classical phenomenon. The corresponding wavelengths for those transmissions are determined by a number of fundamental characteristics as well as by the concentration of free electrons.

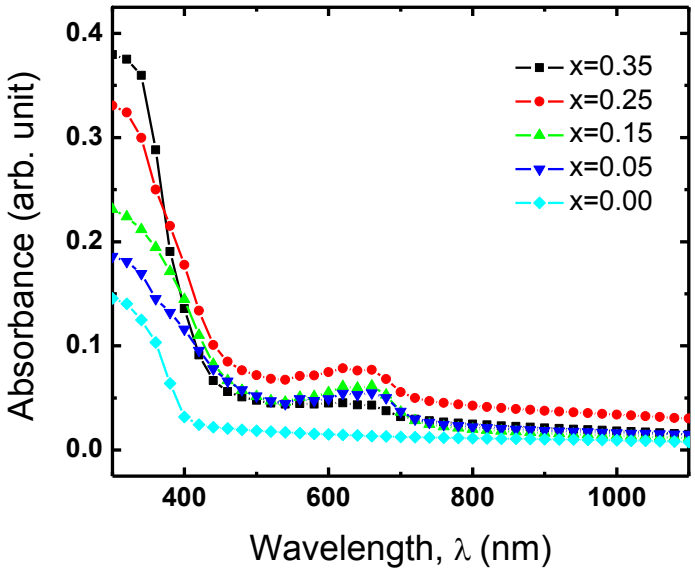

Figure 5.4: Variation of absorbance as a function of wavelength for $Zn_{1-x}Co_xO$ films for different concentrations

Comparing with the undoped ZnO, we find that the higher absorbance in Co doped ZnO, which is due to sp-d exchange interactions between the band electrons and the localized d electrons of Co^{2+} ions. There is a characteristic absorption peak from 550 to 650 nm correlated with the d–d transitions among Co^{+2} ions associated with the tetrahedral crystal field splitting in ZnO lattice. Three absorbance peaks are observed in others research these are:

$^4A_2(F)$	$^2A_1(G)$	560nm
$^4A_2(F)$	$^4T_1(P)$	620nm
$^4A_2(F)$	$^2E(G)$	660nm [4]

Similar results are found by Yang, S. G. et al [5]. Transition metal complexes appear colored because the splitting of the d-orbital matches the energy of certain wavelengths of visible light. The observation of these transitions in the absorbance spectra of our $Zn_{1-x}Co_xO$ films thus clearly reveals that the added cobalt atoms have substituted Zn^{+2} cations and are present in +2 state.

5.3.2 Optical Transmission

Transmission spectra were taken within range of 300 to 1100 nm for films. Fig 5.5 shows the variation of transmittance with wavelength for pure and Co doped ZnO thin films having thickness 200 nm It is seen from the graph that the values of transmittance is high in the visible and IR region it is minimum at wavelength ~ 300 nm. Films prepared at 300 ºC exhibit a transmission of > 80% in the visible and near IR region; again it is found > 70% in the visible and near IR region for Co doped film, which is found to be smaller than that of undoped film. Below 450 nm there is a sharp fall in the %T of the films, which is due to the strong absorbance of the films in this region.It is found that transmittance decreases with increasing concentration of the dopant, which is due to the decrease in the crystalline nature of the doped films as revealed by XRD. The transmittance of the films is also influenced by a number of effects, which include surface roughness and optical inhomogenity in the direction normal to the film surface. Additional absorption peaks appear in the case of Co substituted ZnO films. Similar result was obtained by other researcher [6].

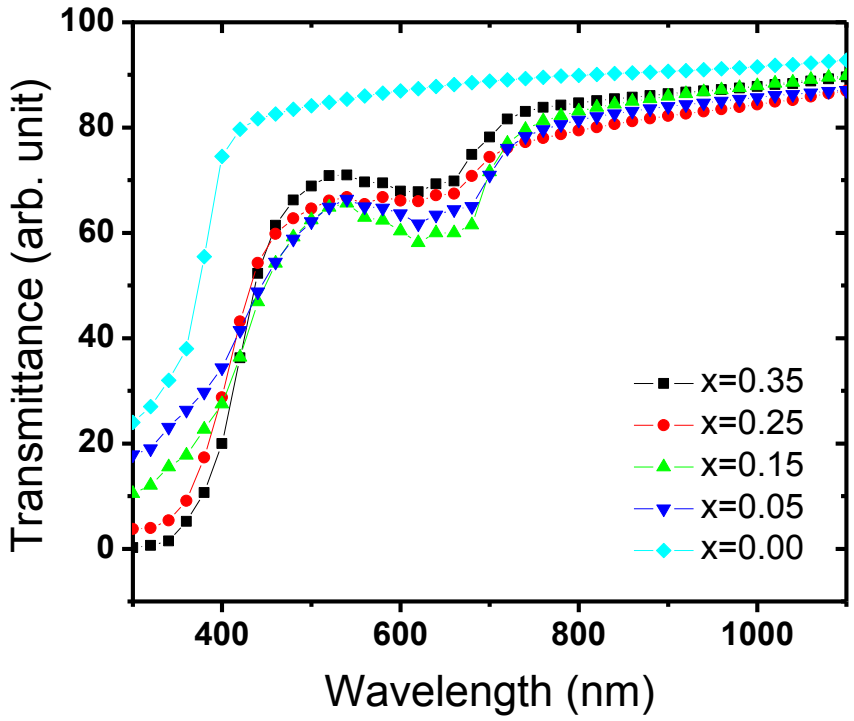

Figure 5.5: Variation of transmittance as a function of wavelength for $Zn_{1-x}Co_xO$ films for different concentrations

5.3.3 Absorption Coefficient

From transmittance spectra, the absorption coefficient and optical band gap were calculated for pure and Co doped ZnO thin films. The absorption coefficient (α) was calculated from the transmission spectra using the relation

$$\alpha = - (\ln T)/t$$

Variation of α with photon energy (hν) for pure and Co doped ZnO thin films is shown in Fig 5.6. This figure shows the distinction of α with photon energy for Co doping. The α is of the order of 10^6 m^{-1} which may also be suitable for a transparent conducting film. From the figure it is observed that α first increases slowly in the low energy region i.e. in the high wavelength region and then increases sharply near the absorption edge. The value of α depends on Co doping.

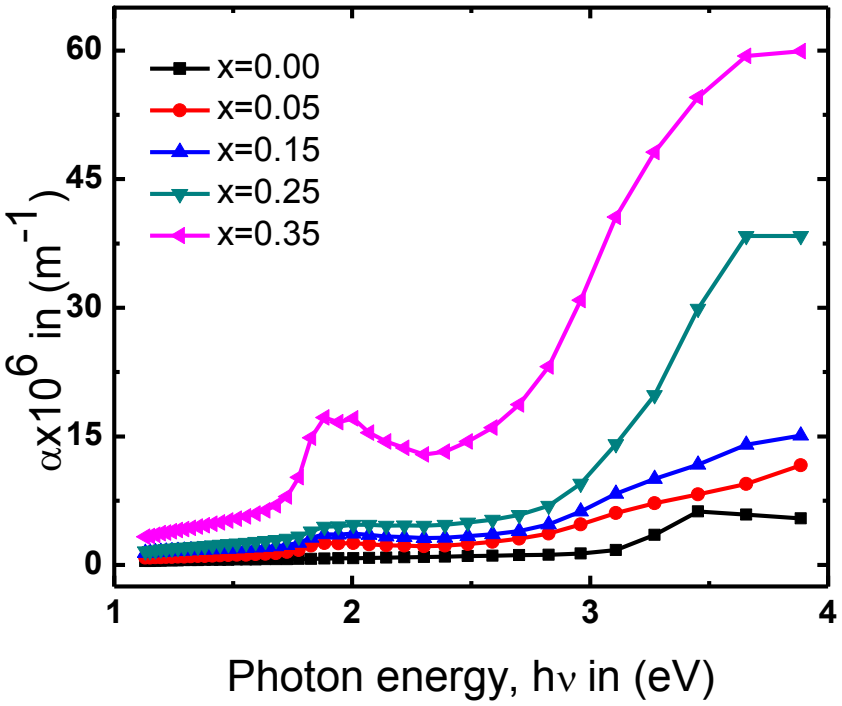

Figure 5.6: Variation of absorption coefficient as a function of wavelength for $Zn_{1-x}Co_xO$ films for different concentrations

5.3.4 Optical Band Gap

The energy gap in a semiconductor is responsible for the fundamental optical absorption edge. The fundamental absorption process is one in which a photon is absorbed and an electron is excited from an occupied valance band state to an unoccupied conduction band state. If photon energy is less than the gap energy, such process is impossible and photon energy will not be absorbed. Such inter band absorption process are possible only if the photon energy is higher than the gap energy. Since α is used to describe the reduction in intensity of light in a medium as a function of distance, therefore higher values of α is an indication of more reduction in intensity. Figure 5.7(a).shows the plots of $(\alpha h\nu)^2$ vs. photon energy ($h\nu$) for direct transition. The optical band gap (Eg) is determined from the plots of $(\alpha h\nu)^2$ vs. photon energy ($h\nu$) for direct transition for $Zn_{1-x}Co_xO$ thin films. The direct band gap energy of the films have been obtained from the intercept on the energy axis after extrapolation of the straight line section of $(\alpha h\nu)^2$ vs. $h\nu$ curve. The band gap of the films varied between 3.2 eV to

2.7 eV. It is observed that small amount of Co present in the films greatly affects the optical band gap of ZnO. The band gap was observed to decrease with an increase of Co in the concentration. A decrease in band gap energy with increase of doping concentration in this case, which was also reported by Kim, K. J. et al and Samanta, K. et al [7, 8]. We think that this shift of the band gap with the Co incorporation interpreted as mainly due to the sp-d exchange interactions between the band electrons and localized d electrons of the Co^{2+} ions substituting Zn ions. The s-p and p-d exchange interactions give rise to a negative and a positive correction to conduction and valance band edges, leading to narrowing of the band gap [9]. The nature of this variation in the band gap energy may be useful to design a suitable window material in fabrication in solar cells. The variations of optical band gap with different film concentrations are shown in fig 5.7 (b).

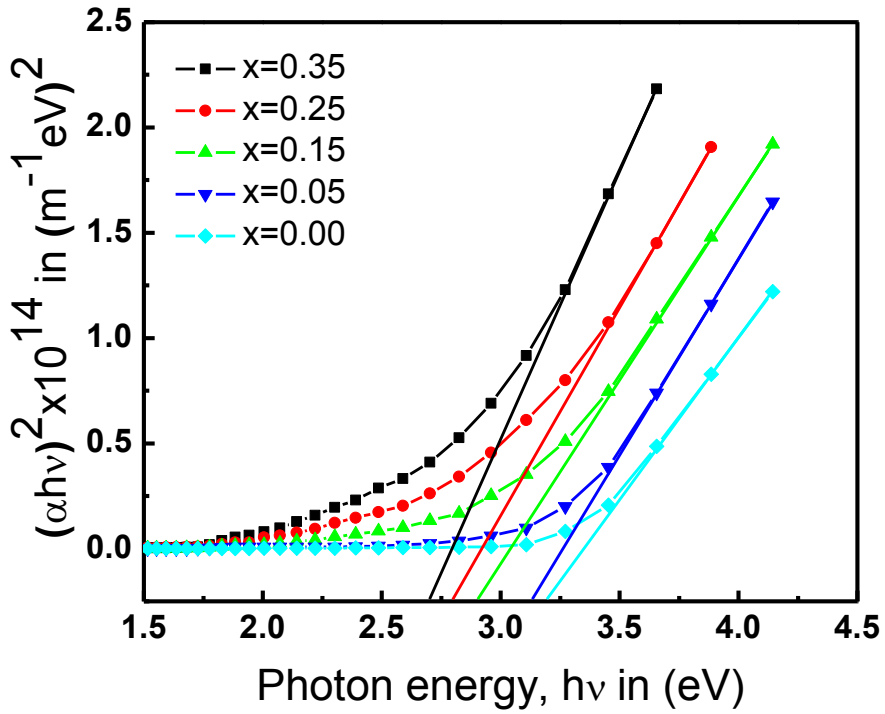

Figure 5.7 (a): Plots of $(\alpha h\nu)^2$ vs. photon energy ($h\nu$) for $Zn_{1-x}Co_xO$ thin films

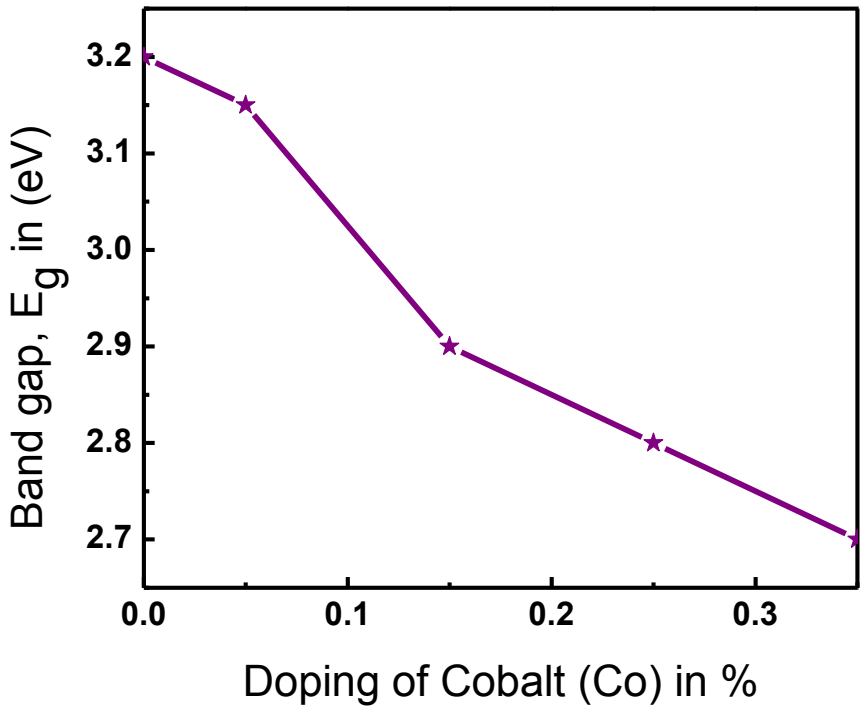

Figure 5.7 (b): Variation of band gap of $Zn_{1-x}Co_xO$ thin films versus compositions

5.3.5 Extinction coefficient

We know α is a quantity that characterizes how easily a material or a medium can be penetrated by a beam of light. Here α can be calculated from observed absorbance data using Beer Lambert's formula $\alpha = 2.303\left(\frac{A}{d}\right)$, where A is the optical absorbance and d is the thickness of the film. The extinction coefficient (k) is the imaginary part of the complex index of refraction, which also relates to light absorption. The extinction coefficient can be obtained from the relation; $K = \frac{\alpha\lambda}{4\pi}$.where λ is the wavelength [10].

The variation of extinction coefficient with wavelength is shown in Figure 5.8. It is observed that the extinction coefficient increases with the increase of Co incorporation. The rise and fall in the extinction coefficient is due to the variation of absorbance. The fall in the extinction coefficient may be due to the absorption of light at the grain boundaries. From figure it is clear that k decreases rapidly with increasing wavelength

from 300 to 400 nm and after that the value of „K" remains constant. The extinction coefficient is almost constant in the higher wavelength region and when the energy exceeds band gap energy it increases rapidly.

Since the extinction coefficient describes the attenuation of light in a medium and increase of k with the increase of hν indicates the probability of raising the electron transfers across the mobility gap with photon energy. Therefore the higher values of k are the representation of greater attenuation of light in a thin film and also the higher probability of raising the electron transfer across the mobility gap with the photon energy.

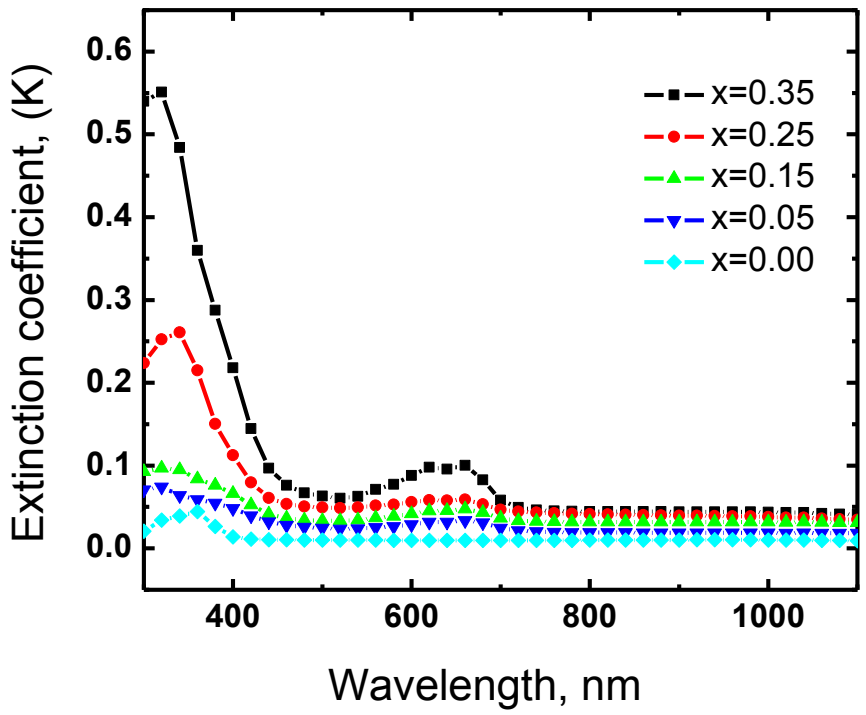

Figure 5.8: Variation of extinction coefficient as a function of wavelength for $Zn_{1-x}Co_xO$ films of different concentrations.

5.3.6 Refractive index

In order to calculate the refractive index of the films, we recorded the reflectance spectra of the films. The refractive index has been calculated using the relation

$$n = \left(\frac{1+R}{1-R}\right) + \sqrt{\left(\frac{4R}{(1-R)^2} - k^2\right)}$$

where k is the extinction coefficient and R is the optical reflectance [11].

The refractive index dependence on the wavelength for various compositions are shown in Figure 5.9. The refractive index of the film significantly changes with the deposition parameter. From the figure it is evident that the refractive index increases with the composition of the film. The increase in the Co incorporation in the film results in the overall increase in the refractive index. The gradual decrease of refractive index with wavelength i.e. increase with photon energy implies that the normal dispersion occurred before the absorption edge followed by anomalous dispersion.

Low refractive index occurs due to successive internal reflections or due to the trapped photon energy within the grain boundary. It is also attributed to the variety of different impurities and defects.

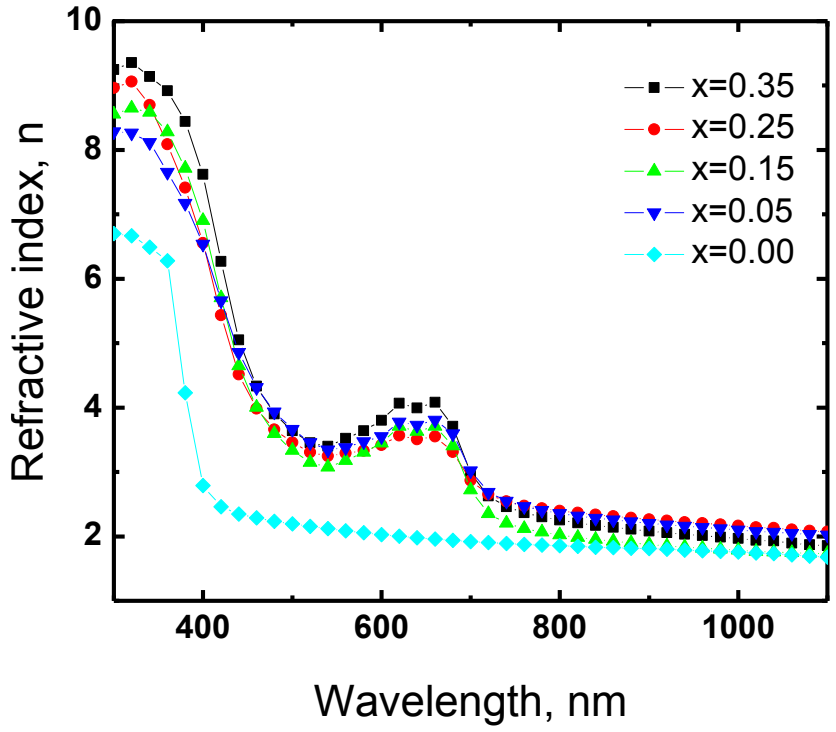

Figure 5.9: Variation of refractive index as a function of wavelength for $Zn_{1-x}Co_xO$ films of different concentrations.

5.3.7 Dielectric constants

The real ε_r and imaginary ε_i parts of the dielectric constant were determined using the formula $\varepsilon_r = n^2 - k^2$ and $\varepsilon_i = 2nk$ [12] .The variation of the real (ε_r) and imaginary (ε_i) parts of the dielectric constant for different film concentrations are illustrated in Figure 5.10(a, b). The complex dielectric constant is fundamental intrinsic material property. The real part of it is associated with the term that how much it will slow down the speed of light in the material and imaginary part gives that how a dielectric absorb energy from electric field due to dipole motion. The real part ε_r is the normal dielectric constant and imaginary part ε_i represents the absorption associated of radiation by free energy. It is seen that both ε_r and ε_i decrease with increasing wavelength. The figures revealed that the values of the real part are higher than that of the imaginary part and follow the same pattern.

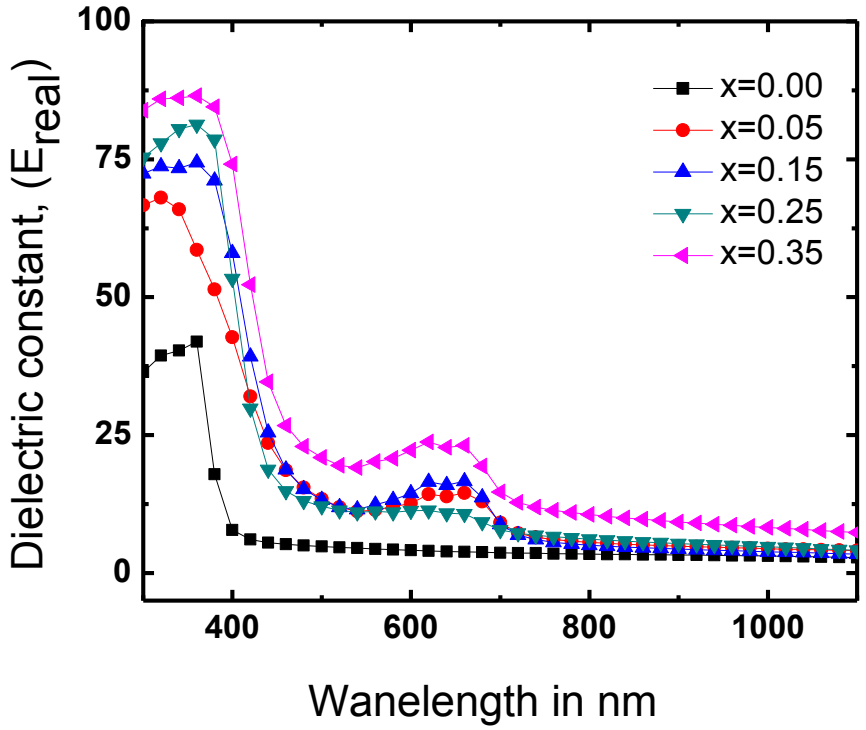

Figure 5.10 (a): Variation of real part of dielectric constants as a function of wavelength for $Zn_{1-x}Co_xO$ films of different concentrations.

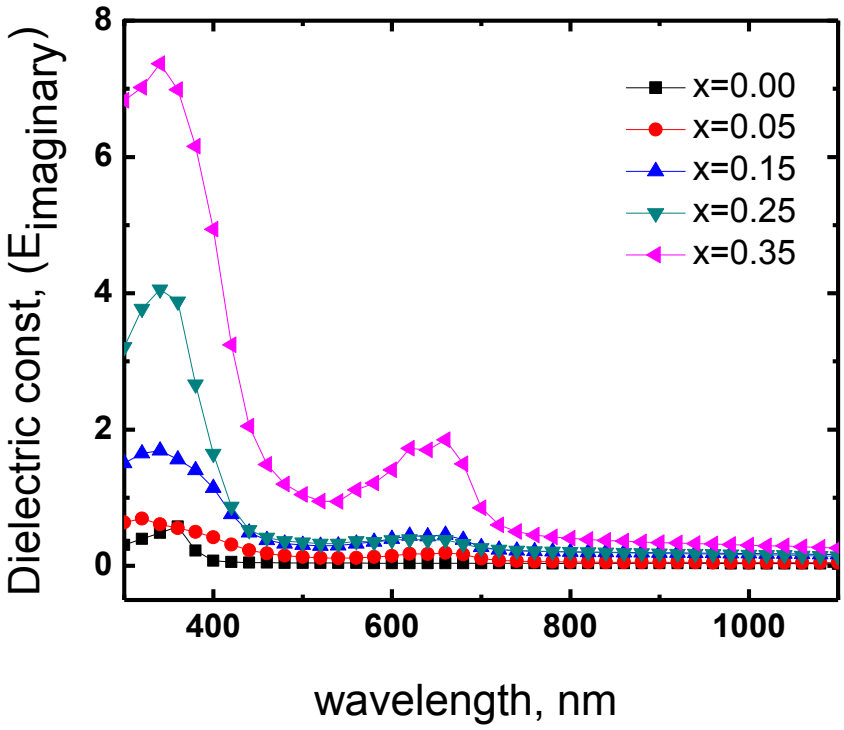

Figure 5.10 (b): Variation of imaginary part of dielectric constants as a function of wavelength for $Zn_{1-x}Co_xO$ films of different concentrations.

5.3.8 Optical conductivity

Figure 5.11 shows the variation of optical conductivity with the incident photon energy. The optical conductivity was determined using the relation $\sigma = \alpha nc/4\pi$ where c is the velocity of light [13]. The increased optical conductivity at high photon energies is due to the high absorbance of thin films in that region. The absorption coefficient, α can be calculated from observed absorbance data using Beer Lambert"s formula

$$\alpha = 2.303\left(\frac{A}{d}\right)$$

where A is the optical absorbance and d is the thickness of the film. The extinction coefficient can be obtained from the relation,

$$K = \frac{\alpha\lambda}{4\pi}$$

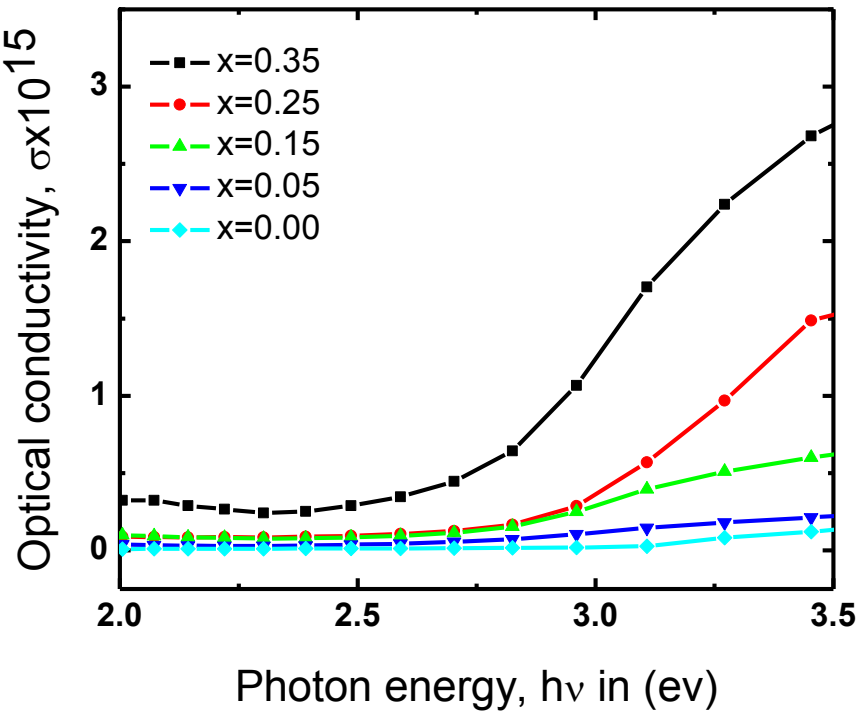

Figure 5.11: Variation of optical conductivity versus photon energy for $Zn_{1-x}Co_xO$ films of different concentrations.

5.4 Electrical Properties

Electrical parameters like resistivity, conductivity, activation energy etc. of the $Zn_{1-x}Co_xO$ films were measured by the van-der Pauw method. D.C electrical resistivity measurements were made in air for freshly deposited films from room temperature 300 K to 430 K by van-der Pauw method and data were taken by increasing the temperature of the film slowly. On increasing up to a maximum temperature (430 K) and then film cooled down slowly to room temperature. Variation of current and voltage corresponding temperature recorded in data and then calculated electrical parameters. For dc conductivity measurement, a 15V dc fixed bias was maintained. A power supply (Heathkit, Model: IP-2717A) was used to pass a constant dc current through the test sample. An electrometer (Keithley, Model: 614) was used to monitor the current through the sample and a digital multimeter (Model: DM-206) was used to measure the potential differences across each sample. The glass substrate was heated by a specially

designed heater and the temperature was measured by a chromel-alumel thermocouple placed on the middle of the substrate.

5.4.1 Variation of Resistivity with Temperature

The variation of electrical resistivity with temperature for as deposited $Zn_{1-x}Co_xO$ thin films are shown in Figure 5.12. From the figure it is seen that resistivity decreases with the increase of temperature. This type of variation indicates the semiconducting behavior of the films. The resistivity decreases with the increasing of cobalt concentration.

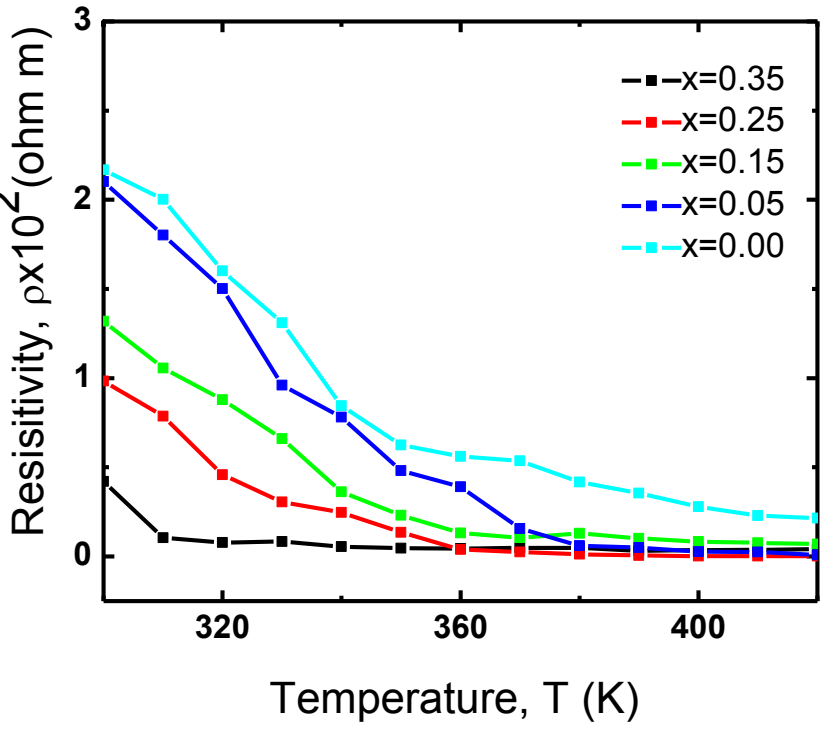

Figure 5.12: Variation of electrical resistivity with temperature for as deposited $Zn_{1-x}Co_xO$ films.

5.4.2 Variation of Conductivity with Temperature

The variation of electrical conductivity with temperature for as deposited $Zn_{1-x}Co_xO$ thin films are shown in Figure 5.13.

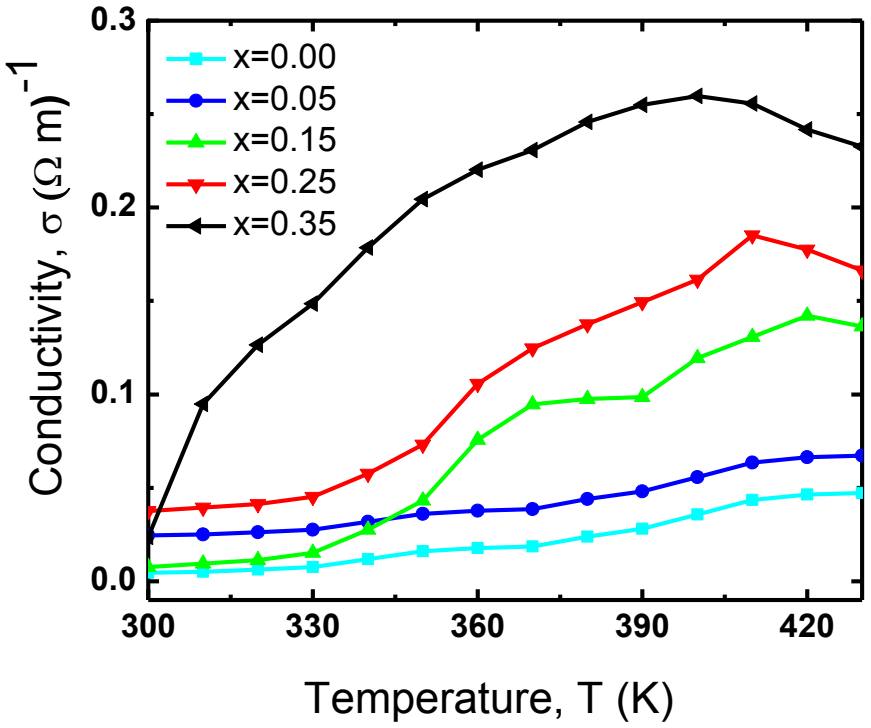

Figure 5.13: Variation of electrical conductivity with temperature for as deposited $Zn_{1-x}Co_xO$ films.

From the figure it is seen that the conductivity increases with the increase of temperature. This type of variation indicates the semiconducting behavior of the films. The conductivity increases with the increasing of cobalt concentration. In semiconductor, the numbers of carriers available for electrical conduction are increased with temperature.

In general for a semiconducting material, dc conductivity increases exponentially with temperature indicating that the conductivity is a thermally activated process. Mathematically, it can be expressed by the well-known Arrhenius relation as

$$\sigma_{dc} = \sigma_o \exp(-\Delta E / 2\,kT)$$

where σ_o is called pre-exponential factor, ΔE is called the activation energy, T is the absolute temperature and k is Boltzmann constant. These parameters are of significance to differentiate the nature of various conduction mechanisms. Figure 5.13 shows temperature dependence of dc conductivity σ_{dc}, for $Zn_{1-x}Co_xO$ film. From the figure, it is clear that the dc conductivity σ_{dc}, varies exponentially with temperature, as lnσ dc vs.

1000/T curves are straight lines. Such behavior is consistent with above equation. The electrical conduction of the films follows a mechanism in which the electron or hole hops from one localized site to the next. Localized state is a state of motion in which an electron may be found anywhere within a region of a material of linear extent smaller than that of the materials. Whenever it is transferred to another site, the surrounding molecules respond to this perturbation with structural changes and the electron or hole is temporarily trapped in the potential well leading to atomic polarization. The electron resides at this site until it is thermally activated to migrate to another site.

Another aspect of this charge hopping mechanism is that the electron or hole tends to associate with local defects. So, the activation energy for charge transport may also include the energy of freeing the hole from its position next to the defects [14,15].

5.4.3 Variation of Activation Energy

The lnσ versus 1/T graph for the as-deposited $Zn_{1-x}Co_xO$ thin films are represented in Figure 5.14. The straight lines for the films of different concentrations are drawn by using least mean square fitting method (not seen here). From the slope, the activation energy of the films of different concentrations has been calculated.

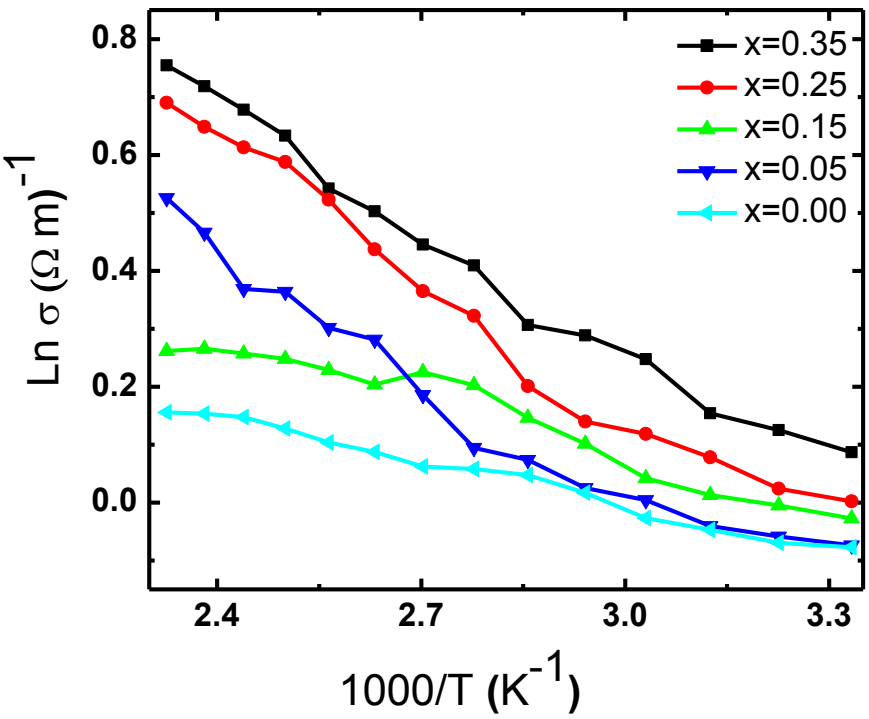

Figure 5.14: Plots of lnσ versus 1/T graph for as-deposited $Zn_{1-x}Co_xO$ thin films.

Figure 5.15 represents the variation of activation energy of different concentration for the as-deposited thin films. It is seen from the graph that the activation energy increases with cadmium incorporation.

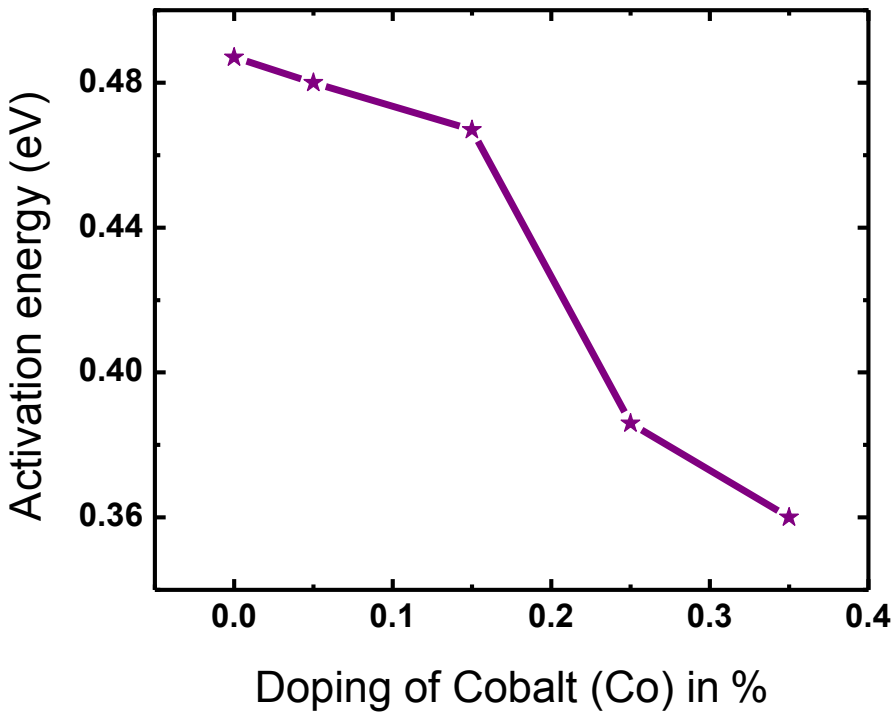

Figure 5.15: Variation of activation energy of different concentration for as-deposited $Zn_{1-x}Co_xO$ films.

References

[1] Islam, M. R., and Podder, J., "Optical Properties of ZnO Nano Fiber Thin Films Grown by Spray Pyrolysis of Zinc Acetate Precursor", Cryst. Res. Techn., Vol-44, No. 3, pp 286-292, 2009.

[2] Llicana, S., Caglara, M., and Yakuphanoglu, F., "Electrical Conductivity, Optical and Structural Properties of Indium-doped ZnO Nanofiber Thin Film Deposited by Spray Pyrolysis Method", Physica E., Vol-35, No. 131, 2006.

[3] Subramanian, M., Tanemura, M., Hihara, T., Ganesan, V., Soga, T., and Jimbo, T., "Magnetic Anisotropy in Nanocrystalline Co-doped ZnO Thin Films", Chem. Phys. Lett., Vol-, No. 487, pp 97-100, 2010

[4] Yoo, Y. Z., Fukumura, T., Jin, Z., Hasegawa, K., Kawasaki, M., Ahmet, P., Chikyow, T., and Koinuma, H., "ZnO-CoO Solid Solution Thin Films",Appl. Phys., Vol-90, pp 4246-4250, 2001.

[5] Yang, S. G., Pakhomov, A. B., Hung, S. T., and Wong, C. Y., "Room Temperature Magnetism in Sputtered (Zn,Co)O Films", IEEE Trans. Magn., Vol-38, No. 5, pp 2877-2879, 2002.

[6] Xue-Chao, L., Er-Wei, S., Zhi-Zhan, C., Hua-Wei, Z., Tao, Z., and Li-Xin, S., "Difference in Magnetic Properties between Co-doped ZnO Powder and Thin Film", Chin. Phys. Soc, Vol-16, No. 6, pp 1770-1774, 2007.

[7] Kim, K. J., and Park, Y. R., "Spectroscopic Ellipsometry Study of Optical Transitions in $Zn_{1-x}Co_xO$ Alloys", Appl. Phys. Lett. Vol-81, No. 19, pp 1420-1422, 2002.

[8] Samanta, K., Bhattachary, P., and Katiyar, R. S., "Optical Properties of $Zn_{1-x}Co_xO$ Thin Films Grown on Al_2O_3 (0001) Substrates", Appl. Phys. Lett., Vol-87, No. 10, 2005.

[9] Furdyna, J. K., "Diluted magnetic semiconductors", Appl. Phys., Vol-64, No. 4, 1988.

[10] Xiao, H. U., Xianogyan, Z., Uddin, A., and leu, C. B., "Preparation and Characterization of Electronic and Optical Properties of Plasma Polymerized Nitrites", Thin Solid Films, Vol-477, pp 81-87, 2005.

[11] Ilican., Caglar, M., and Caglar, Y., "The Effect of Deposition Parameters on the Physical Properties of $Cd_xZn_{1-x}S$ Films Deposited by Spray Pyrolysis Method" Optoelectron. Adv. Mater., Vol-9, No. 5, pp 1414 – 1417, 2007.

[12] Okoli, D. N, Ekpunobi, A.J., and Okeke, C.E., "Growth and Characterization of ZnCdS Thin Films By Chemical Bath Deposition Technique" Academic Open Internet Journal, Vol-18, pp 1-12, 2006.

[13] Sharm, P, Sharma V., and Katyal, S. C., "Variation of Optical Constant in GE10SE60TE30 Thin Film" Chalcogenide Lett Vol-3, No. 10,pp. 73–79, 2006.

[14] Hossaina, M. S., Islama, R,. Khana, K. A., "Electrical Conduction Mechanisms of Undoped and Vanadium Doped ZnTe Thin Films" Chalcogenide Lett. Vol-5, No. 1, pp. 1–9, 2008.

[15] Khan, M. K. A., Rahaman, M. A., Shahjahan, M., Rahama, M. M., Hakim, M. A., Saha, D. K., and Khan, J. U., "Effect of Al-Doping on Optical and Electrical Properties of Spray Pyrolytic Nano-crystalline CdO Thin Films" Curr. Appl. Phys.Vol-1748, pp 7, 2009.

CHAPTER 6

CONCLUSIONS AND SUGGESTIONS FOR FUTURE WORK

6.1 Conclusions

The purpose of this chapter is to summarize the results obtained in this work. As demonstrated, the low-cost SPD technique, described in this study, can be used to obtain uniform conductive layers of pure and Co doped ZnO thin films with good repeatability. The effects of varying the compositions, thickness, structural, optical and electrical properties of the prepared samples were studied. The results of the present work are summarized and the following noteworthy conclusions as follows:

1. Spray pyrolysis is a suitable and novel technique for the production of quality ZnO thin films. The substrate temperature is the most important parameter that should be controlled when spraying. Before spraying, the temperature distribution contributes to the non-uniformity of deposition on the substrate. The structural property, electrical conductivity, and optical transmittance of ZnO thin films depend on the concentration of the dopant, which are optimized in the present work.

2. The average thickness of the film is found to be (200 ± 10) nm. But the samples with thickness 200 nm were studied extensively.

3. Surface morphology of $Zn_{1-x}Co_xO$ thin films was observed using SEM. SEM is shown that all the films are found well covered on the glass substrate. SEM photograph reveals that sprayed particles (atoms) are adsorbed onto the glass substrate. Nanofibers are observed in the pure ZnO thin film. Due to interstitial holes of ZnO are filled with cobalt, nanofibers are observed more clear in 5% doping concentration. But after 5% doping due to Zn are substituted by cobalt nanofibers are observed but unclear in 15% doping and for 25% doping fibers are not observed.

4. X-ray diffraction studies show that spray deposited thin films are polycrystalline in nature with preferential orientation along the (100), (002), (101), (102) and (110) planes and the films coated are ZnO and are found to be n-type semiconductors. Grain size of the film is found 57nm, which is agreed well with previous reported value. The decrease of the grain size due to Co doping is not significant. The shifting in the lattice

parameter values is mainly due to the Co dopant occupying at the interstitial positions in the lattice.

5. Various optical constants such as absorbance, transmittance, refractive index and dielectric constant of the films have been studied for the as-deposited films are recorded in the wavelength ranges from 300 to 1100 nm. The optical transmissions of the films are found to decrease from 80 % to 70 % (at initial) with the addition of Co doping. The UV-VIS spectrum for the $Zn_{1-x}Co_xO$ films show absorption around 570, 620 and 660 nm respectively. The band gap of the films varied between 3.2 to 2.7 eV. The increase in the Co incorporation in the film results in the overall increase in the refractive index. The gradual decrease of refractive index with wavelength i.e. increase with photon energy implies that the normal dispersion occurred before the absorption edge followed by anomalous dispersion.

6. Temperature dependence conductivity indicates that as deposited $Zn_{1-x}Co_xO$ thin film is semiconducting in nature. The conductivity increases with the increasing of cobalt concentration. Activation energy of $Zn_{1-x}Co_xO$ films is found to increases with the incorporation of Co in the solution.

7. The quality of these films prepared by spraying depends on various parameters such as spray rate, substrate temperature and the ratio of the various constituents in the solutions. An oxygen vacancy makes ZnO thin films to possess semiconducting nature. So it is very essential to avoid the complete oxidation of the metal in order to obtain films with good conductivity.

8. Cobalt absorbs UV so for high transmittance and low band gap we can use it in UV sensor. By doping Cobalt the film becomes highly conductive so we can use it in surface acoustic wave devices and transparent conducting electrodes.

In this research work the results obtained from morphological, structural, optical and electrical studies on ZnO thin film deposited by spray pyrolysis method are found to be in good agreement with the results obtained by other techniques.

6.2 Suggestions for Future Work

This is the first time that transition metal such as Co doped ZnO thin films have been prepared in our laboratory. We have deposited ZnO thin films on glass substrate at 575°K substrate temperature and studied some of their structural, electrical and optical properties. To prepare high quality ZnO films and for their details characterization, more studies are necessary. Hence to get better performance from the as deposited pure and Co doped ZnO thin films by spray pyrolysis technique, the following research work may be extended:

- Some magnetic properties are present there because of Co doped into the sample. To investigate the magnetization of the sample is needed by using SQUID magnetometer but we have no opportunity of SQUID magnetometer in our country.

APPENDIX

Table 1: Variation of absorbance as a function of wavelength for $Zn_{1-x}Co_xO$ film for different concentrations.

wavelength	x=0.00	X=0.05	x=0.15	x=0.25	x=0.35
1100	0.007769	0.015013	0.011554	0.030175	0.015063
1080	0.00807	0.015263	0.011955	0.030877	0.015714
1060	0.008446	0.015564	0.012431	0.031654	0.016441
1040	0.008872	0.01594	0.013083	0.032607	0.017293
1020	0.009023	0.016115	0.013308	0.033133	0.017644
1000	0.009323	0.016642	0.01386	0.03396	0.018346
980	0.009599	0.017093	0.014361	0.034712	0.018972
960	0.009825	0.017569	0.014837	0.035464	0.019524
940	0.010025	0.01797	0.015288	0.03619	0.020075
920	0.010226	0.018346	0.015815	0.036967	0.020627
900	0.010401	0.018847	0.016341	0.037744	0.021203
880	0.010627	0.019424	0.016917	0.038571	0.021855
860	0.010777	0.019975	0.017594	0.039474	0.022556
840	0.010927	0.020652	0.018271	0.040451	0.023283
820	0.011103	0.021328	0.019098	0.041454	0.024085
800	0.011328	0.022306	0.02005	0.042556	0.024937
780	0.011504	0.023333	0.021203	0.043835	0.025915
760	0.011779	0.024637	0.022506	0.045213	0.026892
740	0.01208	0.026516	0.024687	0.047018	0.028095
720	0.012356	0.029749	0.028421	0.0499	0.029649
700	0.012707	0.037293	0.036466	0.055539	0.03213
680	0.013058	0.050301	0.052982	0.068221	0.037619
660	0.013459	0.054937	0.061404	0.076967	0.042957
640	0.01396	0.053208	0.059449	0.07614	0.043434
620	0.014511	0.054386	0.061003	0.078421	0.045288
600	0.015013	0.049298	0.055138	0.074887	0.045038
580	0.015539	0.047419	0.051429	0.071479	0.044035
560	0.01619	0.049338	0.050797	0.0711	0.044511
540	0.016967	0.044586	0.045915	0.067419	0.043985
520	0.017769	0.047143	0.047168	0.068371	0.045138
500	0.018596	0.051855	0.051378	0.07183	0.047644
480	0.019424	0.057895	0.057218	0.076566	0.050827
460	0.020602	0.066241	0.066717	0.084787	0.05614
440	0.02188	0.078045	0.082356	0.100902	0.066566
420	0.024511	0.095639	0.11005	0.133734	0.091303
400	0.031779	0.11619	0.144637	0.177845	0.135815
380	0.063885	0.132105	0.171429	0.215088	0.190652
360	0.103358	0.145263	0.194361	0.249975	0.28802
340	0.12504	0.169373	0.211779	0.299699	0.359724
320	0.140419	0.180877	0.22391	0.32391	0.375025
300	0.145504	0.185764	0.231128	0.330727	0.379586

Table 2: Variation of transmittance as a function of wavelength for $Zn_{1-x}Co_xO$ film for different concentrations.

wavelength	x=0.00	x=0.05	x=0.15	x=0.25	x=0.35
1100	0.9281	0.8707	0.8984	0.8699	0.8958
1080	0.9258	0.8689	0.8953	0.8646	0.8925
1060	0.9227	0.8662	0.8912	0.8591	0.8883
1040	0.9193	0.8629	0.8859	0.8522	0.8835
1020	0.918	0.8611	0.8839	0.8491	0.8816
1000	0.9155	0.8571	0.8794	0.8438	0.8781
980	0.9133	0.8538	0.8755	0.8392	0.8751
960	0.9119	0.8505	0.8717	0.835	0.8723
940	0.91	0.847	0.8679	0.8307	0.8698
920	0.9083	0.8438	0.864	0.8264	0.8671
900	0.9067	0.8401	0.8597	0.8219	0.8641
880	0.9052	0.8357	0.8549	0.8171	0.8608
860	0.9038	0.8312	0.85	0.812	0.8579
840	0.9026	0.8263	0.8446	0.8066	0.8545
820	0.9006	0.8209	0.8384	0.8008	0.8512
800	0.899	0.8143	0.8311	0.7946	0.847
780	0.8976	0.8062	0.8224	0.7875	0.8429
760	0.8955	0.7966	0.8123	0.7804	0.8381
740	0.8928	0.7833	0.7964	0.7721	0.8308
720	0.8907	0.7607	0.7698	0.7612	0.8164
700	0.8881	0.7101	0.7156	0.7443	0.7822
680	0.885	0.6506	0.6151	0.7078	0.7486
660	0.8818	0.6441	0.5996	0.6742	0.6985
640	0.8783	0.6339	0.5998	0.6711	0.6932
620	0.8738	0.6174	0.5814	0.66	0.6781
600	0.8695	0.6364	0.6033	0.6614	0.679
580	0.8652	0.6471	0.624	0.6675	0.6949
560	0.8601	0.6497	0.6293	0.6546	0.6969
540	0.854	0.6643	0.6561	0.6678	0.7096
520	0.8479	0.649	0.6487	0.661	0.7089
500	0.8413	0.6218	0.6243	0.646	0.6886
480	0.8347	0.5884	0.5918	0.6276	0.6622
460	0.826	0.5448	0.5422	0.5978	0.6141
440	0.8165	0.4882	0.469	0.5428	0.5227
420	0.7971	0.4149	0.3639	0.4318	0.3623
400	0.7452	0.344	0.2749	0.2877	0.1997
380	0.5547	0.2975	0.2268	0.1736	0.1067
360	0.38	0.2635	0.1777	0.0912	0.0521
340	0.32	0.2312	0.1552	0.0536	0.0149
320	0.27	0.1902	0.1206	0.0392	0.0062
300	0.24	0.1786	0.105	0.0375	0.0023

Table 3: Variation of $(\alpha h\nu)^2$ as a function of hν for $Zn_{1-x}Co_xO$ film for different concentrations.

Hν	x=0.00	x=0.05	x=0.15	x=0.25	x=0.35
1.130114	1.44E+10	2.17E+10	5.61E+10	1.60E+11	5.81E+10
1.151042	1.61E+10	2.33E+10	6.08E+10	1.74E+11	6.10E+10
1.172759	1.84E+10	2.51E+10	6.60E+10	1.89E+11	6.57E+10
1.195313	2.10E+10	2.74E+10	7.25E+10	2.09E+11	7.24E+10
1.21875	2.26E+10	2.91E+10	7.78E+10	2.24E+11	7.72E+10
1.243125	2.51E+10	3.23E+10	8.49E+10	2.45E+11	8.67E+10
1.268495	2.77E+10	3.55E+10	9.29E+10	2.66E+11	9.57E+10
1.294922	3.03E+10	3.90E+10	1.01E+11	2.90E+11	1.07E+11
1.322473	3.29E+10	4.26E+10	1.10E+11	3.15E+11	1.19E+11
1.351223	3.57E+10	4.63E+10	1.20E+11	3.43E+11	1.32E+11
1.38125	3.86E+10	5.11E+10	1.31E+11	3.74E+11	1.48E+11
1.412642	4.22E+10	5.68E+10	1.45E+11	4.08E+11	1.68E+11
1.445494	4.54E+10	6.29E+10	1.60E+11	4.48E+11	1.91E+11
1.479911	4.89E+10	7.04E+10	1.78E+11	4.93E+11	2.19E+11
1.516006	5.30E+10	7.89E+10	1.96E+11	5.43E+11	3.53E+11
1.553906	5.80E+10	9.06E+10	2.19E+11	6.01E+11	3.96E+11
1.59375	6.29E+10	1.04E+11	2.47E+11	6.71E+11	4.55E+11
1.635691	6.95E+10	1.22E+11	2.82E+11	7.52E+11	4.82E+11
1.679899	7.70E+10	1.50E+11	3.33E+11	8.58E+11	6.51E+11
1.726563	8.51E+10	1.99E+11	4.23E+11	1.02E+12	9.06E+11
1.775893	9.53E+10	3.31E+11	6.12E+11	1.34E+12	1.91E+12
1.828125	1.07E+11	6.38E+11	1.09E+12	2.14E+12	3.89E+12
1.883523	1.20E+11	8.08E+11	1.46E+12	2.89E+12	5.44E+12
1.942383	1.38E+11	8.06E+11	1.69E+12	3.01E+12	6.42E+12
2.00504	1.58E+11	8.97E+11	1.87E+12	5.40E+12	7.97E+12
2.071875	1.81E+11	7.87E+11	2.55E+12	6.31E+12	9.78E+12
2.143319	2.08E+11	7.79E+11	3.53E+12	7.53E+12	1.28E+13
2.219866	2.42E+11	7.64E+11	4.07E+12	9.33E+12	1.59E+13
2.302083	2.85E+11	7.95E+11	5.61E+12	1.23E+13	1.96E+13
2.390625	3.38E+11	9.58E+11	6.85E+12	1.47E+13	2.31E+13
2.48625	4.00E+11	1.25E+12	8.33E+12	1.74E+13	2.87E+13
2.589844	4.73E+11	1.70E+12	1.00E+13	2.04E+13	3.33E+13
2.702446	5.80E+11	2.42E+12	1.33E+13	2.62E+13	4.11E+13
2.825284	7.15E+11	3.67E+12	1.67E+13	3.42E+13	5.27E+13
2.959821	9.85E+11	6.04E+12	2.52E+13	4.55E+13	6.90E+13
3.107813	1.82E+12	9.83E+12	3.52E+13	6.10E+13	9.17E+13
3.271382	8.17E+12	2.01E+13	5.09E+13	8.01E+13	1.23E+14
3.453125	2.07E+13	3.87E+13	7.46E+13	1.07E+14	1.68E+14
3.65625	4.85E+13	7.39E+13	1.09E+14	1.45E+14	2.18E+14

Table 4: Variation of Absorption coefficient (α) as a function of wavelength for $Zn_{1-x}Co_xO$ film for different concentrations.

Hν	x=0.00	x=0.05	x=0.15	x=0.25	x=0.35
1.130114	3.27E+06	1.58E+06	1.41E+06	840635.9	443161.9
1.151042	3.38E+06	1.65E+06	1.45E+06	857066.6	457898.7
1.172759	3.52E+06	1.72E+06	1.48E+06	878167.8	477819.4
1.195313	3.70E+06	1.81E+06	1.53E+06	903991.7	499745
1.21875	3.77E+06	1.85E+06	1.55E+06	917945.9	508149.8
1.243125	3.93E+06	1.92E+06	1.59E+06	941279.7	524346.3
1.268495	4.06E+06	1.98E+06	1.62E+06	963368.6	538635.8
1.294922	4.19E+06	2.04E+06	1.66E+06	985544.1	547747.1
1.322473	4.33E+06	2.10E+06	1.69E+06	1.01E+06	560134.8
1.351223	4.47E+06	2.16E+06	1.73E+06	1.03E+06	571240.5
1.38125	4.62E+06	2.22E+06	1.77E+06	1.05E+06	581711.9
1.412642	4.79E+06	2.29E+06	1.81E+06	1.08E+06	591545.6
1.445494	4.96E+06	2.36E+06	1.85E+06	1.11E+06	600738.5
1.479911	5.16E+06	2.43E+06	1.89E+06	1.14E+06	608629.4
1.516006	5.38E+06	2.51E+06	1.94E+06	1.17E+06	621804.4
1.553906	5.65E+06	2.60E+06	1.99E+06	1.21E+06	632365.4
1.59375	5.97E+06	2.70E+06	2.05E+06	1.25E+06	641621.7
1.635691	6.35E+06	2.81E+06	2.11E+06	1.30E+06	655533.3
1.679899	6.95E+06	2.93E+06	2.20E+06	1.38E+06	673467.6
1.726563	7.99E+06	3.09E+06	2.33E+06	1.51E+06	687454.1
1.775893	1.02E+07	3.34E+06	2.59E+06	1.76E+06	704816.4
1.828125	1.48E+07	3.91E+06	3.19E+06	2.28E+06	725584.2
1.883523	1.72E+07	4.46E+06	3.60E+06	2.55E+06	747098.4
1.942383	1.66E+07	4.51E+06	3.56E+06	2.50E+06	770719.1
2.00504	1.71E+07	4.70E+06	3.67E+06	2.57E+06	801227.3
2.071875	1.54E+07	4.68E+06	3.50E+06	2.40E+06	830526.7
2.143319	1.44E+07	4.57E+06	3.34E+06	2.30E+06	859971.4
2.219866	1.37E+07	4.62E+06	3.27E+06	2.25E+06	895084.4
2.302083	1.29E+07	4.57E+06	3.15E+06	2.20E+06	937356.9
2.390625	1.32E+07	4.68E+06	3.19E+06	2.27E+06	979932.3
2.48625	1.44E+07	4.94E+06	3.36E+06	2.45E+06	1.03E+06
2.589844	1.60E+07	5.27E+06	3.58E+06	2.68E+06	1.07E+06
2.702446	1.87E+07	5.82E+06	3.97E+06	3.06E+06	1.14E+06
2.825284	2.31E+07	6.91E+06	4.72E+06	3.66E+06	1.20E+06
2.959821	3.09E+07	9.50E+06	6.25E+06	4.72E+06	1.35E+06
3.107813	4.06E+07	1.41E+07	8.32E+06	6.05E+06	1.75E+06
3.271382	4.81E+07	1.98E+07	1.01E+07	7.20E+06	3.50E+06
3.453125	5.45E+07	2.99E+07	1.17E+07	8.23E+06	6.24E+06
3.65625	5.94E+07	3.84E+07	1.40E+07	9.45E+06	5.86E+06

Table 5: Variation of Extinction coefficient (K) as a function of wavelength for $Zn_{1-x}Co_xO$ film for different concentrations.

wavelength	x=0.00	x=0.05	x=0.15	x=0.25	x=0.35
1100	0.009302	0.018348	0.030968	0.034352	0.040811
1080	0.009487	0.018407	0.031112	0.035186	0.041416
1060	0.009745	0.018479	0.031304	0.036132	0.042218
1040	0.010043	0.018644	0.031638	0.037288	0.043367
1020	0.010017	0.018577	0.03153	0.037313	0.043249
1000	0.010148	0.018654	0.031684	0.038036	0.043648
980	0.010239	0.018739	0.031737	0.038548	0.043997
960	0.010266	0.018756	0.031763	0.038859	0.044147
940	0.010257	0.018756	0.031739	0.039124	0.044106
920	0.01024	0.018787	0.03173	0.039343	0.0441
900	0.010189	0.0188	0.031693	0.039564	0.044193
880	0.010179	0.018885	0.031668	0.039873	0.044309
860	0.010088	0.018925	0.031672	0.040218	0.04424
840	0.009991	0.01903	0.031701	0.040549	0.044324
820	0.00991	0.019067	0.031714	0.040947	0.044419
800	0.009864	0.019184	0.031763	0.041362	0.044583
780	0.009767	0.019373	0.031899	0.041908	0.044806
760	0.009744	0.019647	0.032059	0.042374	0.045138
740	0.00973	0.020226	0.032461	0.043104	0.046257
720	0.009683	0.021587	0.03352	0.044259	0.049272
700	0.009682	0.024534	0.036271	0.04663	0.058052
680	0.009665	0.030864	0.043281	0.053036	0.082628
660	0.009669	0.033677	0.047394	0.058781	0.100415
640	0.009725	0.031992	0.045464	0.057632	0.095776
620	0.009793	0.03183	0.045362	0.058215	0.097809
600	0.009804	0.02873	0.041921	0.056025	0.087966
580	0.00981	0.026642	0.038679	0.052952	0.077258
560	0.009869	0.025156	0.036625	0.051679	0.071233
540	0.009973	0.023682	0.033966	0.049244	0.062713
520	0.010058	0.023562	0.03317	0.048663	0.060593
500	0.010121	0.024448	0.033508	0.04939	0.063133
480	0.010148	0.02574	0.034289	0.050582	0.06708
460	0.010315	0.028097	0.036388	0.053541	0.076117
440	0.010479	0.032157	0.041421	0.060725	0.096745
420	0.011205	0.039458	0.052404	0.079505	0.144431
400	0.013836	0.048293	0.06637	0.112632	0.218021
380	0.026424	0.054606	0.076255	0.150204	0.287652
360	0.044419	0.059018	0.083959	0.214972	0.359749
340	0.039243	0.064052	0.095068	0.260623	0.484164
320	0.033932	0.074118	0.096704	0.252223	0.551135
300	0.020756	0.070837	0.092589	0.22371	0.539955

Table 6: Variation of Refractive index (n) as a function of wavelength for $Zn_{1-x}Co_xO$ film for different concentrations.

wavelength	x=0.00	x=0.05	x=0.15	x=0.25	x=0.35
1100	1.678157	2.021356	1.73109	2.073397	1.853608
1080	1.692278	2.031818	1.734927	2.087934	1.871896
1060	1.711413	2.048022	1.74483	2.107054	1.896402
1040	1.73218	2.067781	1.758855	2.130263	1.927716
1020	1.740178	2.078768	1.765598	2.142649	1.939773
1000	1.755431	2.102274	1.785059	2.163543	1.966368
980	1.768733	2.121578	1.799478	2.182941	1.989267
960	1.776833	2.140737	1.816081	2.20272	2.01168
940	1.788531	2.161797	1.83435	2.221172	2.034294
920	1.79883	2.181023	1.852229	2.241375	2.057057
900	1.808598	2.202843	1.873975	2.261628	2.082566
880	1.817322	2.22899	1.898378	2.288137	2.111153
860	1.825866	2.256077	1.925273	2.310763	2.139756
840	1.833034	2.285149	1.953138	2.338322	2.171854
820	1.845476	2.317799	1.98435	2.364952	2.208449
800	1.854835	2.356868	2.021623	2.395724	2.251867
780	1.863166	2.406357	2.067524	2.432824	2.303777
760	1.87556	2.464947	2.122317	2.476919	2.364782
740	1.891838	2.546646	2.201851	2.541138	2.461005
720	1.904201	2.688357	2.351089	2.653659	2.625225
700	1.919426	3.020788	2.718331	2.865921	2.975772
680	1.938018	3.596357	3.403915	3.311064	3.706516
660	1.95693	3.806592	3.709883	3.549509	4.081491
640	1.97718	3.727614	3.631805	3.504583	3.995726
620	2.003835	3.779523	3.710028	3.564345	4.068262
600	2.029481	3.551805	3.445663	3.416534	3.803018
580	2.054969	3.471196	3.307386	3.330906	3.639763
560	2.085043	3.377261	3.176254	3.289139	3.572611
540	2.121092	3.34348	3.072758	3.243991	3.397919
520	2.157061	3.456559	3.14698	3.307516	3.453169
500	2.196382	3.664807	3.335804	3.45984	3.639533
480	2.235862	3.934897	3.596849	3.66114	3.900735
460	2.287584	4.314321	4.002192	3.983965	4.331353
440	2.344538	4.858122	4.6489	4.513331	5.048618
420	2.462308	5.657978	5.701628	5.434361	6.269527
400	2.789598	6.538966	6.901294	6.554733	7.62218
380	4.22979	7.17126	7.714091	7.415349	8.441399
360	6.277952	7.65481	8.281222	8.086623	8.918537
340	6.491766	8.117996	8.586052	8.697428	9.141088
320	6.666	8.263821	8.649004	9.060432	9.35796
300	6.7006	8.285925	8.556729	8.960885	9.249383

Table 7: Variation of Real part of Dielectric constant as a function of wavelength for $Zn_{1-x}Co_xO$ film for different concentrations.

wavelength	x=0.00	x=0.05	x=0.15	x=0.25	x=0.35
1100	2.816125	4.085751	3.430802	4.102418	7.340135
1080	2.863715	4.128154	3.498771	4.230469	7.503326
1060	2.928841	4.194265	3.590899	4.364136	7.695671
1040	3.000346	4.275589	3.710288	4.536846	7.93179
1020	3.02812	4.321146	3.756944	4.616763	8.056503
1000	3.081436	4.419425	3.860586	4.752096	8.2672
980	3.128312	4.500958	3.950975	4.870979	8.4541
960	3.157029	4.582618	4.040501	4.981791	8.644601
940	3.198737	4.67323	4.131878	5.097297	8.835257
920	3.235685	4.756727	4.224848	5.21452	9.031953
900	3.270922	4.852379	4.330302	5.339089	9.25214
880	3.302555	4.968259	4.450021	5.472913	9.48962
860	3.333684	5.089741	4.57138	5.617256	9.733792
840	3.359914	5.221761	4.709571	5.773489	10.00072
820	3.405684	5.372047	4.869563	5.943924	10.28374
800	3.440316	5.554675	5.062844	6.130253	10.59073
780	3.471291	5.790393	5.298815	6.348751	10.97059
760	3.517632	6.075799	5.583026	6.573023	11.37504
740	3.578957	6.485224	6.046089	6.840414	11.90934
720	3.625887	7.227043	6.878686	7.205306	12.81099
700	3.684103	9.124833	8.834802	7.798456	14.66151
680	3.755819	12.93322	13.69759	9.213134	19.40989
660	3.829483	14.48951	16.6071	10.69456	23.14199
640	3.909146	13.89455	15.92047	10.84324	22.76533
620	4.015259	14.28425	16.50593	11.38087	23.76443
600	4.118696	12.6149	14.42865	11.31346	22.24426
580	4.222803	12.04884	13.21999	11.01667	20.76178
560	4.347309	11.40559	12.38539	11.15779	20.21419
540	4.498933	11.17858	11.52659	11.00347	19.09826
520	4.65281	11.94751	11.90553	11.33368	19.48907
500	4.82399	13.43049	13.22552	12.09725	20.9229
480	4.998978	15.48304	15.1921	13.09433	22.93589
460	5.232935	18.61292	18.73111	14.87155	26.70134
440	5.496747	23.60078	25.4474	18.76715	34.64537
420	6.062837	32.01194	39.24002	29.83202	52.27649
400	7.781666	42.75704	57.99275	53.36742	74.10671
380	17.89043	51.42576	71.12424	78.58491	84.51677
360	41.96189	58.59481	74.38689	81.30044	86.51201
340	40.33642	65.90046	73.39703	80.46542	86.08926
320	39.40881	68.0602	73.7214	77.89204	85.91656
300	36.40881	66.65507	72.38696	75.31141	83.89821

Table 8: Variation of Imaginary part of Dielectric constant as a function of wavelength for $Zn_{1-x}Co_xO$ film for different concentrations.

wavelength	x=0.00	x=0.05	x=0.15	x=0.25	x=0.35
1100	0.031222	0.046138	0.167813	0.139176	0.263748
1080	0.032109	0.046293	0.170457	0.144765	0.270584
1060	0.033355	0.046701	0.173695	0.150986	0.279767
1040	0.034794	0.047379	0.178217	0.158869	0.293647
1020	0.034863	0.047229	0.179002	0.160369	0.294798
1000	0.035629	0.048356	0.182209	0.165857	0.305118
980	0.036221	0.04912	0.18457	0.170181	0.313438
960	0.036482	0.049905	0.186789	0.173493	0.320797
940	0.036691	0.050472	0.188693	0.176689	0.327303
920	0.036839	0.050881	0.190731	0.17971	0.335075
900	0.036856	0.051646	0.192814	0.182862	0.3429
880	0.036996	0.05266	0.195117	0.186589	0.351872
860	0.036839	0.053568	0.197637	0.190669	0.362475
840	0.036628	0.054791	0.200515	0.19489	0.373178
820	0.036576	0.056029	0.20341	0.199686	0.387199
800	0.036594	0.058131	0.206746	0.204845	0.404391
780	0.036394	0.060534	0.211322	0.211219	0.426564
760	0.036552	0.063792	0.216258	0.217304	0.452855
740	0.036816	0.069068	0.224054	0.225502	0.503337
720	0.036878	0.079591	0.239961	0.237638	0.601438
700	0.037166	0.108997	0.277781	0.260474	0.850431
680	0.037461	0.170024	0.381378	0.322013	1.495058
660	0.037841	0.190771	0.456007	0.384521	1.851856
640	0.038455	0.17545	0.433861	0.37961	1.702036
620	0.039247	0.176149	0.442289	0.39284	1.72266
600	0.039796	0.14521	0.395443	0.376939	1.408577
580	0.040318	0.131953	0.352494	0.351555	1.215505
560	0.041154	0.118518	0.328854	0.365291	1.117698
540	0.042307	0.111266	0.296881	0.326736	0.943215
520	0.04339	0.117119	0.292875	0.327689	0.948242
500	0.044458	0.131333	0.306545	0.3436	1.046762
480	0.04538	0.15114	0.328434	0.366106	1.199422
460	0.047193	0.181702	0.376065	0.41299	1.488223
440	0.049136	0.230585	0.487625	0.526182	2.048194
420	0.055183	0.314131	0.757802	0.868579	3.244337
400	0.077196	0.420054	1.142724	1.64582	4.937063
380	0.223535	0.497582	1.402118	2.663437	6.156481
360	0.575493	0.553296	1.561902	3.877765	6.986447
340	0.48597	0.608007	1.691014	4.055465	7.369058
320	0.398088	0.69312	1.651634	3.771635	7.018279
300	0.308088	0.638249	1.506466	3.210978	6.831381

Table 9: Variation of optical conductivity as a function of hν for $Zn_{1-x}Co_xO$ film for different concentrations.

Hν	x=0.00	x=0.05	x=0.15	x=0.25	x=0.35
1.130114	3.92012E+12	5.79E+12	2.11E+13	1.75E+13	3.31154E+13
1.151042	4.10613E+12	5.92E+12	2.18E+13	1.85E+13	3.46028E+13
1.172759	4.346E+12	6.08E+12	2.26E+13	1.97E+13	3.64521E+13
1.195313	4.62063E+12	6.29E+12	2.37E+13	2.11E+13	3.89964E+13
1.21875	4.72064E+12	6.4E+12	2.42E+13	2.17E+13	3.99168E+13
1.243125	4.92075E+12	6.68E+12	2.52E+13	2.29E+13	4.21406E+13
1.268495	5.10465E+12	6.92E+12	2.6E+13	2.4E+13	4.41731E+13
1.294922	5.24853E+12	7.18E+12	2.69E+13	2.5E+13	4.61521E+13
1.322473	5.3909E+12	7.42E+12	2.77E+13	2.6E+13	4.80899E+13
1.351223	5.53038E+12	7.64E+12	2.86E+13	2.7E+13	5.03021E+13
1.38125	5.65581E+12	7.93E+12	2.96E+13	2.81E+13	5.26207E+13
1.412642	5.80634E+12	8.26E+12	3.06E+13	2.93E+13	5.52248E+13
1.445494	5.91619E+12	8.6E+12	3.17E+13	3.06E+13	5.82119E+13
1.479911	6.02229E+12	9.01E+12	3.3E+13	3.2E+13	6.13577E+13
1.516006	6.16052E+12	9.44E+12	3.43E+13	3.36E+13	6.52158E+13
1.553906	6.31755E+12	1E+13	3.57E+13	3.54E+13	6.98141E+13
1.59375	6.4442E+12	1.07E+13	3.74E+13	3.74E+13	7.55303E+13
1.635691	6.64254E+12	1.16E+13	3.93E+13	3.95E+13	8.22959E+13
1.679899	6.87125E+12	1.29E+13	4.18E+13	4.21E+13	9.39419E+13
1.726563	7.07399E+12	1.53E+13	4.6E+13	4.56E+13	1.15369E+14
1.775893	7.33304E+12	2.15E+13	5.48E+13	5.14E+13	1.67793E+14
1.828125	7.60852E+12	3.45E+13	7.75E+13	6.54E+13	2.73656E+14
1.883523	7.91871E+12	3.99E+13	9.54E+13	8.05E+13	3.05521E+14
1.942383	8.29863E+12	3.79E+13	9.36E+13	8.19E+13	3.173E+14
2.00504	8.7427E+12	3.92E+13	9.85E+13	8.75E+13	3.23743E+14
2.071875	9.16045E+12	3.34E+13	9.1E+13	8.68E+13	3.24236E+14
2.143319	9.60068E+12	3.14E+13	8.39E+13	8.37E+13	2.89442E+14
2.219866	1.01497E+13	2.92E+13	8.11E+13	8.52E+13	2.65792E+14
2.302083	1.08206E+13	2.85E+13	7.59E+13	8.36E+13	2.4124E+14
2.390625	1.15243E+13	3.11E+13	7.78E+13	8.7E+13	2.51853E+14
2.48625	1.22805E+13	3.63E+13	8.47E+13	9.49E+13	2.89141E+14
2.589844	1.30573E+13	4.35E+13	9.45E+13	1.05E+14	3.45114E+14
2.702446	1.41695E+13	5.46E+13	1.13E+14	1.24E+14	4.4683E+14
2.825284	1.54233E+13	7.24E+13	1.53E+14	1.65E+14	6.42911E+14
2.959821	1.81462E+13	1.03E+14	2.49E+14	2.86E+14	1.06686E+15
3.107813	2.66542E+13	1.45E+14	3.95E+14	5.68E+14	1.70467E+15
3.271382	8.12444E+13	1.81E+14	5.1E+14	9.68E+14	2.23759E+15
3.453125	1.20785E+14	2.12E+14	5.99E+14	1.49E+15	2.68032E+15
3.65625	1.77407E+14	2.47E+14	6.87E+14	1.65E+15	2.9934E+15

Table 10: Variation of electrical resistivity with temperature for as deposited $Zn_{1-x}Co_xO$ thin films for different concentrations

Temp(K)	x=0.00	x=0.05	x=0.15	x=0.25	x=0.35
300	2.1674	2.10225	1.31957	0.98335	0.42172
310	2.00215	1.80193	1.05566	0.78668	0.10543
320	1.60172	1.50161	0.87971	0.4589	0.07907
330	1.30934	0.96103	0.65979	0.30593	0.08434
340	0.84535	0.78084	0.36224	0.24766	0.05601
350	0.62423	0.48052	0.2315	0.13456	0.04663
360	0.56136	0.39042	0.13196	0.03997	0.04539
370	0.53663	0.15617	0.10557	0.026	0.04744
380	0.41744	0.06006	0.13033	0.01266	0.04858
390	0.35532	0.04914	0.10151	0.00536	0.0328
400	0.27966	0.02628	0.08378	0.0028	0.03575
410	0.22955	0.02503	0.0765	0.00219	0.03765
420	0.21564	0.00948	0.07038	0.00152	0.04137
430	0.21148	0.00522	0.07331	0.00101	0.043

Table 11: Variation of electrical conductivity with temperature for as deposited $Zn_{1-x}Co_xO$ thin films for different concentrations

Temp(K)	x=0.00	x=0.05	x=0.15	x=0.25	x=0.35
300	2.37123	3.75782	0.75782	2.46138	0.46138
310	9.48491	3.94728	0.94728	2.49946	0.49946
320	12.64654	4.13673	1.13673	2.62433	0.62433
330	14.85613	4.51564	1.51564	2.76374	0.76374
340	17.85394	5.76064	2.76064	3.18294	1.18294
350	20.44413	7.31958	4.31958	3.60198	1.60198
360	22.02946	10.57821	7.57821	3.78138	1.78138
370	23.07757	12.47277	9.47277	3.86348	1.86348
380	24.58426	13.75782	9.76064	4.39558	2.39558
390	25.4872	14.94728	9.85168	4.81439	2.81439
400	25.97243	16.13673	11.93569	5.57571	3.57571
410	25.55774	18.51564	13.07242	6.35635	4.35635
420	24.17121	17.76064	14.20915	6.63731	4.63731
430	23.25332	16.64079	13.64079	6.72853	4.72853

Table 12: Variation lnσ as a function of 1/T for the as-deposited $Zn_{1-x}Cd_xS$ thin films for different concentrations.

Temp(K)	x=0.00	x=0.05	x=0.15	x=0.25	x=0.35
3.33333	-0.77353	-0.74301	-0.27731	0.01679	0.86341
3.22581	-0.69422	-0.58886	-0.05416	0.23993	1.2497
3.125	-0.47108	-0.40654	0.12816	0.77893	1.53738
3.0303	-0.26952	0.03975	0.41584	1.1844	2.47285
2.94118	0.168	0.24739	1.01546	1.3957	2.88222
2.85714	0.47124	0.7329	1.46316	2.00572	3.06545
2.77778	0.57739	0.94054	2.02528	3.21954	4.09238
2.7027	0.62245	1.85683	2.24842	3.64979	4.44821
2.63158	0.87362	2.81234	2.0377	4.36896	5.02453
2.5641	1.03474	3.01301	2.28764	5.2281	5.41731
2.5	1.27416	3.63902	2.47953	5.87758	6.33122
2.43902	1.47163	3.68781	2.5705	6.12604	6.77932
2.38095	1.53413	4.65816	2.65389	6.48604	7.18516
2.32558	1.55361	5.25468	2.61306	6.89923	7.54645

CHAPTER - I

INTRODUCTION

CHAPTER – 2

THEORETICAL BACKROUND

CHAPTER – 3

DEPOSITION TECHNIQUES

CHAPTER – 4

EXPERIMENTAL DETAILS

CHAPTER – 5

RESULTS AND DISCUSSION

CHAPTER – 6

CONCLUSIONS AND SUGGESTIONS FOR FUTURE WORK

APPENDIX